

# *Many-body theory of quantum systems*

## *Kumulative Habilitationsschrift*

zur Erlangung des akademischen Grades  
Dr. rer. nat. habil.

vorgelegt der

Naturwissenschaftlichen Fakultät II Chemie und Physik  
der Martin-Luther-Universität Halle-Wittenberg

von

Herrn Dr. rer. nat. Yaroslav Pavlyukh  
geb. am 26. Februar 1976 in Drogobych

Gutachter:

1. Gutachter: Prof. Steffen Trimper, Martin-Luther-Universität Halle-Wittenberg
2. Gutachter: Prof. John J. Rehr, University of Washington
3. Gutachter: Prof. Lucia Reining, École Polytechnique, Université Paris-Saclay

Halle (Saale), den 03. November, 2015



# Abstract/Kurzfassung

---

Cooperation of quantum mechanics and many-body physics stipulates enormous complexity and diversity of systems in Materials Science. Mean-field theories capture some of the electronic properties, whereas the whole complexity is encoded in the notion of electronic correlations. With the advent of ultrafast lasers and nanoscale physics we see the manifestation of electronic correlations in molecular transport, nanoelectronics, attosecond phenomena. In this thesis I view the many-body quantum systems from four different, but related angles: equilibrium and nonequilibrium Green's function theory, exact diagonalization and related quantum chemical approaches, and semi-classical approaches associated with mean-field theories. Important innovations presented here are at the merger of several formalisms: equilibrium methods are used to get a glimpse into nonequilibrium dynamics of excitations in Fermi liquids, or with the help of quantum chemistry methods, decay of excitations in molecular systems is described. Vice versa, nonequilibrium Green's function approach provides a way to construct conserving and positive definite approximations to the equilibrium spectral properties, and complements the description of light-matter interaction covering phenomena of photoemission and photoabsorption. For larger systems, the semi-classical response to electron-magnetic fields is derived starting from the corresponding microscopic expressions for linear and non-linear susceptibilities.

Der Komplexität und Diversität der für Materialwissenschaften relevanten Systeme liegt das Zusammenspiel von Quantenmechanik und Vielteilchenphysik zugrunde. Molekularfeldtheorien sind in der Lage einige elektronische Eigenschaften zu beschreiben, währenddessen die volle Komplexität im Begriff der elektronischen Korrelation enthalten ist. Mit dem Aufkommen von ultraschnellen Lasern und der Nanotechnologie hat man die Manifestation von elektronischen Korrelationen im Ladungstransport durch einzelene Moleküle, in der Nanoelektronik und in Phänomenen auf der Attosekunden Zeitskala erlebt. In dieser Arbeit betrachte ich Vielteilchen-Quantensysteme unter vier verschiedenen, jedoch nicht strikt trennbaren, Gesichtspunkten: Theorie der Green'schen Funktionen im Gleich- und Nichtgleichgewicht, exakte Diagonalisierung und verwandte Methoden aus der Quantenchemie, und semiklassische Ansätze mit den dazugehörigen Molekularfeldtheorien. Die wichtigen Fortschritte, die in dieser Arbeit vorgestellt werden, stellen die Kombination mehrerer Formalismen dar: Gleichgewichtsmethoden erlauben einen Einblick in die Nichtsgleichsdynamik der Anregungen in Fermiflüssigkeiten, während der Zerfall von Anregungen in molekularen Systemen mithilfe von Quantenchemie beschrieben wird. Auf der anderen Seite lassen sich Näherungen, die Erhaltungssätze und positive Definitheit erfüllen, durch den Nichtgleichgewichtsformalismus der Green'schen Funktionen konstruieren. Der Formalismus ergänzt die Beschreibung von Licht-Materie-Wechselwirkung, die die Phänomene von Photoemission und Photoabsorption umfasst. Für größere Systeme wird die semiklassische Reaktion auf das Einwirken elektromagnetischer Felder von den entsprechenden mikroskopischen Ausdrücken für die linearen und nichtlinearen Suszeptibilitäten hergeleitet.



# Preface

---

Clear notations make formulas recognizable and improve comprehension of scientific texts. Therefore, in the preparation of this work I devoted a special attention to make notations consistent across chapters and sections. Consider, for instance, the density-density response function  $\chi$  and its irreducible part  $P$  related by  $\chi = P + P\nu\chi$ . The irreducible part is denoted as  $\tilde{\chi}_{nm}$  by Giuliani and Vignale [1], as  $\chi_{sc}$  by Nozières and Pines [2], as  $Q$  by Gross, Runge and Heinonen [3], and as  $P$  by Hedin [4]. I follow the latter approach here. On the other hand, writing the random phase approximation in the form  $\chi = \chi^{(0)} + \chi^{(0)}\nu\chi$  emphasizes the fact that the Lindhard function (in 3d)  $\chi^{(0)}$  is the zeroth order approximation to both  $\chi$  and  $P$ . This seems to be logical as in this way the optical form of the exact relation  $\chi = \chi^{(0)} + \chi^{(0)}(\nu + f_{xc})\chi$  from the time-dependent density functional theory and the Hedin equation  $W = \nu + \nu PW$  is preserved.

Important well established facts that do not require a proof are presented in shaded boxes. They are included to make the exposition self-contained. Important new results are framed. I tried to provide the full logical way to obtain them starting from basic principles. Mathematical and numerical details are omitted unless they are essential for the comprehension of the idea. They can be found in the appended papers cited in bold face.

I am pleased to express my gratitude for insightful scientific discussions to Dr. Torsten Andersen, Prof. Jamal Berakdar, Dr. Levan Chotorlishvili, Prof. Vitalii Dugaev, Prof. Eberhard K. U. Gross, Prof. Wolfgang Hübner, Prof. Chenglong Jia, Dr. Oleg Kidun, Prof. Jürgen Kirschner, Dr. Georgios Lefkidis, Dr. Andrea Marini, Dr. Andriy Marko, Prof. Luca Guido Molinari, Dr. Andrey Moskalenko, Dr. Oleksandr Ney, Dr. George Pal, Prof. A. Ravi P. Rau, Prof. Angel Rubio, Dr. Khompat Satitkovitchai, Dr. Nicholas Sedlmayr, Prof. Hans Christian Schneider, Dr. Frank Oliver Schumann, Michael Schüler, Stefan Stagraczyński, Dr. Gianluca Stefanucci, Dr. Alexander Sukhov, Dr. Anna-Maija Uimonen, Prof. Claudio Verdozzi, Prof. Robert van Leeuwen, Jonas Wätzel, Prof. Wolf Widdra.

I would like to express my special thanks to Prof. Jamal Berakdar and Prof. Wolfgang Hübner, Prof. Robert van Leeuwen, Prof. Angel Rubio, Prof. Hans Christian Schneider for invaluable support of my scientific endeavours.

Last but not least I would like to thank my parents, my children Nadija and Taras Rakdee, and my wife Khompat, for their loving support, patience and understanding during the preparation of this work.

---

*This work is dedicated to the memory of “Heavenly Hundred” killed during sad events in the fall and winter of 2013-2014, to those who died for the freedom of my country and to a large number of innocent ones.*

# Contents

---

Abstract/Kurzfassung . . . . .	i
Preface . . . . .	iii
<b>1 Introduction</b>	<b>3</b>
<b>2 Equilibrium formalism</b>	<b>5</b>
2.1 Hedin's equations . . . . .	6
2.2 Asymptotic expansions . . . . .	7
2.3 Dealing with singularities . . . . .	9
2.4 Time-evolution of excitations in normal Fermi liquids . . . . .	14
<b>3 Exact propagators from quantum chemistry</b>	<b>21</b>
3.1 Fluctuation-dissipation theorem . . . . .	21
3.2 Lehmann representation of the electronic self-energy . . . . .	24
3.3 Decay of hybridized electronic states of a Na cluster on Cu(001) . . . . .	26
3.4 Superatom molecular orbitals of C <sub>60</sub> molecule . . . . .	28
<b>4 Nonequilibrium approach</b>	<b>33</b>
4.1 Correlators on the Keldysh contour . . . . .	34
4.2 Conserving approximations . . . . .	36
4.3 Positive definite approximations . . . . .	41
4.4 Processes involving emission of particles . . . . .	46
<b>5 Classical and semi-classical approaches</b>	<b>51</b>
5.1 Nonlinear Mie scattering from spherical particles . . . . .	51
5.2 Semi-classical sources . . . . .	55
5.3 Linear scaling approach . . . . .	58
<b>6 Conclusions</b>	<b>65</b>
<b>Bibliography</b>	<b>67</b>
<b>Index</b>	<b>73</b>
<b>Eidesstattliche Erklärung</b>	<b>75</b>
<b>Lebenslauf</b>	<b>77</b>
<b>List of the appended publications</b>	<b>79</b>





# 1 Introduction

---

Beginning of the twentieth century was the golden time of the "new physics". At the birth of quantum mechanics the discoveries were coming at almost monthly pace. Soon after Erwin Schrödinger in 1926 published equation bearing his name, Walter Heitler and Fritz London came up with the first quantum mechanical calculation of a many-particle system — the hydrogen molecule. When they started their calculation they had to "struggle with the proper formulation of the Pauli principle", which was known at that time as "a two-valuedness not describable classically" [5], but no mathematical formulation had yet been given.<sup>1</sup> So, they wrote the two-electron wave-function as a linear combination

$$\Psi(1, 2) = c_1\psi_a(1)\psi_b(2) + c_2\psi_a(2)\psi_b(1),$$

without making any assumption upon the value of coefficients and found two possibilities  $c_1/c_2 = \pm 1$ . The energy difference of between these two states being proportional to the *exchange integral*  $\iint \psi_a(1)\psi_b(2)v(1, 2)\psi_a(2)\psi_b(1) d^3r_1 d^3r_2$ .

The paper was very positively accepted and is truly considered as the birth of quantum chemistry [7]. Soon thereafter Paul A. M. Dirac in the introduction to his paper [8] proclaimed: "the underlying physical laws necessary for the mathematical theory of a large part of physics and the whole of chemistry are thus completely known, and the difficulty is only that the exact application of these laws leads to equations much too complicated to be soluble". By no means this declaration slowed down the pace as already in 1930 Vladimir Fock improved the "self-consistent field" approximation of Douglas R. Hartree [9, 10]. Because the whole bunch of one-particle states are determined by a single potential, the resulting equations are even more simple to implement than the Hartree's equation. The high price due to the non-locality remained to be paid. It was so until Robert T. Sharp and George K. Horton [11] found a way to construct a *local* potential minimizing the Hartree-Fock Hamiltonian establishing, thus, the optimized effective potential method.

These examples illustrate one important philosophical concept: the *reductionism*. In order to describe a complicated system one reduces it to a smaller set of properties to focus on the essential. Already for quite small systems the many-body wave-functions are too complex and it is required to map them onto a more elemental object such as the one-particle density in order to make the numerical treatment feasible. Fortunately, we do not lose any information, as Pierre C. Hohenberg and Walter Kohn proved mathematically [12]. The idea was further corroborated by Walter Kohn and Lu Jeu Sham in the 1965 [13] in the form of the density functional theory which is now the cornerstone of the computational physics and chemistry.

Application of the Green's function approach to the many-body physics is another typical example of the reductionism: almost all information about the observables of a many-

---

<sup>1</sup>"Aber es ist wünschenswert, sich wenigstens darüber klar zu werden, wie diese merkwürdige Zweideutigkeit mathematisch zustande kommt" [6].

body system is contained in one and two-particle propagators. Here, a lot of input came from particle physics after the observation that the Feynman diagram technique is equally well applicable to the scattering problems in high-energy physics and to electrons in solids under very normal conditions. In 1961 Julian Schwinger published a paper [14] on the Brownian motion of a quantum oscillator. The main message of his highly mathematical work was, however, more general: to give an action principle that would allow to compute expectation values in the time-dependent formulation of quantum mechanics. In fact, he invented what is now commonly known as the Keldysh contour [15], the basic concept of nonequilibrium Green's function theory.

"More is different" is a philosophical paper of Philip W. Anderson [16] where he refutes mindless application of the reductionist hypothesis to science in general: the method development is not more important than the method application. And many-body physics is not a mere application of the Green's function methods. Phenomenology and models development are as productive as designing methods for their solution. The notion of the *Fermi liquid* introduced by Lev Landau [17] was the reflection of an idea that elemental excitations in the interacting electron gas — the quasiparticles — act like non-interacting particles. How good is this approximation is possible to judge only by contrasting them with excitations in one-dimensional systems: in Luttinger liquids the elemental excitations are given by spin and charge density waves.

The theory of many-body systems is rich on beautiful models and elegant solutions [18]. In 1967 Philip Anderson realized that photoemission from a deep core state leads to the orthogonality catastrophe [19]: zero overlap of many-body states before and after the photon absorption event. Soon thereafter a brilliant, but mathematically very involved, solution by Philippe Nozières and Cyrano De Dominicis [20] demonstrated the power of Green's function approach. Interestingly, two more solutions using the so-called parquet approximation and the bosonization technique are known. They are now standard topics of books on strongly correlated systems [21].

It is rather unexpected that "less correlated systems", typically represented by metals and semiconductors are less susceptible to analytic methods. In 1965 Lars Hedin formulated a system of integral equations [4] relating the one and two-particle Green's functions and providing a systematic way to improve upon the mean field theories. The lowest order approximation, in which the electron self-energy is given as a product of the electron Green's function and the screened Coulomb interaction (the so called *GW* approximation [22]), demonstrated a high potential in improving results of the density functional theory. However, it is extremely difficult to go beyond.

Going "beyond" is the main topic of this work. The zero-temperature formalism is common to all the topics covered here and the emphasis is given to the time-evolution aspect of many-body problems. It is tackled using both the equilibrium (Chapters 2 and 3) and non-equilibrium (Chapter 4) approaches. Chapter 5 is devoted to the semi-classical and classical descriptions of large but finite systems, again, from the many-body perspective.

## 2 Equilibrium formalism

---

A naive thinking suggests that any mathematically valid perturbation theory should provide an expansion of a desired quantity such as total energy or the Green's function in terms of some small parameter. Furthermore, one expects that the perturbative expansion is a power series in terms of this parameter. It is often mentioned in this context that the fine-structure constant  $\alpha \approx 1/137.036$  is a small parameter for the perturbative expansions of quantum electrodynamics. Or by writing the Coulomb interaction in the homogeneous electron gas (HEG) in the form  $\alpha r_s/r$  one expects to treat it as a small perturbation<sup>1</sup>.

Fortunately, the nature is not that simple. In fact, none of the statements is valid. From mathematical point of view perturbative expansions are asymptotic expansions which often means that the radius of convergence of a series is zero at each point. It is known, for example, that the correlation energy of HEG in the high density limit  $r_s \ll 1$  can be written in the form  $a_0 + a_1 \ln r_s + a_2 r_s \ln r_s + a_3 r_s + \mathcal{O}(r_s^2 \ln r_s)$ . In the low density limit the gas undergoes a phase transition to the Wigner crystal and the total energy is  $A_1 r_s^{-1} + A_2 r_s^{-3/2} + A_3 r_s^{-2} + A_4 r_s^{-5/2} + \mathcal{O}(r_s^{-3})$ . Clearly, these are non-analytic functions and, therefore, cannot be represented in terms of power series<sup>2</sup>.

The expression for the weak-correlation limit ensues from the infinite re-summation of certain classes of Feynman diagrams. The re-summations are often done by replacing the bare propagators with the "dressed" ones. The dressed propagators are typically obtained as solutions of some integral equations and already contain an infinite number of diagrams. In fact, it is not only the single-particle propagators that can be dressed. The same approach is applicable to the interparticle interaction, which can also be dressed or "screened". The interaction is of bosonic nature, and therefore the screening follows from the dressing of the particle-hole propagator. There is no indication that the "dressing procedure" cannot be implemented for other correlators.

Functional differentiation is a very natural tool to represent these relations. After a short introduction of functional relations between the propagators (Sec.2.1) I present exact analytical results for the enumeration of Feynman diagrams for these quantities in Sec. 2.2. Diagrammatic solution of the  $S$ -model is given in Sec. 2.3. Finally, in the discourse of Sec. 2.4 it is shown how non-analytic terms in the short time-limit of the electron spectral function follow from the re-summation of diagrams using the cumulant expansion technique.

---

<sup>1</sup>Here,  $\alpha$  has a different meaning being just a numerical constant  $(4/(9\pi))^{1/3}$  and the Seitz radius  $r_s$  is a standard measure of the electron density.

<sup>2</sup>The  $a_0 + a_1 \ln r_s$  terms in high density limit were computed by Gell-Mann and Brueckner [23] by resummation of all bubble diagrams, whereas the first coefficient of the energy of the Wigner crystal was calculated by Fuchs [24].

## 2.1 Hedin's equations

Most many-body or field theory books derive perturbative expansions in terms of propagators starting from the path integral formalism. On this way the Feynman diagrams are introduced graphically and a set of rules is given allowing to transform these into analytical expressions. There is an alternative approach where propagators are expressed in terms of variational derivative of a certain functional with an advantage that various integral relations between them can readily be found. It was introduced in the arsenal of the condensed matter physics through the work of Hedin [4] and a very pedagogical introduction is due to Strinati [25]. There is a self-contained system of five variational equations describing many-body physics of interacting fermions:

$$\Gamma(12, 3) = \delta(12)\delta(13) + \frac{\delta\Sigma(12)}{\delta V(3)}, \quad (2.1a)$$

$$\Sigma(12) = i\hbar \int W(13)G(14)\Gamma(42, 3)d(34), \quad (2.1b)$$

$$P(12) = -i\hbar \int G(23)G(42)\Gamma(34, 1)d(34), \quad (2.1c)$$

$$\frac{\delta G(12)}{\delta V(3)} = \int G(14)G(52)\Gamma(45, 3)d(45), \quad (2.1d)$$

$$\frac{\delta W(12)}{\delta V(3)} = \int W(14)W(52)\frac{\delta P(45)}{\delta V(3)}d(45), \quad (2.1e)$$

where  $\Gamma(12, 3)$  is the vertex function,  $\Sigma(12)$  is the electron self-energy,  $P(12)$  is the polarization propagator, and  $V(3)$  is the external  $[\varphi(3)]$  plus the induced field in the system.<sup>3</sup> All these quantities are functionally dependent on the external field and on the full electron propagator  $G(12)$ . By the use of chain rule

$$\frac{\delta\Sigma(12)}{\delta V(3)} = \int \frac{\delta\Sigma(12)}{\delta G(45)} \frac{\delta G(45)}{\delta V(3)} d(45)$$

one arrives at the Bethe-Salpeter equation for the vertex function, and, analogically for the screened interaction  $W$ :

$$W(12) = v(12) + \int W(13)P(34)v(42)d(34), \quad (2.2a)$$

$$\Gamma(12, 3) = \delta(12)\delta(13) + \int \frac{\delta\Sigma(12)}{\delta G(45)} G(46)G(75)\Gamma(67, 3)d(4567). \quad (2.2b)$$

and the whole system is transformed into the system of Hedin's equations. Setting for the vertex function  $\Gamma = \delta(12)\delta(13)$  leads to celebrated  $GW$ -approximation for the self-energy and random phase approximation (RPA) for the screened interaction:

$$\Sigma(12) = iW(12)G(12), \quad P(12) = -iG(21)G(12). \quad (2.3)$$

<sup>3</sup>For the rest of this chapter atomic units are used, i. e.,  $e = m_e = \hbar = 1$ .  $i = 1, 2, \dots$  stand for a collection of space  $\mathbf{r}_i$ , spin  $\sigma_i$  and time  $t_i$  variables, i. e.,  $i \equiv (\mathbf{r}_i, \sigma_i, t_i)$ .

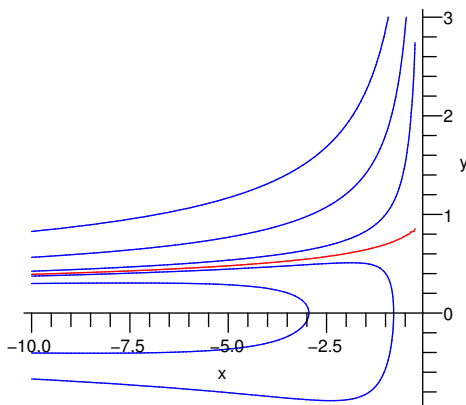


Figure 2.1: The solution of Eq. (2.7) can be represented in the following implicit form  $\sqrt{-x} \exp\left[\frac{1}{2} \frac{(1+xy)^2}{x}\right] + \sqrt{\frac{\pi}{2}} \operatorname{erf}\left[\frac{(1+xy)}{\sqrt{-2x}}\right] = C$ . It is shown here for different values of  $C$ . The initial condition  $y(0) = 1$  is satisfied when  $C = \sqrt{\pi/2}$  (red curve).

## 2.2 Asymptotic expansions

The enumeration of Feynman diagrams for the electron propagator  $G(1, 2)$ , the self-energy operator  $\Sigma(1, 2)$ , the effective potential  $W(1, 2)$ , the polarization  $P(1, 2)$ , and the vertex function  $\Gamma(1; 2, 3)$  can be accomplished by writing Hedin's equations in zero dimensions of space-time where they transform into a set of ordinary differential equations (ODE) [1].

$$G = g + g\Sigma G, \quad W = v + vPW, \quad \Sigma = GW\Gamma, \quad P = \ell G^2\Gamma, \quad \Gamma = 1 + g^2 \frac{d\Sigma}{dg}. \quad (2.4)$$

The parameter  $\ell$  denotes the degeneracy due to the spin summation, and  $g$  is the Green's function of interacting electrons in the Hartree approximation. The expansion of the generating functions in powers of the parameter  $x = g^2v$  yields a number of topologically distinct diagrams with a given number of fermionic loops (corresponds to the power of  $\ell$ ). With  $\Sigma \equiv gvs(x)$  and  $G = g/(1 - g\Sigma) = g/[1 - xs(x)] \equiv gy(x)$  the differential equation for the electron propagator can be obtained:

$$2x^2 \frac{dy}{dx} [y^\ell + (1 - \ell)] + x\ell y^2 - y[1 - x(1 - \ell)] + 1 = 0. \quad (2.5)$$

This Abel ODE has a power series solution:

$$y(x) = 1 + x + (3 + \ell)x^2 + (15 + 11\ell + \ell^2)x^3 + (105 + 116\ell + 26\ell^2 + \ell^3)x^4 + \mathcal{O}(x^5), \quad (2.6)$$

where the number of  $m$ -th order Feynman diagrams with  $n$  fermionic loops is given by the coefficient in front of  $\ell^n x^m$ . Enumeration of *all* Feynman diagrams can then be obtained by setting  $\ell = 1$ :

$$2x^2 y \frac{dy}{dx} + y^2 x - y + 1 = 0. \quad (2.7)$$

Analytic solution of Abelian Eqs. (2.5, 2.7) are rather complicated and given in terms of Whittaker functions [26] (Fig. 2.1). This solution has interesting applications for the correlated electronic calculations in realistic systems [27, 28]. Also, more insight can be obtained by analyzing the coefficients of the power series solution of Eqs. (2.5, 2.7) and noticing a correspondence to other combinatorics objects — the chord diagrams.

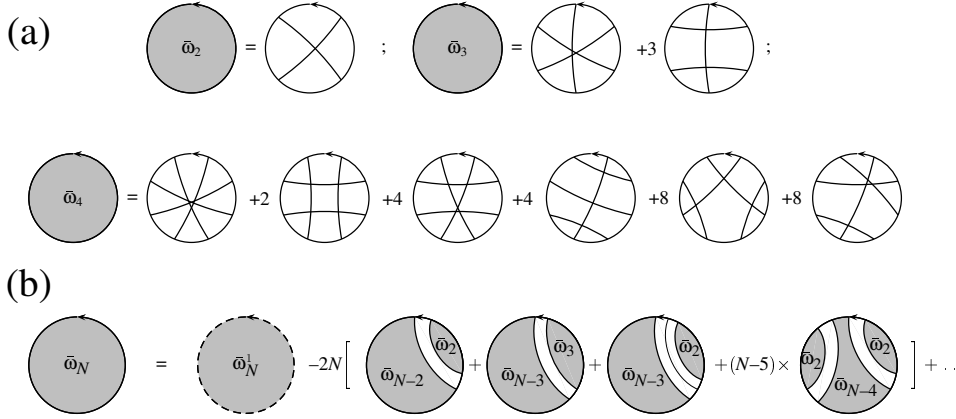


Figure 2.2: (a) Non-degenerate chord diagrams of the lowest order. (b) Graphical representation of Eq. (2.11) that shows the relation between the non-degenerate chord diagrams and degenerate CD that do not contain an isolated chord of length 1.

*Chord diagrams* are well studied combinatorics objects [29] possessing an additional algebraic structure — graded co- and commutative Hopf algebra which is dual to the algebra of Vassiliev knot invariants [30, 31]. A *chord diagram* is defined as  $2N$  points on a circle labeled  $1, 2, \dots, 2N$  and joined in a pairwise fashion by  $N$  chords. The number of such objects is given by  $\lambda_N = (2N - 1)!!$ . Similarly, one can compute the number of CD containing  $k$  strands with  $2N$  vertices

$$\lambda_{N,k} = \binom{2N+k-1}{2N} (2N-1)!! \quad (2.8)$$

The CD is called *degenerate* if it has at least one isolated chord, i. e. one not crossed by any other. The number of these objects is  $\omega_N$ . By  $\bar{\omega}_N$  we denote the corresponding count of non-degenerate CD (the first few of these objects are depicted in Fig. 2.2 (a)). It is remarkable that their number yields exactly the counting of the Feynman diagrams for the electron propagator  $\bar{\omega}_N = y_{N-1}$  allowing to obtain an asymptotic formulas for all generating functions in (2.4). The number of degenerate CDs that do not contain an isolated chord of length 1 is given by an explicit formula [32]:

$$\bar{\omega}_N^1 = \sum_{k=0}^N (-1)^k (\lambda_{N-k,k+1} + \lambda_{N-k,k}). \quad (2.9)$$

Using the asymptotic expression for  $\frac{\bar{\omega}_N^1}{\lambda_N}$ :

$$\frac{\bar{\omega}_N^1}{\lambda_N} = \frac{1}{e} \left[ 1 - \frac{3}{4N} - \frac{7}{32N^2} + \dots \right] \quad (N \rightarrow \infty). \quad (2.10)$$

and a diagrammatic relation (Fig. 2.2 (b)) between the number of degenerate CDs that do not contain an isolated chord of length 1 the number of non-degenerate CDs:

$$\bar{\omega}_N = \bar{\omega}_N^1 - 2N [\bar{\omega}_{N-2} + 5\bar{\omega}_{N-3} + (N-5)\bar{\omega}_{N-4}] + \dots, \quad (2.11)$$

we obtain:

$$\frac{\bar{\omega}_N}{\lambda_N} = \frac{1}{e} \left[ 1 - \frac{5}{4N} - \frac{63}{32N^2} + \dots \right] \quad (N \rightarrow \infty) \quad (2.12)$$

This allows us to obtain the large- $n$  behavior of the number of the Feynman diagrams of all quantities related by the Hedin equations, see Tab. 2.1.

Table 2.1: Asymptotic expansion for the Feynman diagrams counting.

Generating function	Asymptotic $\times \frac{(2n+1)!!}{e}$
$G$	$1 - \frac{5}{4n} - \frac{23}{32n^2} - o(n^{-2})$
$\Sigma, \chi$	$2n \left[ 1 - \frac{5}{4n} - \frac{23}{32n^2} - o(n^{-2}) \right]$
$\Gamma$	$2(n-1) \left[ 1 - \frac{7}{4n} - \frac{27}{32n^2} - o(n^{-2}) \right]$

### 2.3 Dealing with singularities

Introduction of the Green's function methods in the electronic structure calculations is the most striking achievement of the field-theoretic methods on par with the density functional theory having immediate technological applications [22]. Even in the lowest (beyond the mean field) order one obtains significant improvements of e. g. the band gap through the correlational shifts ( $\Delta$ ). Including higher-order diagrams (vertex correction) is numerically demanding and generates *asymptotic series*. Despite non-convergence, the asymptotic expansion is useful when truncated to a finite number of terms. This is the reason for popularity of first-order methods such as  $GW$  approximation in condensed matter, molecular and atomic physics. Emerging implementation of the higher-order (vertex correction) approximations for realistic systems are plagued with numerical difficulties such that systematic investigation of the convergence is not possible. Here I demonstrate that Hamiltonian describing a core electron coupled to a single plasmonic excitation not only leads to exactly solvable model, but also allows to realize a solution purely diagrammatically.

*Model specification and known results* The model originates in the work of Lundqvist [33] who considered coupling of the deep hole to plasmonic excitations in metals. Similar to the coupling to particle-hole excitations giving rise to the singularities in x-ray absorption and emission spectra [19, 34–37] the model permits the analytic solution [38, 39].

The Hamiltonian of the Lundqvist  $S$ -model in its simplest form reads:

$$\hat{H} = \epsilon \hat{c}^\dagger \hat{c} + \hat{c} \hat{c}^\dagger \gamma (\hat{a} + \hat{a}^\dagger) + \Omega \hat{a}^\dagger \hat{a}, \quad (2.13)$$

where  $\hat{c}$  is the creation operator of the deep hole with energy  $\epsilon$ ,  $\hat{a}^\dagger$  is the bosonic creation operator of the plasmon with the energy  $\Omega$ .

The Hamiltonian (2.13) is quite versatile and is applicable to other scenarios such as resonant-tunneling through a single level coupled to wide-band phonons [40]. Remarkably, also the two particle Green's function can be found analytically [41], the model can be solved at finite temperatures, and its non-equilibrium properties have also been studied thoroughly [42, 43]. I will return to this model in a more general setup in the next section where a realistic plasmon dispersion in 3d homogeneous electron gas will be considered.

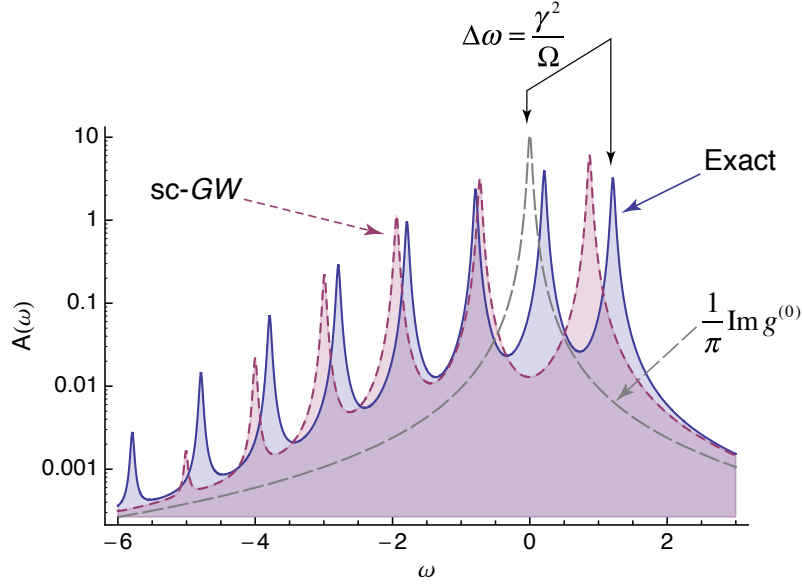


Figure 2.3: (Color online) Spectral function at different levels of theory: exact (full line), self-consistent first-order (short dashes), zeroth iteration (long dashes).

We define the following Green's function

$$g(t - t') = -i \langle \psi | T \{ \hat{c}(t) \hat{c}^\dagger(t') \} | \psi \rangle,$$

where  $|\psi\rangle$  is the exact ground state of the *no-hole system*. By writing the cumulant expansion for the Green's function

$$g(t) = g^{(0)}(t) e^{C(t)}$$

and observing that only a single diagram contributes to the *cumulant function* resulting in

$$C(t) = - \left( \frac{\gamma}{\Omega} \right)^2 (1 + i\Omega t - e^{i\Omega t}). \quad (2.14)$$

one obtains the well known spectral function

$$A(\omega) = \sum_{n=0}^{\infty} \frac{\left( \frac{\gamma}{\Omega} \right)^{2n}}{n!} \frac{\exp \left[ - \left( \frac{\gamma}{\Omega} \right)^2 \right]}{\omega - \epsilon - \left( \frac{\gamma}{\Omega} \right)^2 \Omega + n\Omega - i\eta}. \quad (2.15)$$

It is depicted at Fig. 2.3 together with the zeroth order and spectral function from the self-consistent *GW* calculation (*sc-GW*). The results are plotted for a strongly correlated regime ( $\gamma > \Omega$ ) and can be characterized as follows: (i) The spectral function consist of a main peak shifted by the energy of  $\Delta\omega = \frac{\gamma^2}{\Omega}$  compared to the noninteracting case; (ii) the quasiparticle peak is followed by the ladder of plasmonic satellites; (iii) the self-consistent *GW* method predicts the satellites, however, the position even of the main peak is wrong. This inaccuracy is the main motivation for performing higher-order diagrammatic calculations.

*Diagrammatic properties* The ground state is a no-hole state. Therefore,  $c^\dagger|\psi\rangle$  vanishes and the non-interacting time-ordered Green's function only consists of the hole propagator:

$$g^{(0)}(t - t') = i\theta(t' - t)e^{-i\epsilon(t-t')},$$



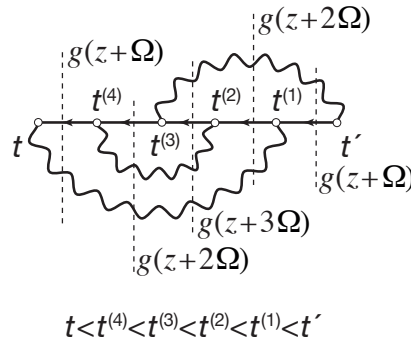
This fact simplifies diagrams considerably: (i) in the expansion for the Green's function ( $g$ ) and the self-energy ( $\Sigma$ ) all intermediate points are time-ordered (Fig. 2.4); (ii) diagrams containing loops necessarily yield a zero contribution. These properties allow to write the self-energy for this model explicitly. Because there is no spatial degrees of freedom, the problem is similar to that of the Feynman diagrams enumeration considered in the previous section. Here, we present an analytic solution of a more complicated one-dimensional case, i. e. we treat the time argument explicitly.

Let  $\Sigma^{(n,\alpha)}(\omega)$  be an  $n$ th-order self-energy term corresponding to a particular diagram which will be denoted as  $\alpha$ . We will prove below that the corresponding expression in the frequency representation is given by the product of the Green's functions:

$$\Sigma^{(n,\alpha)}[g; \omega] = (\gamma^2)^n \prod_{i=1}^{2n-1} g(\omega + k_i^{(n,\alpha)} \Omega), \quad (2.16)$$

where the integer number of absorbed plasmons in each fermionic line ( $k_i^{(n,\alpha)}$ ) is computed as a number of bosonic lines crossing each vertical line (Fig. 2.4).  $2n - 1$  vertical lines are positioned such that they cut each fermionic line. This equation can be derived by using the nonequilibrium Green's function formalism (more on that in chapter 4). Let a vertical line separate times lying on the forward and backward branches of the Keldysh contour in a expression for the *lesser* self-energy ( $\Sigma^<$ ). Consider, for instance, a third vertical line at Fig. 2.4. It contributes  $g^<(z - y_1 - y_2 - y_3)W^<(y_1)W^<(y_2)W^<(y_3)$  to  $\Sigma^<$ . Here,  $W^<(y) = \gamma^2 \delta(y + \Omega)$  is the lesser bosonic propagator. Performing three frequency integrals (over  $y_1, y_2, y_3$ ) we obtain a contribution proportional to  $g^<(z + 3\Omega)$ . Similar considerations can be repeated for each vertical line and fermionic propagator yielding in total  $2n - 1$  terms for each  $n$ th-order self-energy diagram  $\Sigma^<(z) = \sum_{i=1}^{2n-1} f_i(z)g^<(z + k_i\Omega)$ . Now, since  $f_i(z)$  are non-singular the generic expression for the time-ordered self-energy (2.16) is obtained.

Expansion (2.16) is a new exact result for the  $S$ -model which also permits generalizations for more general scenarios, e. g., interaction with phonons [44]. Electronic spectra of numerous realistic materials have been rationalized in terms of the time-ordered [45–48] or retarded [49] cumulant expansions which, we see above, are exact for the considered model. The presence of multiple plasmonic satellites is a marked feature of these materials. The plasmon dispersion is the only modification needed for generalization to this case. It



$$\Sigma(z) = (\gamma^2)^3 g(z + \Omega)g(z + 2\Omega)g(z + 3\Omega)g(z + 2\Omega)g(z + \Omega)$$

Figure 2.4: Example of the self-energy in time domain. The system only contains holes. Therefore there is only one possible time-ordering as shown below the diagram. Bosonic propagators are denoted as wavy-lines. In view of the time-ordering for fermionic lines, only the negative time part of the bosonic propagator is used. It means that in the frequency space one needs to take into account only the  $\delta(\omega + \Omega)$  part of its spectral function.

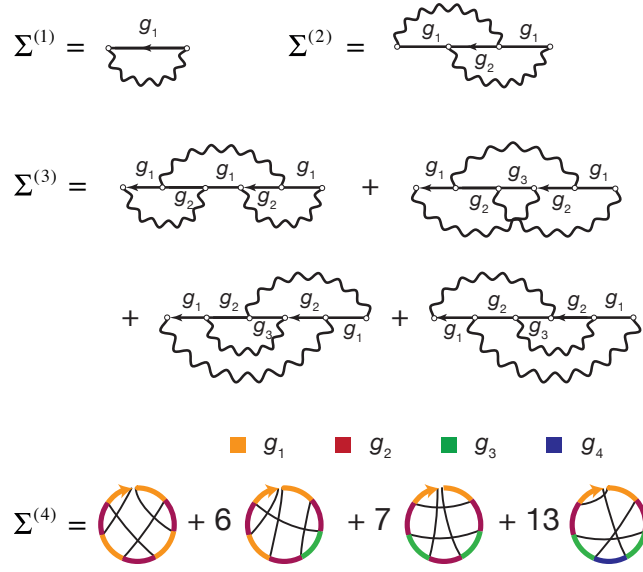


Figure 2.5: Four lowest orders of the diagrammatic expansion of the self-energy for the  $S$ -model in frequency space. Notice that two diagrams of the third-order containing loops are not shown because they are equal to zero. The fourth-order self-energy is given in terms of chord diagrams with color-coding. Only one representative for each class is shown. Due to the absence of loops an isomorphism between the Feynman diagrams and the chord diagrams can be established.

amounts to introducing additional sums over the plasmonic moment at each vertex, but does not change the diagrammatic structure.

Eq. (2.16) serves as the starting point for numerics; complexity goes into the generation of Feynman diagrams and determination of the coefficients  $k_i^{(n,\alpha)}$ . This is second important ingredient of our approach. By iterating the variational equations using MATHEMATICA computer algebra system we obtain diagrams shown at Fig. 2.5. The chord diagram representation is natural in this case because according to the analysis above the fermionic loops yield zero contribution. In order to further facilitate the interpretation of the graphs in frequency space we use a color coding for the coefficients  $k_i^{(n,\alpha)}$  entering the Green's function arguments. The graphs were generated by our symbolic algorithm in MATHEMATICA computer algebra system. Conversion from the time to frequency domains is likewise performed using a symbolic algorithm. The self-energy accurate to the sixth order comprises 1, 1, 4, 27, 248, and 2830 diagrams of the first to sixth orders, respectively, and has the following algebraic representation:

$$\begin{aligned}
 \Sigma = & \alpha g_1 + \alpha^2 g_2 g_1^2 + \alpha^3 (g_2^2 g_1^3 + 3g_2^2 g_3 g_1^2) \\
 & + \alpha^4 (g_2^3 g_1^4 + 6g_2^3 g_3 g_1^3 + 7g_2^3 g_3^2 g_1^2 + 13g_2^2 g_3^2 g_4 g_1^2) \\
 & + \alpha^5 (g_2^4 g_1^5 + 9g_2^4 g_3 g_1^4 + 23g_2^4 g_3^2 g_1^3 + 26g_2^3 g_3^2 g_4 g_1^3 \\
 & + 15g_2^4 g_3^3 g_1^2 + 58g_2^3 g_3^3 g_4 g_1^2 + 45g_2^2 g_3^3 g_4^2 g_1^2 + 71g_2^2 g_3^2 g_4^2 g_5 g_1^2) \\
 & + \alpha^6 (g_1^6 g_2^5 + 12g_1^5 g_2^5 g_3 + 48g_1^4 g_2^5 g_3^2 + 72g_1^3 g_2^5 g_3^3 \\
 & + 31g_1^2 g_2^5 g_3^4 + 39g_1^4 g_2^4 g_3^2 g_4 + 194g_1^3 g_2^4 g_3^3 g_4 + 183g_1^2 g_2^4 g_3^4 g_4 \\
 & + 90g_1^3 g_2^3 g_3^3 g_4^2 + 313g_1^2 g_2^3 g_3^4 g_4^2 + 145g_1^2 g_2^2 g_3^4 g_4^3 \\
 & + 142g_1^3 g_2^3 g_3^2 g_4^2 g_5 + 310g_1^2 g_2^3 g_3^3 g_4^2 g_5 + 470g_1^2 g_2^2 g_3^3 g_4^3 g_5 \\
 & + 319g_1^2 g_2^2 g_3^2 g_4^3 g_5^2 + 461g_1^2 g_2^2 g_3^2 g_4^2 g_5^2 g_6) + \mathcal{O}(\alpha^7), \tag{2.17}
 \end{aligned}$$

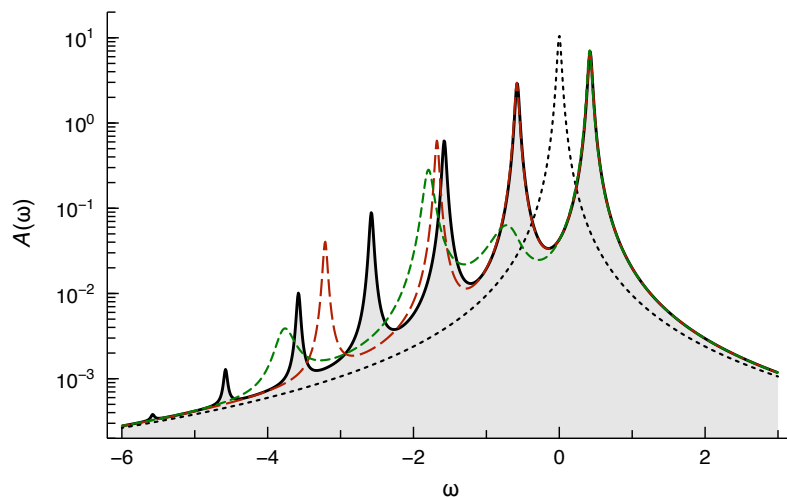


Figure 2.6: Spectral function of the  $S$ -model at different levels of theory: exact (full line), self-consistent third-order (short dashed), sixth-order (long dashed), zeroth iteration (dotted) for the following values of parameters:  $\epsilon = 0$ ,  $\Omega = 1$ ,  $\gamma = 0.65$ ,  $\eta = 0.03$ .

where  $g_k \equiv g(\omega + k\Omega)$ . Setting all  $g_k \equiv 1$  we obtain a generating function for the enumeration of all chord diagrams (cf. Eq. (2.6) and set  $\ell = 1$  there):

$$y(\alpha) = \alpha + \alpha^2 + 4\alpha^3 + 27\alpha^4 + 248\alpha^5 + 2830\alpha^6 + \mathcal{O}(\alpha^7).$$

Our explicit form for the self-energy dictates that the singularities of  $\Sigma$  should be located exactly at the Green's function poles. Physically it is wrong as it is well known that the self-energy poles lie between the poles of the corresponding exact Green's function [50]. These two facts can be reconciled noticing that already starting with the second order

$$\Sigma^{(2)}(\omega) = (\gamma^2)^2 g(\omega + \Omega)g(\omega + 2\Omega)g(\omega + \Omega)$$

the self-energy contains *higher-order* poles in the frequency domain. They are responsible for the shift of quasiparticle energies.

*Self-consistent calculation* Assume that in the course of a self-consistent calculation an approximation for the Green's function,  $g^{(i)}(\omega)$ , has been obtained. Using the diagrammatic expansion viz. Eq. (2.17) we compute an approximation to the self-energy  $\Sigma[g^{(i)}](\omega^*)$  at a chosen frequency point. The point  $\omega^*$  should belong to the domain where the perturbative expansion converges. In order to obtain the self-energy in the vicinity of Green's function poles where the series diverge we perform the Padé approximation  $\Sigma[g^{(i)}](\omega^*) \rightarrow \tilde{\Sigma}^{(i)}(\omega)$  and use the new self-energy in order to update the Green's function according to the Dyson equation

$$g^{(i+1)}(\omega) = \frac{1}{\omega - \epsilon - \tilde{\Sigma}^{(i)}(\omega)}. \quad (2.18)$$

Iterations are started from the noninteracting Green's function  $g^{(0)}(\omega) = (\omega - \epsilon - i\eta)^{-1}$  and typically converge within some tens of cycles. The quality of the resulting spectral function strongly depends on the order of perturbative expansions and on the strength of the electron-plasmon scattering  $\gamma$ . For weakly correlated regime  $\gamma \simeq 0.1\Omega$  already the  $GW$  approximation faithfully reproduces the exact spectral function. This approximation

ceases to be valid in the *correlated regime* as Fig. 2.3 demonstrates. The energy of the main quasiparticle peak is the major discrepancy. However, for  $\gamma = 0.65$  already third-order treatment yields very good results for its energy and strength (Fig. 2.6, short dashed line). The first satellite, which has a rather large contribution to the density of states at this value of  $\gamma$  (notice logarithmic scale), represents a substantially more complicated feature. It can only be captured with the self-energy accurate to the 6th order (long dashed line). However, even 3111 diagrams are not sufficient to reproduce the second-order satellite. With the help of more optimized algorithms we may extend the calculations to higher orders in order to predict position of even more satellites. However, any symbolic algorithm based on the Hedin's equations (2.1) will eventually hit the wall as the number of diagrams grows super-exponentially (Tab. 2.1).

In summary, it is more than computational complexity that prevents applications of many-body perturbation theory beyond the leading order. Resulting asymptotic series lead to Green's functions with incorrect physical properties: non-positive densities, higher-order poles already for the second order. Some of these aspects will be re-iterated and studied in details in subsequent chapters. Here, we proposed to use the Padé approximation to regularize the electron self-energy. With the help of nonequilibrium Green's function theory the self-energy of the  $S$ -model was derived explicitly and a connection of its diagrammatic expansion to a certain class of chord diagrams was demonstrated. Our symbolic algorithm generates analytical expressions up to the sixth order in the electron-plasmon interaction. For  $\omega^* \gg \frac{\gamma^2}{\Omega}$  the series converge rapidly, however, there are no interesting spectral features in this domain. Therefore, to recursively update the Green's function in the whole spectral range the self-energy is regularized before plugging it in into the Dyson equation. In this way, even in the correlated regime ( $\gamma = 0.65\Omega$ ) our approach allows to accurately describe the quasiparticle peak and the first-order satellite. Hence, for realistic electronic structure calculations and self-consistent methods the Padé approximation is unavoidable.

## 2.4 Time-evolution of excitations in normal Fermi liquids

In the previous section we considered a very simplified model describing the coupling of the electronic and bosonic degrees of freedom. The cumulant expansion (2.14) gives an exact solution in this case. I will demonstrate now that the method is beneficial for other scenarios as well. The approach gained its wide recognition after Nozières and de Dominicis [36] proposed an exact solution of a complex integral equation for the cumulant function  $C(k, t)$  for the Fermi edge singularity model. Other numerous results are summarized in [2].

### Fluctuation potential and the $GW$ approximation

Typically the method is applied to systems which allow for a distinct separation of the Hamiltonian into the parts allowing for the analytical treatment and a coupling that needs to be treated perturbatively. Consider a generalization of the  $S$ -model (2.13) — the electron-boson Hamiltonian with dispersion

$$\hat{H} = \sum_k \epsilon_k \hat{c}_k^\dagger \hat{c}_k + \sum_q \omega_q \hat{a}_q^\dagger \hat{a}_q + \sum_{k,k'} \sum_q \mathcal{V}_{k,k'}^q (\hat{a}_q^\dagger + \hat{a}_q) \hat{c}_k^\dagger \hat{c}_{k'}. \quad (2.19)$$

Here  $\omega_q$  describes the energies of bosonic excitations,  $\epsilon_k = k^2/2$  is the usual particle dispersion in a weakly interacting Fermi liquid, and  $\mathcal{V}_{k,k'}^q$  is the fluctuation potential [51]

with matrix elements:

$$\mathcal{V}_{\mathbf{k},\mathbf{k}'}^q = \frac{4\pi}{|\mathbf{k} - \mathbf{k}'|^2} \rho_{\mathbf{k}-\mathbf{k}'}^q, \quad (2.20)$$

where  $\rho_{\mathbf{k}}^q$  are the matrix elements of fluctuation density. The choice of the interaction form is not arbitrary: it guarantees that the lowest order diagram for  $\mathcal{G}(k, t)$  in the model (2.19) corresponds to the *GW* approximation for the initial fermionic system:

$$\Sigma(k, t) = i \int \frac{d\mathbf{q}}{(2\pi)^3} \mathcal{W}(\mathbf{q} - \mathbf{k}, t + \delta) \mathcal{G}^0(\mathbf{q}, t), \quad \delta \rightarrow +0, \quad (2.21)$$

with the screened Coulomb interaction given by:

$$\mathcal{W}(k, \omega) = v(k) + v^2(k) \chi(k, \omega) = v(k) + \sum_q \frac{2\omega_q |V_k^q|^2}{\omega^2 - \omega_q^2}, \quad (2.22)$$

where  $v(k) = 4\pi/k^2$  is the Coulomb potential,  $V_k^q \equiv \mathcal{V}_{\mathbf{k}'+\mathbf{k},\mathbf{k}'}^q$  and  $\chi(k, \omega)$  is the full bosonic propagator or the *density-density response function* in this particular case. The latter is related by the *fluctuation-dissipation theorem* to the *dynamical structure factor*:

$$S(k, \omega) = -\frac{1}{\pi} \text{Im} \chi(k, \omega),$$

and the *static structure factor* is defined as

$$S(k) = \frac{1}{n} \int_0^\infty d\omega S(k, \omega). \quad (2.23)$$

The cumulant function  $C(k, t)$  can be written very accurately in terms of the dynamical structure factor  $S(k, \omega)$ :

$$C(k, t) = - \sum_q v^2(q) \int_0^\infty d\omega S(q, \omega) f(\epsilon_{|\mathbf{k}|} - \epsilon_{|\mathbf{k}+\mathbf{q}|} - \omega, t), \quad (2.24)$$

where  $f(v)$  is defined as:

$$f(v) \equiv \int_0^t d\tau \int_0^\tau d\tau' e^{iv(\tau-\tau')} = \frac{1 + ivt - e^{ivt}}{v^2}. \quad (2.25)$$

The central quantity of this study — the dynamical structure factor — although expressed almost identically in the many-body perturbation and in the cumulant expansion theories, originates from different approximations. In the former case it is the vertex function in the expression for the self-energy that is neglected, while for the latter it is assumed that the Hamiltonian can be written in the electron-boson form (2.19). Under some circumstances the model (2.19) is exact: typically this is the case when certain matrix elements of the Coulomb interactions between a test particle (such as a deep core hole [38] or a high-energy photoelectron [51]) are vanishingly small. For a more general scenario, such as considered here, the accurateness of (2.19) is less obvious [47, 52, 53]. In view of this fact it is interesting to consider the connections with other theories. Parallels between the cumulant expansion and the many-body perturbation theories (MBPT) in terms of the electron self-energy were explored by Aryasetiawan *et al.* [45], Kas *et al.* [49].

### Short time limit

As a first application we compute the leading expansion coefficients<sup>4</sup> of the cumulant function in the short-time limit:

$$C(k, t) = -\frac{\sigma^2(k)}{2!}t^2 + \frac{c_3(k)}{3!}t^3 + \dots \quad (2.26)$$

The prefactor of the quadratic decay (Eq. (3.23)) can be computed by evaluating the second derivative of (2.24) at  $t = 0$ :

$$\sigma^2 = n \sum_q v^2(q) S(q). \quad (2.27)$$

It follows then that  $\sigma^2$  is independent of  $k$  and coincides with the local contribution to the zeroth spectral moment of the electron self-energy obtained by Vogt *et al.* [54]. The long wave-length expression in Eq. (2.23) follows from the exactness of the random phase approximation (RPA) in this limit.

It is not obvious from the outset that the  $c_3(k)$  coefficient should take a finite value: this heavily relies on the exact form of the structure factor in the asymptotic ( $q \rightarrow \infty$ ) limit. By using the  $f$ -sum rule:

$$\int_0^\infty d\omega \omega S(q, \omega) = n\epsilon_q, \quad (2.28)$$

where  $n$  is the electron density we obtain:

$$c_3(k) = -in \sum_q v^2(q) [(\epsilon_{|k|} - \epsilon_{|k+q|}) S(q) + \epsilon_q]. \quad (2.29)$$

In the simplest case of a hole state at the band's bottom the convergence of the integral regardless of the system's dimension ( $z$ ) is guaranteed by the limit

$$\lim_{q \rightarrow \infty} q^{z+1} [S(q) - 1] = -\pi 2^z n g(0), \quad (2.30)$$

where  $g(0)$  is the value of the pair correlation function for two electron at the same position and  $z$  is the dimensionality of a system. For  $k > 0$  the term linear in  $k$  vanishes after the angular integration and we finally obtain the  $k$ -independent result:

$$c_3 = in \sum_q v^2(q) \epsilon_q [S(q) - 1]. \quad (2.31)$$

Finally we notice that the leading terms of Eq. (2.24) in the long time-limit are the constant and the linear ones, i. e.,  $C(k, t) \xrightarrow{t \rightarrow \infty} \gamma - i \Sigma(k, \epsilon_k) t$  as expected from the exponential quasiparticle decay.

In the  $t \rightarrow 0$  case, the non-analytic terms originate from the coupling to the particle-hole ( $p$ - $h$ ) continuum. We can split the momentum integration into a finite interval  $q < q_c$  yielding just the well-behaved analytic part of  $C(k, t)$  and the interval extending to infinity. The value of  $q_c$  can always be chosen large enough so that the real part of the dielectric function on the second interval approaches unity. This considerably simplifies the dynamical structure factor which results now from the imaginary part of the Lindhard formula:

---

<sup>4</sup>Such expansion does not imply analyticity of the function in vicinity of  $t = 0$ . Just the opposite, higher expansion coefficients diverge starting from  $c_6$  in 2d case and from  $c_7$  in 3d based on very general properties of the density-density response function ( $\text{Im } \chi(k, \omega) \sim \omega^{-4-d/2}$  [1]).

$$S(q, \omega) = \frac{1}{\pi} \frac{1}{v(q)} \frac{\alpha r_s}{\tilde{q}^3} \left( 1 - \frac{1}{4} \left( \tilde{q} - \frac{\tilde{\omega}}{\tilde{q}} \right)^2 \right),$$

where the tilde denotes the use of rescaled quantities, i. e.  $q = \tilde{q}k_F$ ,  $\omega = \tilde{\omega}\epsilon_F$ .

For small momenta the computation can be performed explicitly yielding the leading term:

$$C(0, t) = -\frac{8}{45} (\alpha r_s)^2 \left( \frac{2it}{\pi} \right)^{5/2}. \quad (2.32)$$

Such time-dependence is easy to reconcile with well known asymptotic behavior of the electron self-energy as a function of frequency [54, 55]:

$$\text{Im } \tilde{\Sigma}(k, \tilde{\omega}) \xrightarrow{\omega \rightarrow \infty} = -\mathcal{O}(\omega^{-3/2}).$$

To see the connection we express asymptotically the spectral function as  $A(k, \omega) \sim C/\omega^{2+3/2}$  and perform the Fourier transform. Since at  $\omega \rightarrow -\infty$  the spectral function decays faster it is sufficient to perform the transform on a semi-bounded interval:

$$A(k, t) \sim \int_{\omega_c}^{\infty} \frac{d\omega}{2\pi} \frac{C}{\omega^{7/2}} e^{-i\omega t}.$$

Among several resulting terms one has to pick up the one independent of the cut-off  $\omega_c$ . It exhibits the same time-dependence and the density scaling  $\sim (\alpha r_s)^2$  as Eq. (2.32).

To summarize, Eqs. (2.27, 2.29, 2.31) provide analytic expressions for the coefficients of the holonomic part of the electron spectral function at short times. The leading term of the nonholonomic part is given by Eq. (2.32). To study the opposite limit it is convenient to work in the frequency representation.

## Quasiparticle decay and Paley-Wiener theorem

It is commonly believed that HEG in two or three dimensions serves as a perfect illustration of the Fermi liquid concept [1], that is a many-body fermionic systems with long-lived excitations: *quasiparticles*. Two marked properties distinguish them from other excited states: i) they can be brought in a direct correspondence with real particles (electrons) of a fictitious non-interacting many-body system; ii) they are characterized by the life-time, which tends to infinity as the particle's energy approaches the Fermi level ( $\epsilon_F$ ). It also implies that asymptotically the decay is exponential  $\exp(-\gamma t)$ , with the decay constant being quadratically dependent on the energy ( $\gamma(\epsilon) \sim \epsilon^2/\epsilon_F$ ). At  $\epsilon \rightarrow \epsilon_F$  this constant can be computed perturbatively, and it is sufficient to consider the lowest-order term giving a non-vanishing imaginary part of the self-energy. In view of this it is intriguing that a rigorous proof can be given that the lowest-order diagram yield the spectral function inconsistent with the asymptotic exponential decay.

To do so we recall that pronounced features in the spectral function appear at energies  $E_k$  that are approximately given by  $E_k = \epsilon_k + \Sigma(k, E_k)$ , where  $\text{Im } \Sigma(k, \omega) \sim \delta(\omega - \epsilon_{|\mathbf{k}+\mathbf{q}|} \pm \omega_q)$ . These resonances are surrounded by the incoherent background which has the same extent as the self-energy:

$$A(k, \omega) = \frac{1}{\pi} |\text{Im } \mathcal{G}(k, \omega)| = \frac{1}{\pi} \frac{|\text{Im } \Sigma(k, \omega)|}{|\omega - \epsilon_k - \text{Re } \Sigma(k, \omega)|^2 + |\text{Im } \Sigma(k, \omega)|^2}. \quad (2.33)$$

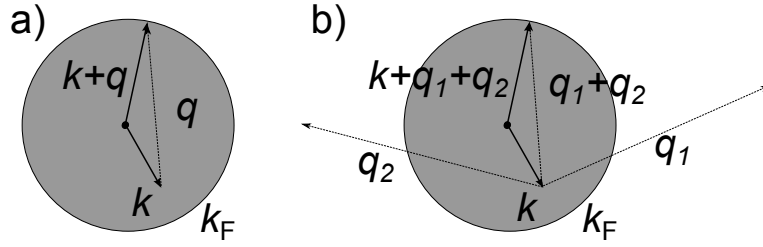


Figure 2.7: a) First and b) second order hole scattering mechanisms. While the two excitations in b) carry in total the same momentum as a single excitation in a) the energy transfer is much larger.

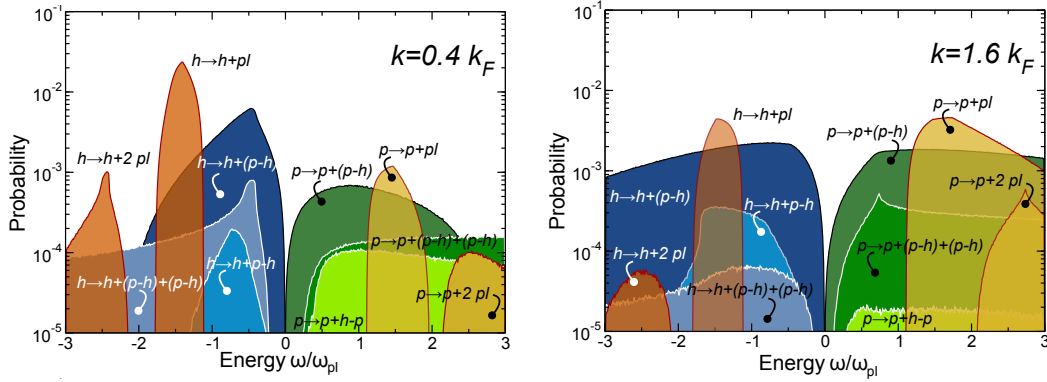


Figure 2.8: Monte-Carlo calculation for 3d HEG at  $r_s = 5$  density of the first and second order self-energy diagrams. The Fermi energy is set to zero.

In the lowest order of the screened interaction a particle can only loose its energy ( $\epsilon_k$ ) by generating a *single* bosonic excitation  $\omega_q$ . Since only a finite momentum can be transferred also  $\omega_q$  is finite and, thus, the self-energy has a semi-bounded support (limited from below) (Fig. 2.7). From this, in view of (2.33) follows  $A(k, \omega) = 0$  for  $\omega < \omega^*(k)$ .

According to the Paley-Wiener theorem [56] the Fourier transform of  $A(k, \omega)$  behaves as  $A(k, t) \xrightarrow{t \rightarrow \infty} \exp(-Bt^\alpha)$  ( $0 < \alpha < 1$ ) for large times: a result in a clear contradiction with the Fermi liquid theory. Quasiparticle calculations of the two-dimensional surface bands by Gumhalter [57] give an example of realistic spectral function (in the frequency domain) and survival probability (in the time domain) in this approximation.

The paradox is resolved by considering the second-order self-energy  $\Sigma[\mathcal{G}^0, \mathcal{W}^0]$ :

$$\Sigma^{(2)}(1, 2) = i^2 \iint \mathcal{W}^0(1^+, 4) \mathcal{G}^0(1, 3) \mathcal{G}^0(3, 4) \mathcal{G}^0(4, 2) \mathcal{W}^0(3^+, 2) d(34). \quad (2.34)$$

Our representation of the screened Coulomb interaction allows to compute the electronic self-energy relatively easy using the MATHEMATICA computer algebra system. The remaining momentum integrals are performed using the Monte-Carlo approach (Fig. 2.8).

In agreement with our simple argument we see that the phase-space for the first order processes is limited. The same is observed in the simplest second order process (it includes also contribution from two bare interaction lines) in view of the same arguments. The existence of a critical upper momentum for the plasmons also restricts the phase-space available for the  $h \rightarrow h + 2pl$  scattering. The situation is completely different for the  $h \rightarrow h + (p-h) + (p-h)$  events: even though the hole can only loose a finite momentum the shares of each excitation can be large (Fig 2.7b), resulting in an arbitrarily large energy transfer. Hence, the



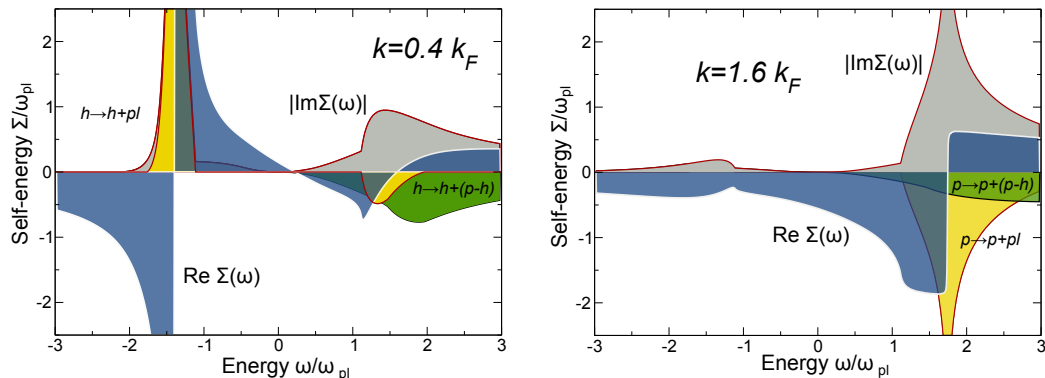


Figure 2.9: Exact first order self-energy of the 3d HEG at  $r_s = 5$  density. The Fermi energy is set to zero. The real part is shown without including the static (exchange) part. The values are  $e_x = -1.490\omega_p$  and  $e_x = -0.225\omega_p$  for  $k = 0.4k_F$  and  $k = 1.6k_F$ , respectively. The plasmon energy in the long wave-length limit is  $\omega_p = 2.103\epsilon_F$ .

self-energy has an unbounded support, the Paley-Wiener theorem cannot be applied and the Fermi liquid behavior is restored in the second order.

Our analysis is also important for practical calculations since it allows to determine *a priori* where a certain diagram might contribute. It is interesting to notice a sequence of plasmonic peaks in the sea of  $p$ - $h$  excitations. By expanding the cumulant function  $C(k, t) \sim e^{i\omega_p t}$  and computing the Fourier transform one sees that their weight decays as  $e^{-a} a^n / n!$ . Therefore, plasmons will only be important at low orders whereas the tails of the spectral functions are shaped by the  $p$ - $h$  scattering mechanisms which lead to the power-law decay. Where such a crossover occurs depends, of course, on the specific system parameters.

The phase-space arguments provide a partial account of the problem. The inclusion of matrix elements can modify the self-energy substantially as the comparison of Fig. 2.8 and Fig. 2.9 shows. This can be best seen at the Fermi level (set to zero in our calculations). While both methods lead to a vanishing self-energy in this limit, the way how it approaches zero is rather different. Realistic calculations of next order diagrams are also feasible as will be demonstrated in Chapter 4.

To summarize, in this section we studied the electron spectral function in the frequency space by considering the diagrammatic expansion of the self-energy up to the second order in the screened Coulomb interaction. We have shown on the basis of the Paley-Wiener theorem that in the first order, as implemented in typical one-shot  $G^0W^0$  calculations, the quasiparticle decay at long times must deviate from exponential. On the other hand, the inclusion of the second order terms leads to a spectral function different from zero on the whole frequency axis. This is consistent with the exponential decay postulated by the Landau theory of the Fermi liquids.



## 3 Exact propagators from quantum chemistry

---

Working with dressed correlation-functions is a great possibility of many-body perturbation theory. It is very easy, for example, to find the screened Coulomb interaction for a homogeneous system: in the random phase approximation the integral equation for the polarization function, if recasted in the momentum space, turns into the algebraic one. For inhomogeneous periodic systems the idea is still fruitful, but not free from numerical complications: while for the electron Green's function (and the self-energy) it is sufficient to know its representation  $G(\mathbf{k}, \omega)$  in the first Brillouin zone, the polarization propagator must be known at all values of the momentum transfer, i. e.  $\chi_{\mathbf{G}, \mathbf{G}'}(\mathbf{q}, \omega)$ . Here  $\mathbf{G}$  and  $\mathbf{G}'$  are reciprocal lattice vectors, and  $\mathbf{k}$  and  $\mathbf{q}$  belong to the first Brillouin zone. This is due to the fact that for the calculation of the self-energy the integration over the whole momentum space is performed requiring the knowledge of the screened interaction at all momenta [22].

The problem aggravates in the case of finite systems. There, the supercell calculations are still possible, but seem to be an overshoot as the periodicity is lost. The methods of quantum chemistry provide a more convenient way to evaluate the screening in molecules and clusters. The idea is based on the exact Lehmann representation of the particle-hole propagator. Its constituents, the excited states and the transition matrix elements are readily computed using methods derived either from the configuration interaction (CI) or the equation of motion coupled-cluster (EOM-CC) approaches. For them the whole ladder of approximations, ranging from the virtually exact full CI to the simplest configuration interaction singles (CIS) is known. They are very controllable in terms of the accuracy and performance. Excited states can also be obtained from the time-dependent density functional theory which makes the approach suitable for the treatment of correlated solids [58, 59].

The following sections present the material in logical, but not exactly chronological order: the theory and the computational method is first applied to small systems that permit exact diagonalization study [3] (Sec. 3.2), then the method is pushed to its computational limits: the decay of hybridized electronic states of a Na cluster on the Cu(001) surface [4] (Sec. 3.3) and superatomic molecular orbitals of the  $C_{60}$  molecule: peculiar long-lived electronic states in fullerenes [5] (Sec. 3.4). In both cases, it considerably enhances the efficiency of the conventional  $GW$  approach and shows the feasibility of a high-level correlated calculation for large systems without periodicity.

### 3.1 Fluctuation-dissipation theorem

If a system obeys the detailed balance condition and in an equilibrium it responses to a small perturbation in the same way as it does to a spontaneous fluctuation *the fluctuation-dissipation theorem* can be proven. Consider a quantum system at zero temperature and two operators  $\hat{A}$  (the observable) and  $\hat{B}$  (the perturbation) such that their averages over the ground state are zero. For a weak time-dependent perturbation  $\hat{B}F(t)$  the linear relation

between them is given in terms of the *retarded response function*:

$$\langle \hat{A} \rangle(t) = \int_{-\infty}^{\infty} \chi_{AB}(\tau) \hat{F}(t - \tau) d\tau, \quad (3.1)$$

which is itself an average over the ground state of the commutator:

$$\chi_{AB}(\tau) = -\frac{i}{\hbar} \theta(\tau) \langle [\hat{A}(\tau), \hat{B}(0)] \rangle. \quad (3.2)$$

Now set  $\hat{B} \equiv \hat{A}^\dagger$  and compute the spectrum of time-dependent fluctuations of  $\hat{A}$ :

$$S_{AA^\dagger}(\omega) = \frac{1}{2\pi} \int_{-\infty}^{\infty} \langle \hat{A}(\tau) \hat{A}(0) \rangle e^{i\omega\tau} d\tau. \quad (3.3)$$

The fluctuation-dissipation theorem (FDT) then reads

$$\text{Im } \chi_{AA^\dagger}(\omega) = -\frac{\pi}{\hbar} S_{AA^\dagger}(\omega). \quad (3.4)$$

By the detailed balance condition the probabilities  $P_{mn}$  and  $P_{nm}$  of the transition between two quantum states  $m$  and  $n$  are equal. Take these states to be the eigenstates of the unperturbed Hamiltonian. In this case the response function can be represented in terms of the eigenstates — the Lehmann representation. The proof of FDT (3.4) amounts to showing that the left and the right side of this identity is given by the Fermi Golden rule formula:

$$S_{AA^\dagger}(\omega) = \sum_n |A_{0n}|^2 \delta(\omega - \omega_{0n}), \quad (3.5)$$

where 0 denotes the ground state. In the Chapter 4 we will see examples where response functions cannot be represented in this form. However, this can only occur for approximate correlators of the many-body perturbation theory. Exact correlators can always be written in this form provided conditions for the FDT hold. For the following discussion we will explicitly need the density-density response function, i. e.  $\hat{A} = \hat{A}^\dagger = \delta\hat{n} \equiv \hat{n} - \langle \hat{n} \rangle$ :

$$\chi^R(\tau) \equiv \chi_{nn}(\tau) = -\frac{i}{\hbar} \theta(\tau) \langle [\delta\hat{n}_H(\tau), \delta\hat{n}_H(0)] \rangle. \quad (3.6)$$

In the previous chapter we operated with various propagators using functional relations among them. It is time now to introduce these quantities explicitly. The time-ordered correlators are the main constituents of the equilibrium many-body perturbation theory:

$$\chi(1, 2) = -\frac{i}{\hbar} \langle T[\delta\hat{n}_H(1), \delta\hat{n}_H(2)] \rangle, \quad (3.7)$$

$$G(1, 2) = -\frac{i}{\hbar} \langle T[\hat{\psi}_H(1), \hat{\psi}_H^\dagger(2)] \rangle. \quad (3.8)$$

$$\Sigma^c(1, 2) = -\frac{i}{\hbar} \langle T[\hat{\gamma}_H(1), \hat{\gamma}_H^\dagger(2)] \rangle_{\text{irr}}, \quad (3.9)$$

where  $\Sigma^c$  denotes the correlated part of the self-energy. Its expression excludes the reducible diagrams, i. e., the expansion of the self-energy (3.9) contains all the diagrams of the two-particle-one-hole ( $2p1h$ ) correlation function [60] in which the entrance and exit channels cannot be separated by cutting one Green's function line [50, 61]. I adopt here the shorthand notations  $\mathbf{x}_i \equiv (\mathbf{r}_i, \sigma_i)$ ,  $i \equiv (\mathbf{x}_i, t_i)$ , etc., and express the field operators in the Heisenberg picture  $\hat{\psi}_H(1)$  as an expansion over real  $[\phi_i^*(\mathbf{x}) = \phi_i(\mathbf{x})]$  basis functions:

$$\hat{\psi}_H(1) = \sum_i \hat{c}_i(t_1)\phi_i(\mathbf{x}_1), \quad \hat{\psi}_H^\dagger(1) = \sum_i \hat{c}_i^\dagger(t_1)\phi_i(\mathbf{x}_1).$$

In following  $H$  index on creation and annihilation operators is consistently removed. The constituents of the response function and the self-energy are defined as follows:

$$\hat{n}(\mathbf{x}) = \hat{\psi}^\dagger(\mathbf{x})\hat{\psi}(\mathbf{x}), \quad (3.10)$$

$$\hat{\gamma}(\mathbf{x}) = \int d\mathbf{y} \nu(\mathbf{x}, \mathbf{y})\hat{\psi}^\dagger(\mathbf{y})\hat{\psi}(\mathbf{y})\hat{\psi}(\mathbf{x}). \quad (3.11)$$

This allows to write the real space representation of the propagators:

$$\chi(\mathbf{x}_1, \mathbf{x}_2; \omega) = \sum_{ijkl}^{D^1} \left\{ \sum_{n \neq 0}^{D^N} \langle 0 N | \hat{c}_i^\dagger \hat{c}_j | n N \rangle \langle n N | \hat{c}_k^\dagger \hat{c}_l | 0 N \rangle \left[ \frac{1}{\omega - E_n} - \frac{1}{\omega + E_n} \right] \right\} \times \phi_i(\mathbf{x}_1)\phi_j(\mathbf{x}_1)\phi_k(\mathbf{x}_2)\phi_l(\mathbf{x}_2), \quad (3.12)$$

$$G(\mathbf{x}_1, \mathbf{x}_2; \omega) = \sum_{ij}^{D^1} \left\{ \sum_p^{D^{N+1}} \frac{\langle 0 N | \hat{c}_i | p N + 1 \rangle \langle p N + 1 | \hat{c}_j^\dagger | 0 N \rangle}{\omega - \varepsilon_p^+} + \sum_q^{D^{N-1}} \frac{\langle 0 N | \hat{c}_i^\dagger | q N - 1 \rangle \langle q N - 1 | \hat{c}_j | 0 N \rangle}{\omega - \varepsilon_q^-} \right\} \phi_i(\mathbf{x}_1)\phi_j(\mathbf{x}_2). \quad (3.13)$$

The summations are performed over the single particle states ( $D^1$ ), over the states of the Hilbert space of  $N$ -particle system ( $D^N$ ), over the Hilbert space of the ionized states ( $D^{N-1}$ ), and over the electron-attached states ( $D^{N+1}$ ). The self-energy cannot be explicitly written in such a form because reducible diagrams must be excluded. We see that matrix elements of creation and annihilation operators are important ingredients of the Lehmann representation. For the following discussion it is useful to define these quantities explicitly:

$$Q_{ij}^n = \langle n N | \hat{c}_i^\dagger \hat{c}_j | 0 N \rangle, \quad E_n = E_n^N - E_0^N - i\delta; \quad (3.14a)$$

$$X_i^p = \langle p N + 1 | \hat{c}_i^\dagger | 0 N \rangle, \quad \varepsilon_p^+ = E_p^{N+1} - E_0^N - i\delta; \quad (3.14b)$$

$$Y_i^q = \langle q N - 1 | \hat{c}_i | 0 N \rangle, \quad \varepsilon_q^- = E_0^N - E_q^{N-1} + i\delta; \quad (3.14c)$$

$$\bar{X}_{ij}^p = \langle p N + 2 | \hat{c}_i^\dagger \hat{c}_j^\dagger | 0 N \rangle, \quad \bar{\varepsilon}_p^+ = E_p^{N+2} - E_0^N - i\delta; \quad (3.14d)$$

$$\bar{Y}_{ij}^q = \langle q N - 2 | \hat{c}_i \hat{c}_j | 0 N \rangle, \quad \bar{\varepsilon}_q^- = E_0^N - E_q^{N-2} + i\delta. \quad (3.14e)$$

### 3.2 Lehmann representation of the electronic self-energy

The exact self-energy has a Lehmann representation. This will be explicitly demonstrated in the next chapter. Approximate theories do not necessarily have this property because MBPT does not respect Fermi Golden rule form. There are, however, two approximations that do permit to write an explicit expression for the  $\hat{\gamma}(\mathbf{x})$  operators and such that reducible diagrams are excluded per construction. They correspond to two possibilities to factorize the product of three field operators in (3.11) or to factorize the  $2p1h$ -Green's function.

In the spectral representation of the self-energy it is convenient to separate the particle and the hole terms as it was done for the Green's function (3.13):

$$\Sigma^c(\mathbf{x}_1, \mathbf{x}_2; \omega) = \sum_{\nu} \frac{V_+^{\nu}(\mathbf{x}_1)V_+^{\nu}(\mathbf{x}_2)}{\omega - \omega_{\nu}^+} + \sum_{\nu} \frac{V_-^{\nu}(\mathbf{x}_1)V_-^{\nu}(\mathbf{x}_2)}{\omega - \omega_{\nu}^-}. \quad (3.15)$$

For the  $(p-h)-p$  factorization following expressions hold [3]:

$$V_+^{np}(\mathbf{x}) = \sum_{ijkl}^{D^1} X_i^p \langle ij|kl \rangle Q_{kl}^n \phi_j(\mathbf{x}), \quad \omega_{np}^+ = E_n + \varepsilon_p^+, \quad (3.16a)$$

$$V_-^{nq}(\mathbf{x}) = \sum_{ijkl}^{D^1} Y_i^q \langle ij|kl \rangle Q_{kl}^n \phi_j(\mathbf{x}), \quad \omega_{nq}^- = \varepsilon_q^- - E_n. \quad (3.16b)$$

where the Coulomb matrix elements are defined as

$$\langle ij|kl \rangle = \int d(\mathbf{r}_1 \mathbf{r}_2) \frac{\phi_i(\mathbf{r}_1)\phi_j(\mathbf{r}_1)\phi_k(\mathbf{r}_2)\phi_l(\mathbf{r}_2)}{|\mathbf{r}_1 - \mathbf{r}_2|}. \quad (3.17)$$

As can be seen from Eq. (3.15) the self-energy matrix is symmetric, complex, non-hermitian. As a function of frequency it has poles in the complex upper half-plane for  $\omega < -(E_{IP} + E_1)$  and in the lower half-plane for  $\omega > -(E_{EA} - E_1)$ .  $E_{IP}$ ,  $E_{EA}$  and  $E_1$  denote the ionization potential, electron affinity, and the energy of the first excited state. Thus, the energy gap for the self-energy in  $GW$  approximation is larger than that for the Green function. For the  $(p-p)-h$  factorization we additionally need the two-particle matrix elements [60]:

$$V_+^{pq}(\mathbf{x}) = \sum_{ijkl}^{D^1} Y_i^q \langle ij|kl \rangle \bar{X}_{ik}^p \phi_j(\mathbf{x}), \quad \omega_{pq}^+ = \bar{\varepsilon}_p^+ - \varepsilon_q^-, \quad (3.18a)$$

$$V_-^{qp}(\mathbf{x}) = \sum_{ijkl}^{D^1} X_i^p \langle ij|kl \rangle \bar{Y}_{ik}^q \phi_j(\mathbf{x}), \quad \omega_{qp}^- = \bar{\varepsilon}_q^- - \varepsilon_p^+. \quad (3.18b)$$

Eqs. (3.15, 3.16, 3.18) are main results of this section. They allow to assess the validity of the approximate self-energies on the basis of configuration interaction calculations and to perform calculations for larger systems where quantum chemistry approach provides a viable alternative to the random phase approximation calculations of the response function.

## Application

We demonstrate that for molecular systems the self-energy in the  $GW$  approximation can be exactly computed by using the Configuration Interaction (CI) method. The method found its broad application in quantum chemistry where, however, it is rarely used without any additional truncation of the full Hilbert space. A full CI wave function includes all possible Slater determinants which can be formed for a given number of electrons and orbitals. Thus, the full CI method provides an exact treatment of electron correlations by diagonalizing the many-body Hamiltonian within the space spanned by the given one-electron basis set [62, 63]. As a result of iterative diagonalization it gives the ground state energy and the energy of the lowest excited states. Due to the efficient implementations [64] the method can be applied for the benchmarking of small systems (usually described by localized Gaussian basis functions).

*Comparison of approximations* As a prototypical system I consider the widely studied  $\text{Na}_9^+$  cluster [65]. For the current purpose it is advantageous for several reasons: i) it contains a small number of electrons making it accessible to full CI [3, 4], ii) it can be seen as a generalization of 3d HEG to a finite number of particles (the jellium model [66]). In accordance with the prediction of the jellium model the 8 valence electrons complete the  $1s^2$  and  $1p^6$  shells typical for a spherical Coulomb potential well. Because the  $\text{Na}_9^+$  cluster has nearly spherical shape, this explains its high stability and large electron affinity. The energy of the highest occupied molecular orbital (HOMO) is  $-7.00$  eV, and the lowest unoccupied molecular orbital (LUMO) is at  $-2.57$  eV. These energies also yield good estimates for the electron affinity and ionization potential that come out as a result of this CI calculation. We use an algorithm by Olsen *et al.* [63] based on the graphical unitary group approach [62] for the generation of the restricted active space (RAS) and full CI Hamiltonians. The calculations are performed for each spin multiplicity separately using spin-adapted basis functions [67]. The configuration interaction including single, double, triple, and quadruple excitations (CISDTQ) in the subspace of 12 orbitals and 4 electron pairs is the highest level correlated method we use for this system. It yields  $E_{IP} = 6.93$  eV and  $E_{EA} = 2.77$  eV.

Let us compare the self-energy of the cluster computed using the  $(p-h)-p$  ( $GW$  approximation) and  $(p-p)-h$  (ladder approximation) factorizations with the exact self-energy from the inversion of the Dyson equation. The quasiparticle energy corrections resulting from the real part of self-energy are slightly overestimated on the  $GW$  level leading to the value of HOMO-LUMO gap of 4.05 eV compared to 4.17 eV according to the graphical solution of the Dyson equation as depicted on Fig. 3.1.

In order to get a better insight about the accuracy of the  $GW$  approximation we plot the state-resolved (diagonal) elements of the self-energy (Fig. 3.1). Although the differences are more pronounced here, the  $GW$  self-energy in the vicinity of the corresponding states yields a good estimate of their life-times. This finding supports the use of the  $GW$  approximation for calculations of life-times in order to describe time-resolved two-photon photoemission experiments in systems with simple electronic structure.

*Total energy* The electron Green function (3.13) and self-energy (3.15) allow to compute the total energy of the system in a variety of ways. The Galitskii-Migdal equation requires the knowledge of the spectral function only. In our approach it translates into:

$$E_{GM} = \frac{1}{2} \left[ T + \sum_q^{D^{N-1}} \left( \epsilon_q^- \sum_\alpha^{D^1} Y_\alpha^q Y_\alpha^q \right) \right], \quad (3.19)$$

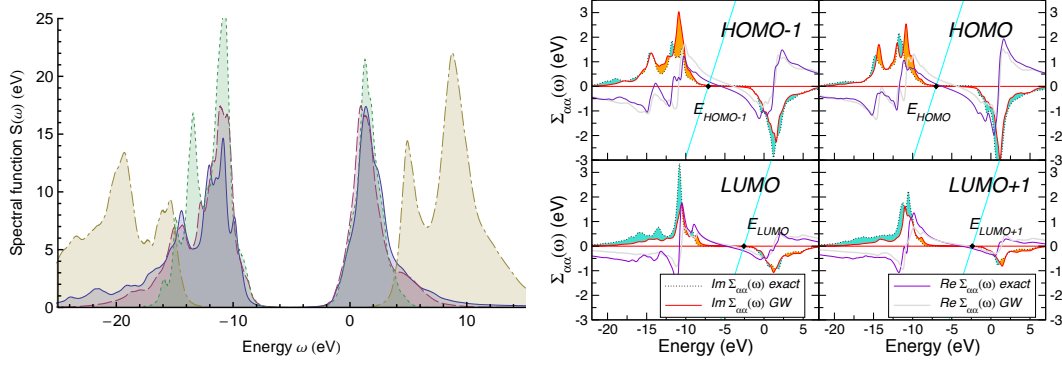


Figure 3.1: *Left*: The spectral function of the exact (solid),  $(p-h)-p$  (dashed) and  $(p-p)-h$  (dash-dotted) self-energies. *Right*: The diagonal matrix elements of the self-energy of the  $\text{Na}_9^+$  cluster from the inversion of the Dyson equation (exact) compared to the  $GW$  approximation. Computations are performed using the CISDTQ method. The straight lines demonstrate the graphical solution of the Dyson equation.

where  $T$  is the one-particle part of the energy of the system. The total energy in the form given by Eq. (3.19) does not provide a test of the  $GW$  approach accuracy since it depends on the quantities that are directly obtained from the diagonalization of the many-body Hamiltonian. Here I use a more universal approach that allows to directly test the accuracy of the  $GW$  self-energy based on the following expression (cf. Eq. (7) of Ref. [4] and Eq. (3) of Ref. [68]) for the correlated part of the total energy:

$$E_c = -\frac{i}{2\pi} \int_{-\infty}^{\infty} d\omega \frac{1}{2} \text{Tr} [\boldsymbol{\Sigma}(\omega) \mathbf{G}(\omega)]. \quad (3.20)$$

By substituting here the expressions for the matrix elements of the Green function  $\mathbf{G}(\omega)$  and the electron self-energy  $\boldsymbol{\Sigma}(\omega)$  in Eq. (3.20) and performing the frequency integration we obtain:

$$E_c = \sum_{n \neq 0} \sum_p \sum_q \frac{\sum_{\alpha} \sum_{\gamma} \sum_{ij}^{D^1 D^1 D^2} \left[ X_{\alpha}^p Y_{\gamma}^q \langle \alpha \gamma | ij \rangle Q_{ij}^n \right]^2}{(\epsilon_q^- - \epsilon_p^+) - E_n}. \quad (3.21)$$

### 3.3 Decay of hybridized electronic states of a Na cluster on Cu(001)

Physics of atoms or clusters of them adsorbed on metal surfaces is very rich. Electronic correlations often play a decisive role in phenomena accompanying the adsorption. They strongly influence the geometry of the constituent system and modify the single-particle electronic properties such as density of states or band structure. *Excited transient states*, localized on an adsorbate are very often invoked as intermediate states in scanning tunneling microscope manipulations of individual adsorbates and chemical reactions. The development of time-resolved two-photon photoemission (TR-2PPE) has allowed for the direct study of the transient states at surfaces and their life-times [69].



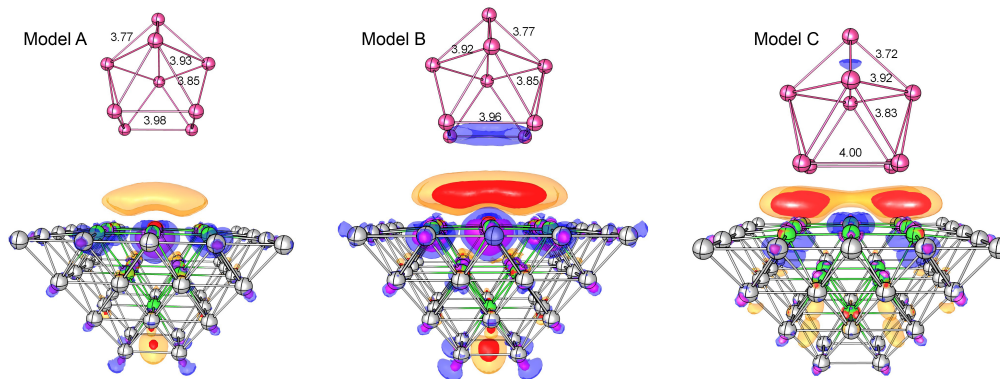


Figure 3.2: (Calculated isosurfaces of the electron density in the metal-adsorbate system minus superposition of bare-metal and free cluster densities. Three snapshots of the geometry optimization (models A, B, C) of  $\text{Na}_3^+ @ \text{Cu}(001)$  surface are shown (shortest distances between Na atoms and the top Cu plane are a)  $h_1=6.023 \text{ \AA}$ , b)  $h_1=4.894 \text{ \AA}$ , c)  $h_1=3.096 \text{ \AA}$ ).

The standard theoretical approach to compute the *electron-electron scattering* rate is the *GW* approximation known from many-body perturbation theory [4, 22]. The complete absence of translational invariance in such systems makes the use of the reciprocal space methods very difficult and calls for the development of new methods working solely in the real space representation. In the previous section (see also Ref. [3]) I have outlined a *GW* computational scheme based on a quantum chemistry approach. The use of CI for the computation of the screened Coulomb interaction enables us to treat extremely large systems and to properly account for the symmetry of the system in order to reduce the computational effort. Thus, we completely abandon the random phase approximation (RPA) usually adopted in condensed matter physics for the computation of  $W$ . While for bulk systems this is still a necessity, a CI approach proves to be a much more efficient tool for the evaluation of  $W$  in the systems without periodicity and, thus, for the description of inelastic electron scattering processes. The idea to use methods outside of many-body perturbation theory in order to facilitate the *GW* computations is not new. In particular, time-dependent density functional theory was used to derive expressions for the many-body vertex, polarizability, and self-energy functions [58] or to go beyond the RPA in the computation of the electronic screening in confined systems [70].

The non-self-consistent  $G^0W$  calculations of the electronic self-energy shown here are performed starting from the mean-field electronic structure. The spectral representation of the electronic Green's function is obtained by summation over the single particle states  $(\phi_\alpha, \epsilon_\alpha)$ , eigenstates of the Hartree-Fock (HF) Hamiltonian. This method is applied to the test case of a  $\text{Na}_3^+$  cluster adsorbed on Cu(001) surface. The geometry optimization performed with the GAUSSIAN 03 quantum chemistry package. Excited states and corresponding transition densities are computed using symmetry-adapted cluster expansion (SAC-CI) method [71]. The (001) surface of Cu is represented by a  $\text{Cu}_{54}$  cluster with  $5 \times 5$ ,  $4 \times 4$ ,  $3 \times 3$ , and  $2 \times 2$  atoms in the first, second, third, and fourth layers, respectively (Fig. 3.2).

Due to the delocalization of the valence electrons the  $\text{Na}_3^+$  cluster investigated in this work (Fig. 3.2) is well described by the jellium model and can be considered as an artificial atom with occupied  $1s$  and  $1p$  states typical for the spherical potential well [72]. In contrast to Cu(111), the surface states of Cu(001) are mostly located inside the bulk continuum [73], i. e., express themselves as resonance states. One of the questions that arises is whether the hybridized electronic states described above can indeed be observed using a cluster approach. At first sight there is little hope to separate these states from a huge number of unoc-

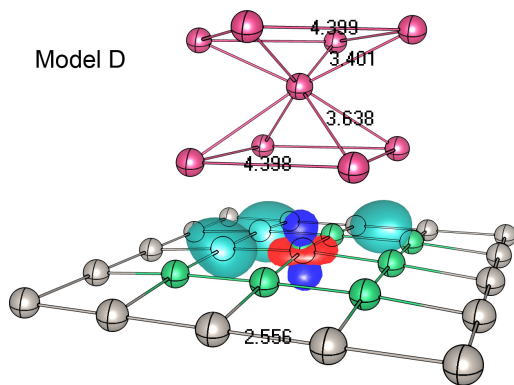


Figure 3.3: Partly occupied Wannier functions (WF) for the optimized geometry of  $\text{Na}_9^+@Cu(001)$  (model D).  $d$ - and  $s$ -bands of Cu give rise to five atom-centered  $d$  orbitals (one located on the central Cu atom is shown in red and blue) and to a single  $s$  orbital centered in one of the two interstitial sites (not shown). Besides the WFs located on each Na atom there are 4 symmetrically situated orbitals (3 are shown as a green cloud) above the last Cu plane originating from the hybridization of surface states with the unoccupied states of the  $\text{Na}_9^+$  cluster.

cupied molecular orbitals. One can use some localization techniques in order to analyze the system in terms of localized molecular orbitals. Their applicability, however, is limited to occupied orbitals only. Thus, we construct “partly occupied Wannier orbitals” [74], in this way prove the existence of the excited hybridized adsorbate states and get a clear picture of chemical bonding (Fig. 3.3).

The computation of the imaginary part of the self-energy is performed using 240 excited states from the SAC-CI calculation within the active space comprising 26 occupied and 86 virtual molecular orbitals. The state and energy resolved electronic self-energy (Fig. 3.4) gives access to life-times of excited states directly measurable in TR-2PPE experiments. The convergence of our calculations is tested on model A (Fig. 3.4, inset B). We find that the self-energy is very sensitive to the geometry of the system, systems further away from the equilibrium geometry have larger self-energy corrections. This is in line with the common knowledge in quantum chemistry that indicates a degradation of the accuracy of mean-field methods for stretched geometries. Although the broadening of the states obtained with our method is dependent on the state symmetry and energy, inset A on Fig. 3.4 enables us to make a statement about the average life-time of the quasiparticle states above the Fermi level. Based on the broadening of 20 to 40 meV we deduce the life-time to be of the order of 33 to 16.5 fs.

Summarizing, for the optimized geometry the life-time of excited states is larger than reported in the literature for  $\text{Cs}@Cu(001)$  ( $6\pm 4$  fs), but in line with the results for  $\text{Cs}@Cu(111)$  system ( $15\pm 6$  fs) [75, 76]. The variety of relaxation times in aforementioned systems indicates a delicate interplay among various factors such as details of the geometric and electronic structure, position of excited states with respect to bulk band structure etc., and suggests that only *ab initio* methods accounting for all these factors can provide an adequate description of the experiment.

### 3.4 Superatom molecular orbitals of $\text{C}_{60}$ molecule

The quasiparticle decay times in a Buckminsterfullerene can be likewise computed from first principles based on the many-body perturbation theory. A particularly lucid representation arises when the broadening of the quasiparticle states is plotted in the angular momentum ( $\ell$ ) and energy ( $\epsilon$ ) coordinates [5]. In this representation the main spectroscopic features of the fullerene consist of two occupied nearly parabolic bands, and delocalized plane-wave-like unoccupied states with a few long-lived electronic states (the superatom molecular orbitals, SAMOs) embedded in the continuum of Fermi-liquid states. SAMOs were recently discovered experimentally by M. Feng, J. Zhao, and H. Petek using scan-

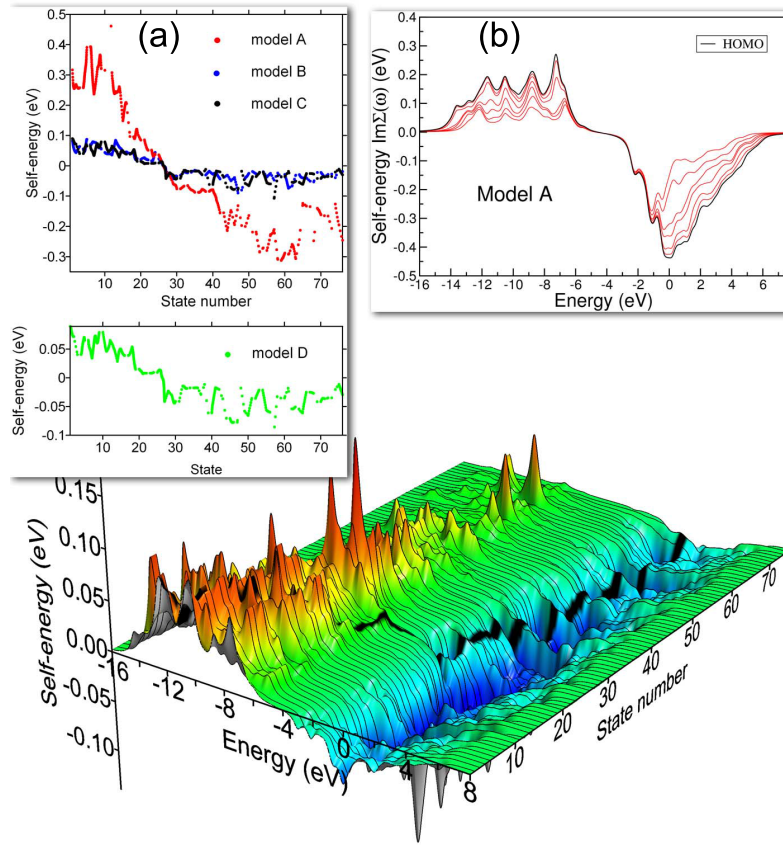


Figure 3.4: Energy and state resolved electronic self-energy for the converged geometry (model D). The black curve shows the energies of the quasiparticle states, its intersection with the self-energy curves yields an approximate solution of the Dyson equation for the imaginary part of the state energy. Panel (a) shows the main result of this work, the broadening of quasiparticle states. It can be seen that the life-times are highly sensitive to the geometrical structure of the system. Panel (b) shows the convergence of  $\text{Im}\Sigma(\omega)$  for the highest occupied molecular orbital (HOMO) of model A with the number of excited states included in the calculation ( $D^N = 60, 90, 120, 180, 210, 240$ ).

ning tunneling spectroscopy [77] as universal characteristics of  $C_{60}$  molecules and their aggregates. Further experiments on endohedral systems [78] and calculations for a series of quasi-spherical molecules [79] showed that SAMOs are associated with the whole system (rather than with a particular atom), have a well defined spherical symmetry (Fig. 3.5, angular momentum  $\ell = 0, 1, 2$ , principal quantum number  $n = 3$ ) and are capable of forming chemical bonds. Being markedly different from other unoccupied delocalized states they hold a promise for unique applications in molecular electronics. Hitherto theory was not able to answer why these states are so resilient to the chemical environment and why their character is not washed out by the hybridization. The clarification of these issues is of a critical importance for the SAMO-mediated charge transport [80].

Results of quantum chemical calculations for  $C_{60}$  molecule using a recently developed self-energy formalism resolve these issues. We have shown [60] that the spectral function for a large class of relevant electronic systems can be represented in the form

$$\mathbf{A}_\alpha(t) = \exp\left(-\gamma_\alpha \frac{t^2}{t + \tau_\alpha}\right), \quad (3.22)$$

where the set-in time of the exponential decay is given by  $\tau_\alpha = 2\gamma_\alpha/\sigma_{\alpha\alpha}^2$ . The spectral

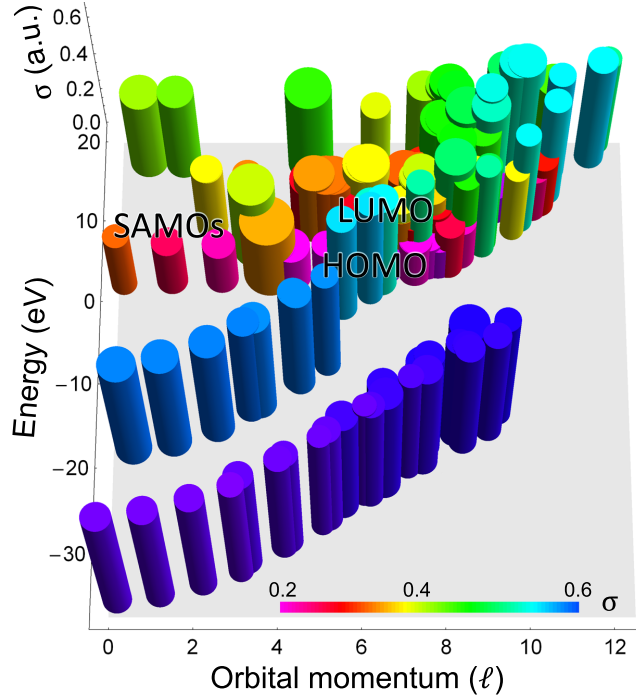


Figure 3.5: Single-particle states of  $C_{60}$  molecule. Each group of the degenerate states is represented by a cylinder and is characterized by the averaged orbital momentum  $\ell$  ( $x$ -axis), the energy ( $y$ -axis), the energy uncertainty  $\sigma$  (atomic units (a.u.),  $z$ -axis or colour coding) and the orbital momentum uncertainty ( $\delta\ell$ , the area of the cylinder base).  $\ell$  and  $\delta\ell$  are determined by projecting the states onto the spherical harmonics  $\phi_\alpha = \sum_{\ell} \sum_{m=-\ell}^{\ell} C_{\ell,m}^{\alpha} Y_{\ell,m}$  and interpreting  $\sum_{m=-\ell}^{\ell} |C_{\ell,m}^{\alpha}|^2$  as a probability to be in the angular momentum state  $\ell$ .

function  $\mathbf{A}_\alpha(t)$  has the following short and long time-limits:

$$\frac{d}{dt}\mathbf{A}_\alpha(t) \xrightarrow{t \rightarrow 0} -\sigma_{\alpha\alpha}^2 t, \quad (3.23)$$

$$\mathbf{A}_\alpha(t) \xrightarrow{t \rightarrow \infty} e^{-\gamma_\alpha t}, \quad (3.24)$$

meaning that for short times ( $t \ll \tau_\alpha$ ) we have the quadratic decay

$$\mathbf{A}_\alpha(t) \sim 1 - \sigma_{\alpha\alpha}^2 t^2 / 2. \quad (3.25)$$

$\sigma_{\alpha\alpha}^2$  is the central quantity for our theory. It can be determined as follows. A simple substitution of the asymptotic expansions into the Dyson equation leads to the exact relations between the spectral moments of the self-energy  $\Sigma(\omega)$  and of the spectral function  $\mathbf{A}(\omega)$  [54]:

$$\mathbf{M}^{(0)} = \mathbf{I}, \quad \Sigma_\infty = \mathbf{M}^{(1)} - \epsilon, \quad (3.26)$$

$$\Sigma^{(0)} = \mathbf{M}^{(2)} - [\mathbf{M}^{(1)}]^2, \quad (3.27)$$

where  $\Sigma_\infty$  is the frequency independent real part of the self-energy [81].  $\epsilon$  is a diagonal matrix with the elements given by the zeroth-order state energies. By defining the matrix of the spectral functions in terms of the imaginary part of the single-particle Green function ( $\mathbf{A}(\omega) = \frac{1}{\pi} |\text{Im}\mathbf{G}(\omega)|$ ) and likewise for the spectral function of the self-energy ( $\mathbf{S}(\omega) = \frac{1}{\pi} |\text{Im}\Sigma(\omega)|$ ), and by the use of the superconvergence theorem [82] one can redefine

the matrices in terms of the frequency integrals:

$$\mathbf{M}^{(n)} = \int_{-\infty}^{\infty} d\omega \omega^n \mathbf{A}(\omega), \quad n = 0 \dots 2, \quad (3.28)$$

$$\mathbf{\Sigma}^{(0)} = \int_{-\infty}^{\infty} d\omega \mathbf{S}(\omega). \quad (3.29)$$

Using the spectral representation of the self-energy (3.15), the frequency integral is expressed in terms of the matrix elements  $V_{\pm}$ . They should be written in a finite basis and coupled with an appropriate approximation for the self-energy operator. We consider the  $GW^0$  [83] approximation and treat the screened Coulomb interaction on the random phase approximation level. This is equivalent to the configuration interaction singles (CIS) treatment of the excited states. The final result can be expressed in terms of populations  $n_i$  and the Coulomb matrix elements only:

$$\sigma_{\alpha\beta}^2 = 2 \sum_i \sum_{j,k} \langle \alpha i | j k \rangle \langle \beta i | j k \rangle n_k (1 - n_j). \quad (3.30)$$

The main computational burden in this approach is the transformation of the Coulomb matrix elements from the atomic to molecular orbital basis which scales as  $\mathcal{O}(N^5)$ . Very large basis sets (up to 6-311++G(3df,3pd)) resulting in  $N = 2340$  functions for  $C_{60}$  were needed to obtain convergent results. Integral transformations for this number of basis functions is not feasible with any standard quantum chemistry package and required a parallelized implementation fully accounting for the symmetry of the system [84].

My calculations clearly indicate a peculiarity of SAMOs: a strong localization in the energy domain (cf.  $\sigma_{\text{HOMO}} = 16.0$  eV and  $\sigma_{\text{SAMO}_d} = 6.1$  eV) (Fig. 3.5) or their extended life-time even in comparison with the life-time of HOMO or LUMO states. This finding endorses the potential of SAMOs as transport channels in molecular electronic devices, since the energy is hardly dissipated during the short transport time. Our results are also unexpected from the Landau's theory of Fermi liquids [2] and illustrate that finite systems possess electronic excitations that differ drastically from quasiparticles in extended matter. Namely, a particle excitation may decay into two particles and one hole. This process may recur for many generations or it may stop after a few. For the former case a large number of many-particle peaks form a Lorentzian envelope, the so-called *quasiparticle*. If the decay stops after a finite number of branchings, only Dirac peaks appear in the single particle spectrum (denoting a localization in the Fock space). A decisive discriminating factor was shown to be the particle's energy ( $\epsilon$ ) [85]. Our *ab initio* approach suggests that it is actually the kinetic energy  $\epsilon_K$  that governs the decay. We find that even though the energies of electrons with different radial character may be very similar, their kinetic energy is substantially different (as follows from the specific form of the Kohn-Sham potential for this system [86]). It imposes strong restrictions on the Coulomb matrix elements and leads to the localization of SAMOs in the Fock space. This hints on the prolonged life-times and stipulates the observed high stability of these states.



## 4 Nonequilibrium approach

---

Time-resolved spectroscopies such as attosecond streaking [87] or two-photon photoemission [88] (TR-2PPE) allow to trace the dynamics of electronic excitations in real time. As the measurements inadvertently drive the system out of equilibrium, the many-body wavefunction describing the whole system evolves in time. The evolution is reflected in a number of observables like the total energy, dipole moment or the spectral density, etc. The equilibrium theory such as presented in the previous chapter can only be applied when the external influence already ceased to act. One can still substantiate the theory in the limit of weak or slowly varying in time perturbations. But it is impossible to do so for intrinsically non-equilibrium experimental conditions, such as during the transport measurements: even in the steady regime the system is out of equilibrium.

The non-equilibrium Green's function (NEGF) approach allows to tackle exactly these scenarios [89]. Unlike the ordinary  $T = 0$  MBPT with propagators being formally functions of two real times, but practically only depending on their difference, the propagators of NEGF theory are defined on the Keldysh contour. The time is then an abstract complex quantity, whereas projections on the real time axis define Green's functions with different orderings of the time-arguments. Consequently, one works with a set of four Green's functions, but diagrammatic rules and the whole methodology remain unchanged.

The propagators contain now a lot more of information: to elucidate consider the electron spectral function which is natural to define in energy  $\omega$  and time  $T$  coordinates. The dependence on  $T$  reflects the transient behavior of the system during the perturbation, while the  $\omega$ -dependence results from the Fourier transform with respect to the relative time coordinate  $t$ :

$$A(T, \omega) = i \int \frac{dt}{2\pi} e^{i\omega t} [G^> - G^<] (T + \frac{t}{2}, T - \frac{t}{2}).$$

At equilibrium the lesser  $G^<(t_1, t_2)$  and the greater  $G^>(t_1, t_2)$  functions only depend on the time difference and, thus, are reduced by the fluctuation-dissipation theorem to the product of the hole/particle distribution function and the difference of the retarded and advanced components, i. e., the whole expression is reduced to spectral function of the equilibrium theory. In the non-equilibrium regime the two-arguments  $A(T, \omega)$  contains information about both: the transient electronic structure and the time-dependent distribution function. It be-

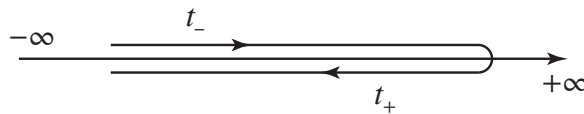


Figure 4.1: The Keldysh time-loop contour  $C$ . The forward branch is denoted with a “-” label while the backward branch is denoted by a “+” label.

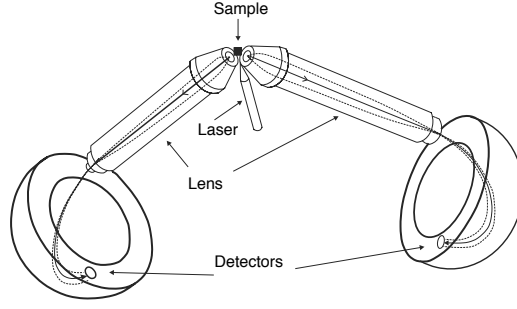


Figure 4.2: Sketch of the coincidence electron spectrometer.

comes evident when one considers the generalized Kadanoff-Baym Ansatz (GKBA) [90]:  $-iG^<(t_1, t_2) = G^R(t_1 - t_2)G^<(t_2) - G^<(t_1)G^A(t_1 - t_2)$ . This approximation will be used in the following sections together with the requirement on the theory to be conserving at one and two-particle levels [91, 92] to devise a practical numerical scheme applicable for equilibrium and non-equilibrium situations [6, 7] (Sec. 4.2).

Positive definiteness of spectral functions is another requirement that perturbation theories should fulfill. A model example presented in Sec. 2.3 demonstrates that its violation is a direct consequence of the asymptotic character of perturbative series. In Sec. 4.3 I zoom into the origin of this problem. A diagrammatic solution using the NEGF tools [8] is then illustrated by the vertex function calculations for the homogeneous electron gas.

Evolution of a quantum state on the Keldysh contour is very similar to the preparation and observation of a wave packet in scattering experiments [93, 94]. That is why it is natural to apply the machinery of NEGF theory to the process of electron photoemission. In Sec. 4.4 I focus on one particular experiment (Fig. 4.2) where two electrons are observed in coincidence after a quantum system absorbs one photon, the so-called double photoemission (DPE). As the minimal coupling of the incident laser field to any many-body system is of the single-particle type, the simultaneous emission of two electrons must be mediated by the electron-electron interaction [95] and is a manifestation of *extrinsic* losses in a single photoemission [96, 97]. Diagrammatic formulation of the plasmon assisted DPE is the major innovation here [9].

## 4.1 Correlators on the Keldysh contour

In Chapter 3 the time-ordered correlators  $\chi(1, 2)$ ,  $G(1, 2)$  and  $\Sigma^c(1, 2)$  have been defined as the ground state average of products of field operators (Eqs. (3.7)-(3.9)). They all depend on two time-arguments and, therefore, can be written in the following generic form:

$$\mathcal{F}(\mathbf{x}_1 t_1, \mathbf{x}_2 t_2) = -i \langle \Psi_0 | T[\hat{f}_H^\dagger(\mathbf{x}_1 t_1) \hat{f}_H(\mathbf{x}_2 t_2)] | \Psi_0 \rangle_{\text{irr}}, \quad (4.1)$$

where  $\langle \dots \rangle_{\text{irr}}$  signifies that after the correlator was computed according to the Wick's theorem some reducible diagrams need to be removed.  $T$  denotes the time-ordering operator.

We can consider a more general situation where the time arguments lie on an arbitrary contour (such as shown at Fig. 4.1). In the following I adhere to notations of Stefanucci and van Leeuwen [89], denote points on the contour as  $z_i \in C$ , and introduce the order relation  $z_i < z_j$  and the corresponding *contour-ordering* operator  $\mathcal{T}$ .



The definition of the correlator (4.1) is then naturally extended

$$\mathcal{F}^C(\mathbf{x}_1 z_1, \mathbf{x}_2 z_2) = -i \langle \Psi_0 | \mathcal{T} \hat{\ell}_H(\mathbf{x}_1 z_1) \hat{\ell}_H^\dagger(\mathbf{x}_2 z_2) | \Psi_0 \rangle_{\text{irr}}, \quad (4.2)$$

where the contour Heisenberg picture is introduced with the help of the contour evolution operators

$$\hat{\ell}_H(\mathbf{x}z) = \hat{U}(z_0, z) \hat{\ell}_H(\mathbf{x}) \hat{U}^\dagger(z, z_0). \quad (4.3)$$

We see that for each real time point correspond two points on the Keldysh contour (Fig. 4.1) such that  $t_-$  precedes  $t_+$  ( $t_- < t_+$ ). Thus, it is natural to introduce four possible correlators  $\mathcal{F}^{\alpha\beta}(\mathbf{x}_1 z_1, \mathbf{x}_2 z_2)$  ( $\alpha, \beta = \pm$ ) according to the branch to which  $z_1$  and  $z_2$  belong to. In these notations the time-ordered correlator has its both time-arguments on the forward branch and denoted as  $\mathcal{F}^{--}$ , whereas the anti-time-ordered correlator has two time arguments on the backward branch, i. e.  $\mathcal{F}^{++}$ . They are known to us from standard (equilibrium) formulation of MBPT.  $\mathcal{F}^{-+}$  and  $\mathcal{F}^{+-}$  have slightly different meaning and are denoted as the *lesser* and *greater* correlators:

$$\mathcal{F}^<(\mathbf{x}_1 z_1, \mathbf{x}_2 z_2) = +i \langle \Psi_0 | \hat{\ell}_H^\dagger(\mathbf{x}_2 z_2) \hat{\ell}_H(\mathbf{x}_1 z_1) | \Psi_0 \rangle_{\text{irr}}, \quad (4.4)$$

$$\mathcal{F}^>(\mathbf{x}_1 z_1, \mathbf{x}_2 z_2) = -i \langle \Psi_0 | \hat{\ell}_H(\mathbf{x}_1 z_1) \hat{\ell}_H^\dagger(\mathbf{x}_2 z_2) | \Psi_0 \rangle_{\text{irr}}. \quad (4.5)$$

In frequency space and at zero temperature  $-iG^<(\omega)$  is the spectral function below the Fermi energy, whereas  $iG^>(\omega)$  is the spectral function above the Fermi energy.

From physical perspective all observables are given by the *retarded* correlation functions, that is between an excitation and the system's response is a causal relation. It can be expressed in terms of already defined correlators on the Keldysh contour:

$$\begin{aligned} \mathcal{F}^R(\mathbf{x}_1 t_1, \mathbf{x}_2 t_2) &= \mathcal{F}^\delta(\mathbf{x}_1 t_1, \mathbf{x}_2 t_2) \delta(t_1 - t_2) \\ &\quad + \theta(t_1 - t_2) [\mathcal{F}^>(\mathbf{x}_1 t_1, \mathbf{x}_2 t_2) - \mathcal{F}^<(\mathbf{x}_1 t_1, \mathbf{x}_2 t_2)], \end{aligned} \quad (4.6)$$

where  $\mathcal{F}^\delta$  is the instantaneous function. It vanishes for the electron propagator and is equal to the bare Coulomb interaction for the screened Coulomb interaction. To make the picture complete one considers the anti-causal relations described by the *advanced* correlators  $\mathcal{F}^A(\mathbf{x}_1 t_1, \mathbf{x}_2 t_2) = \mathcal{F}^R(\mathbf{x}_1 t_2, \mathbf{x}_2 t_1)$ .

Diagrammatically the non-equilibrium Green's function theory is not different from its equilibrium counterpart. Also equations of motion on the Keldysh contour have the same functional form. The difference is in the way how products and convolutions are evaluated. They are known as *Langreth rules*. Consider, for instance, the convolution of two functions on the contour

$$c(z_1, z_2) = \int_C dz a(z_1, z) b(z, z_2).$$

Following identities hold

$$c^<(t_1, t_2) = \int dt [a^<(t_1, t)b^A(t, t_2) + a^R(t_1, t)b^<(t, t_2)], \quad (4.7)$$

$$c^R(t_1, t_2) = \int dt a^R(t_1, t)b^R(t, t_2). \quad (4.8)$$

The products  $c(z_1, z_2) = a(z_1, z_2)b(z_2, z_1)$  are evaluated as follows

$$c^<(t_1, t_2) = a^<(t_1, t_2)b^>(t_2, t_1), \quad (4.9)$$

$$c^>(t_1, t_2) = a^>(t_1, t_2)b^<(t_2, t_1). \quad (4.10)$$

Other identities are listed in Ref. [89].

## 4.2 Conserving approximations

In this section I present a general approach for  $GW$  calculations of quasiparticle (QP) properties, in which an accurate screened Coulomb potential is calculated based on consistency requirements between the single-particle Green's function (determined by the self-energy) and the screened potential (determined by the density-density correlation function). Such an approach is particularly well suited for metal clusters, which combine features of finite systems with those of extended ones [65, 98, 99].

The calculation of the screened Coulomb potential is the main difference of our approach from standard  $GW$ -RPA and its selectively improved versions. The motivation for this change in approach is that  $W$  as computed in the  $GW$ -RPA is an auxiliary quantity, which lacks some of the properties of a physical screened potential [100]. To be more specific,  $GW$ -RPA does not obey the charge/current conservation law as it applies to the density-density correlation function, unless the screened potential  $W$  is calculated from single-particle Green's function in the Hartree approximation [91]. This approximation, however, is clearly not good enough for clusters. Using Green's functions determined self-consistently instead of the Hartree Green's function seems to be a straightforward improvement for the calculation of  $W$ , but it leads to a violation of the  $f$ -sum rule [92], and therefore is in conflict with our goal of improving the quality of the screened Coulomb potential.

To obtain a screened Coulomb potential that does not violate sum rules, we choose the self-energy first, and obtain the *consistent* screened potential (including vertex corrections):

$$W^R(1, 2) = v(1, 2) + \int d(34) v(1, 3)\chi^R(3, 4)v(4, 2), \quad (4.11)$$

by the physical constraint that the polarization function (or density-density correlation function) fulfills charge/current conservation [91, 101]. This can be achieved by determining the density-density correlation function as a functional derivative of the Green's function with respect to an external potential [91, 102]:

$$\chi^R(1, 2) = \left. \frac{\delta \langle \hat{n}(1) \rangle}{\delta \varphi(2)} \right|_{\varphi=0}. \quad (4.12)$$

Using the functional derivative technique, the concept of  $\Phi$ -derivability is not explicitly needed [103], if one starts from conserving Green's functions, as is the case in our calculations. The functional derivative is computed by solving a linearized quantum-kinetic equation for the one-particle Green's function in the presence of a weak external potential  $\varphi$  with a generalized quasiparticle ansatz.

In the previous chapters I have already demonstrated that in the framework of MBPT the quality of approximations for the self-energy and the irreducible polarization function is controlled by the level of approximation adopted for the calculation of the vertex function  $\Gamma$ . One can also use *general* criteria derived from physical conservation laws or invariance principles. Such an approach has been used for transport calculations [91] and electronic structure calculations [92, 101, 104]. Since the conservation laws imply important consistency conditions for the one and two-particle correlation functions [91, 101], they prevent a choice of the vertex contributions that optimizes, say, the one-particle properties at the cost of the two-particle correlation functions. The choice of vertex corrections, which are inconsistent in the sense that they do not obey the charge-current conservation law, may be suitable for a particular calculation, but such a choice is more likely to encounter problems with calculations where both the single-particle quantities (i. e.,  $G$  and  $\Sigma$ ) and the two-particle quantities (i. e.,  $W$  and  $P$ ) are intimately connected. The question of consistency between the different "ingredients" for the calculation also arises if one uses, for instance, density-functional based single-particle states as input in  $GW$  calculations, which are then used as input to Bethe-Salpeter equation calculations [22].

## Quantum kinetics

In our basis function representation, the single-particle density matrix is given in terms of a single-particle nonequilibrium Green's function

$$iG_{n_2 n_1}^<(t, t) = -\langle \hat{n}_{n_1 n_2}(t) \rangle = -\langle \hat{c}_{n_1}^\dagger(t) \hat{c}_{n_2}(t) \rangle, \quad (4.13)$$

where  $\hat{c}_n^\dagger$  and  $\hat{c}_n$  are the creation and the annihilation operators of particles in the molecular orbital  $n$ , respectively.

In the following, I relate the determination of  $\chi^R$  to a quantum-kinetic calculation of a nonequilibrium Green's function under the action of a weak external field  $\varphi$ . For this, we start from the time-dependent Hamiltonian  $\hat{H}(t) = \hat{H}_0 + \sum_{n_1 n_2} \varphi_{n_1 n_2}(t) \hat{c}_{n_1}^\dagger \hat{c}_{n_2}$  with

$$\hat{H}_0 = \sum_{n_1 n_2} T_{n_1 n_2} \hat{c}_{n_1}^\dagger \hat{c}_{n_2} + \frac{1}{2} \sum_{n_1 \dots n_4} \langle n_1 n_2 | v | n_4 n_3 \rangle \hat{c}_{n_1}^\dagger \hat{c}_{n_2}^\dagger \hat{c}_{n_3} \hat{c}_{n_4}, \quad (4.14)$$

where  $\hat{T}$  is the kinetic part, which in our case includes the core potential, and  $v$  is the bare Coulomb matrix element. With this Hamiltonian, the Green's function (4.13) evolves in time according to

$$\begin{aligned} i \frac{\partial}{\partial t_1} G_{n_1 n_2}^<(t_1, t_2) &= \delta(t_1 - t_2) \delta_{n_1 n_2} + \sum_{n_3} (T + \varphi)_{n_1 n_3}(t_1) G_{n_3 n_2}^<(t_1, t_2) \\ &+ \sum_{n_3} \int dt_3 (\Sigma_{n_1 n_3}^R(t_1, t_3) G_{n_3 n_2}^<(t_3, t_2) + \Sigma_{n_1 n_3}^<(t_1, t_3) G_{n_3 n_2}^A(t_3, t_2)). \end{aligned} \quad (4.15)$$

There is also the adjoint equation, corresponding to the derivative with respect to  $t_2$ . For the evaluation of Eq. (4.15) we use a relation (4.6) between the components of  $G$ ,  $W$  and  $\Sigma$  on the Keldysh contour and recall that the instantaneous HF self-energy is given by:

$$\Sigma_{n_1 n_2}^{\text{HF}}(t_1) = -i \sum_{n_3 n_4} [\langle n_1 n_3 | v | n_2 n_4 \rangle - \langle n_1 n_2 | v | n_3 n_4 \rangle] G_{n_3 n_4}^<(t_1, t_1). \quad (4.16)$$

Finally, for  $\Sigma^{\geq}(t_1, t_2)$  we use the  $GW$  form

$$\Sigma_{n_1 n_2}^{\geq}(t_1, t_2) = i \sum_{n_3 n_4} G_{n_3 n_4}^{\geq}(t_1, t_2) \langle n_1 n_2 | W^{\leq}(t_2, t_1) | n_3 n_4 \rangle. \quad (4.17)$$

Similarly for the imaginary part of the retarded correlated self-energy we have

$$\text{Im} \Sigma_{n_1 n_1}^c(\omega) = \sum_{n_2} \int \frac{d\omega'}{\pi} [n_B(\omega') + n_F(\omega + \omega')] \text{Im} G_{n_2 n_2}^R(\omega + \omega') \text{Im} \langle n_1 n_1 | W^R(\omega') | n_2 n_2 \rangle, \quad (4.18)$$

where  $n_B(\omega)$  and  $n_F(\omega)$  are the Bose and Fermi distribution functions, respectively, i. e.  $n_{B/F}(\omega) = [\exp \beta \omega \pm 1]^{-1}$ . The real part of  $\Sigma^c(\omega)$  is calculated from a Kramers-Kronig transformation.

Equation (4.15) for the dynamical Green's functions depending on two real time arguments is an extremely complex integro-differential equation, whose solution is possible only for small or homogeneous systems [105]. For systems of intermediate size, our aim is to develop a flexible approximate numerical scheme which works only with Green's functions depending on a single time argument. We introduce approximations, so that the resulting equations depend only on  $G^R(t_1 - t_2)$ , i. e., the equilibrium retarded Green's function, whose Fourier transformation  $G^R(\omega)$  has a simple physical interpretation, instead of  $G^R(t_1, t_2)$ . An important consequence of this approximation is that the equilibrium  $G^R(t_1 - t_2)$  does not need to be calculated *together* with the dynamical Eq. (4.15). Rather, the response of the system described by Eq. (4.15) now becomes implicitly dependent on  $G^R(\omega)$ .

Here, I concentrate on the numerical procedure for a consistent "one-shot"  $GW$  calculation. Using HF spin orbitals as single-particle quantum numbers, the retarded GF becomes diagonal

$$G_{n_1 n_2}^R(\text{HF})(\omega) = \frac{1}{(\omega + i\gamma) - \epsilon_{n_1}^{\text{HF}}} \delta_{n_1 n_2}. \quad (4.19)$$

In equilibrium, this corresponds also to a diagonal kinetic Green's function

$$G_{n_1 n_2}^<(\text{HF})(\omega) = 2\pi i f_{n_1 n_2}^{(\text{HF})} \delta(\omega - \epsilon_{n_1}^{\text{HF}}) \quad (4.20)$$

$$f_{n_1 n_2}^{(\text{HF})} = n_F(\epsilon_{n_1}^{\text{HF}}) \delta_{n_1 n_2}, \quad (4.21)$$

Employing Eq. (4.20) as a description of the HF ground state, we determine the dielectric function via Eq. (4.12). To do this, we need several additional steps and an approximation for the two-time kinetic Green's function. We first note that, to first order in the weak perturbation, only density *fluctuations*, i. e., averages of the form  $\langle \hat{n}_{n_1 n_2}(t) \rangle$  with  $n_1 \neq n_2$ , are driven away from their equilibrium value (4.21), while the level occupations  $\langle \hat{n}_{n_1 n_1} \rangle$  remain equal to  $f_{n_1 n_1}^{(\text{HF})} = n_F(\epsilon_{n_1}^{\text{HF}})$  for all times.

Transcribing this back into the language of Green's functions using Eq. (4.13), we need to calculate off-diagonal matrix elements  $iG_{n_1 n_2}^<(t, t)$ . The quantum kinetic equation for these quantities is derived by subtracting Eq. (4.15) and the adjoint equation, making the substitution  $t = (t_1 + t_2)/2$  and  $\tau = t_1 - t_2$  and finally considering the equal-time limit  $\tau = 0$ :

$$\left( i \frac{\partial}{\partial t} - \epsilon_{\alpha}^{\text{HF}} \right) G_{\alpha}^<(t) + n_{\alpha} \Omega_{\alpha}^{\text{eff}}(t) = S_{\alpha}(t). \quad (4.22)$$

Here,  $\alpha = (n_1, n_2)$  is a pair-state index for the off-diagonal Green's function,  $\epsilon_{\alpha}^{\text{HF}} = \epsilon_{n_1}^{\text{HF}} - \epsilon_{n_2}^{\text{HF}}$  the energy difference between two levels, and  $n_{\alpha} = n_F(\epsilon_{n_1}) - n_F(\epsilon_{n_2})$  is the difference in level

distribution between the two spin-orbitals of the pair state. The latter quantity is sometimes referred to as the Pauli-blocking factor. The generalized *driving term*

$$\Omega_{\alpha}^{\text{eff}}(t) = i\varphi_{\alpha}(t) + \sum_{\beta} (v_{\alpha\beta}^{\text{dir}} - v_{\alpha\beta}^{\text{exc}}) G_{\beta}^{<}(t) \quad (4.23)$$

contains Coulomb enhancement contributions involving direct and exchange terms:

$$v_{\alpha\beta}^{\text{dir}} \equiv v_{(n_1 n_2)(n_3 n_4)}^{\text{dir}} = \langle n_1 n_3 | v | n_2 n_4 \rangle, \quad v_{\alpha\beta}^{\text{exc}} \equiv v_{(n_1 n_2)(n_3 n_4)}^{\text{exc}} = \langle n_1 n_2 | v | n_3 n_4 \rangle. \quad (4.24)$$

The right hand side of Eq. (4.22) is the *correlation term*

$$S_{n_1 n_2}(t) = \sum_{n_3} \int_{-\infty}^t d\bar{t} [\Sigma_{n_1 n_3}^{>}(t, \bar{t}) G_{n_3 n_2}^{<}(\bar{t}, t) + G_{n_1 n_3}^{<}(t, \bar{t}) \Sigma_{n_3 n_2}^{>}(\bar{t}, t) - (\lesseqgtr)] \quad (4.25)$$

that accounts for interaction effects beyond HF. For the self-energies, we use Eq. (4.17).

### Generalized Kadanoff-Baym ansatz

The aim of our approach is to reduce the computational complexity of the Green's functions depending on two time arguments by splitting the problem into the determination of the equilibrium  $G^{\text{R}}(\omega)$  from the calculation of the density-response function, i. e.,  $G^{<}(t, t)$  in the presence of an external perturbation. The main approximation involved is that the two-time Green's functions  $G^{<}(t, \bar{t})$ , which are contained in the correlation contribution (4.25) need to be related to the dynamics of the density response, i. e., the time-diagonal Green's function by virtue of Eq. (4.13). To this end, GKBA in the following form [106] is employed:

$$G_{n_1 n_2}^{\gtrless}(t, \bar{t}) = iG_{n_1 n_1}^{\text{R}}(t - \bar{t}) G_{n_1 n_2}^{\gtrless}(\bar{t}) - iG_{n_1 n_2}^{\gtrless}(t) G_{n_2 n_2}^{\text{A}}(t - \bar{t}). \quad (4.26)$$

To evaluate the correlation contribution using GKBA I substitute for the retarded  $G^{\text{R}}$  and advanced  $G^{\text{A}}$  Green's functions the Hartree-Fock Green's functions in the time domain and obtain:

$$S_{n_1 n_2}(t) = i \sum_{n_3 n_4 n_5} \int_{-\infty}^t d\bar{t} [e^{-i(\tilde{\epsilon}_{n_4} - \tilde{\epsilon}_{n_2}^*)(t - \bar{t})} \langle n_1 n_3 | W^{<}(t, \bar{t}) | n_4 n_5 \rangle G_{n_3 n_2}^{<}(\bar{t}) G_{n_4 n_5}^{>}(\bar{t}) + e^{-i(\tilde{\epsilon}_{n_1} - \tilde{\epsilon}_{n_5}^*)(t - \bar{t})} \langle n_3 n_2 | W^{<}(t, \bar{t}) | n_4 n_5 \rangle G_{n_1 n_3}^{<}(\bar{t}) G_{n_4 n_5}^{>}(\bar{t}) - (\lesseqgtr)]. \quad (4.27)$$

Because we wish to determine the *linear* density response to the weak external perturbation,  $S(t)$  is linearized with respect to the off-diagonal  $G^{\gtrless}$ s that are driven by  $\varphi$ . In the spirit of linear response, the Green's functions appearing in one term together with one off-diagonal Green's function are replaced by the equilibrium relations  $G_{n_1 n_1}^{<} = -i(1 - f_{n_1})$  and  $G_{n_1 n_1}^{>} = -if_{n_1}$ , where we have defined  $f_{n_1} \equiv f_{n_1 n_1}^{(\text{HF})}$ ; and use  $G_{n_1 n_2}^{>}(\bar{t}) = G_{n_1 n_2}^{<}(\bar{t})$  for  $n_1 \neq n_2$ .

### The density-density response

The equation for  $\chi^R$  is obtained by functional differentiation of Eq. (4.22) with respect to  $\varphi(t')$  and letting  $\varphi \rightarrow 0$  afterwards. This is done by replacing everywhere the term  $\delta G_{n_1 n_2}^<(t)/\delta \varphi_{n_3 n_4}(t')$  with  $-i\langle n_1 n_2 | \chi^R(t-t') | n_3 n_4 \rangle$ . In the correlation contributions, terms such as  $\delta W^{\lessgtr}/\delta \varphi$  are consistently neglected, because we assume that the external potential is weak enough as not to cause changes in the screening properties of the system [107]. The resulting equation can be cast in the form

$$\begin{aligned} \left( i \frac{\partial}{\partial t} - \epsilon_{\alpha}^{\text{HF}} \right) \chi_{\alpha\beta}^R(t, t') + n_{\alpha} \left( \delta_{\alpha\beta} + \sum_{\gamma} (v_{\alpha\gamma}^{\text{dir}} - v_{\alpha\gamma}^{\text{exc}}) \chi_{\gamma\beta}^R(t, t') \right) \\ = \sum_{\gamma} \int_{-\infty}^t d\bar{t} \Delta_{\alpha\gamma}(t, \bar{t}) \chi_{\gamma\beta}^R(\bar{t}, t'). \end{aligned} \quad (4.28)$$

The correlation kernel  $\Delta$  only depends on the time-difference allowing us to perform the Fourier transformation of Eq. (4.28) with respect to time and to determine the frequency-dependent  $\chi^R$  by

$$\left( \omega - \epsilon_{\alpha}^{\text{HF}} \right) \chi_{\alpha\beta}^R(\omega) + n_{\alpha} \left( \delta_{\alpha\beta} + \sum_{\gamma} (v_{\alpha\gamma}^{\text{dir}} - v_{\alpha\gamma}^{\text{exc}}) \chi_{\gamma\beta}^R(\omega) \right) = \sum_{\gamma} \Delta_{\alpha\gamma}(\omega) \chi_{\gamma\beta}^R(\omega). \quad (4.29)$$

The integration of terms contributing to  $\Delta$  is quite tedious and presented in full in [7].

Equation (4.29) completes the development of our method: it allows to determine  $\chi^R$  and therefore via Eq. (4.11) the retarded screened potential  $W^R$ . This in turn enters the calculation of the equilibrium Green's function via the Dyson equation and (4.18). Thus, we have access to single-particle properties of a system [6] (density of states) via the Green's function and to neutral excited states [7] via the density-density response function on equal footing.

The real part of  $\Delta$  contributes to transition-energy renormalizations and the imaginary part to resonance broadening. The diagonal contributions  $\Delta_{\alpha=\gamma}$  only shift and broaden two-particle resonances whereas the off-diagonal  $\Delta_{\alpha\neq\gamma}$  together with  $v_{\alpha\gamma}^{\text{dir}}$  and  $v_{\alpha\gamma}^{\text{exc}}$  can lead to collective features in the  $\text{Im}\epsilon^{-1}(\omega)$  spectrum. We reiterate that the quasiparticle properties are conserving on the one and two-particle levels in the sense of Baym and Kadanoff because the one-particle Green's function is calculated from a dielectric function (density response-function) that is related by a functional differentiation to a one-particle conserving equation of motion for  $G^<$ .

Figure 4.2 shows the comparison between the experimental and the theoretical cross sections of the optical absorption of  $\text{Na}_{21}^+$  cluster. The measured spectrum displays a large absorption line centered around 2.74 eV [108]. Two different cluster geometries were used in the calculation: one corresponding to a prolate (i. e., elongated) cluster and one structure with  $C_{6v}$  symmetry. The qualitative agreement between theory and experiment is very good with respect to the position and the shape of the peak for the prolate  $\text{Na}_{21}^+$ .

In summary, I have presented an approach to compute the absorption and quasiparticle spectra for finite systems based on a linear response theory for the dynamical electron-hole coherences in the presence of an external field. Using a quasiparticle ansatz in the quantum kinetic equation for the electron-hole coherence, which includes HF and scattering contributions, allows us to derive a Bethe-Salpeter equation for the electron-hole correlation function with a complex, frequency-dependent kernel yielding the scattering (or correlation) contributions to the electron-hole coherence dynamics.

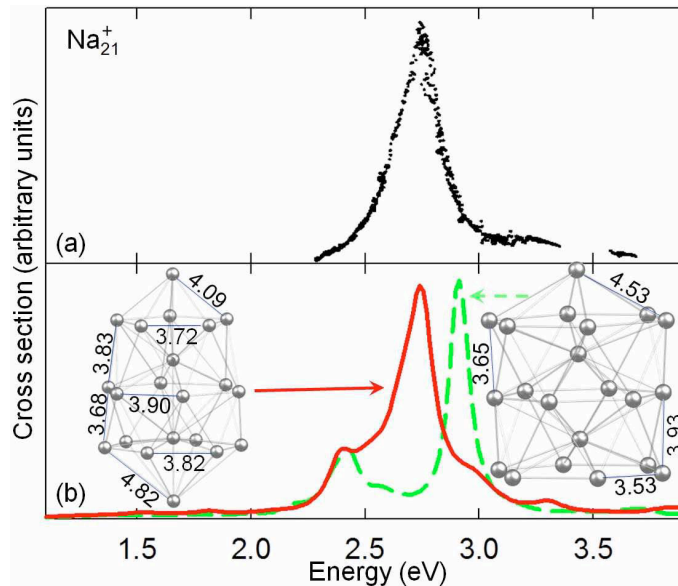


Figure 4.3: Measured (a) and computed (b) absorption cross section for  $\text{Na}_{21}^+$ . The experimental result is adapted from Ref. [108]. The theoretical spectra are calculated for the prolate cluster (solid line), and the structure with  $C_{6v}$  symmetry (dashed line). The insets show the cluster geometries with distances in Å.

### 4.3 Positive definite approximations

In Section 2.2 I have already emphasized the asymptotic character of perturbative expansions. Important observation was made for the electron gas by Minnhagen [109]. He noticed that the straightforward inclusion of vertex corrections beyond the  $GW$  level leads to negative spectral densities in some frequency regions. Such unpleasant property is not limited to the electron gas as it has also been observed in a study of vertex corrections in finite systems [110, 111]. This deficiency not only prohibits the usual probability interpretation of the spectral function but also generates Green's functions with the wrong analytic properties. In particular the latter feature prevents an iterative self-consistent solution of the Dyson equation since the analytic properties deteriorate with every self-consistency cycle. This problem was circumvented in Sec. 2.2 by performing calculations in the frequency domain where perturbative expansions are known to converge and by making an analytic continuation using the Padé approximation.

The non-positivity of spectral functions is not pertinent to single-particle properties. Starting from Hubbard [112] who introduced what is now known as the *local field factor*, numerous works were devoted to the diagrammatic computations of the density response function [1]. In a full generality the frequency dependent first-order results were obtained by Holas, Aravind, and Singwi [113]. In Fig. 4.4 we depict its momentum and energy resolved spectral function computed according to their expression. The pink shaded area denotes a part of the particle-hole continuum where the 1st order spectral function is negative. This fact again prevents any self-consistent calculations where screening is treated beyond RPA. To resolve this issue we first inspect the positivity property of exact correlators and use this fact to modify MBPT to generate positive definite approximations.

### Positivity of the exact self-energy and response function

From the Dyson equation on the Keldysh contour one can show [89] that in equilibrium following relations hold:

$$G^{\lessgtr}(\omega) = G^R(\omega)\Sigma^{c,\lessgtr}(\omega)G^A(\omega), \quad (4.30)$$

where  $\Sigma^c$  is the correlation self-energy. Since  $G^A(\omega) = [G^R(\omega)]^\dagger$  the PSD of  $\mp iG^{\lessgtr}$  implies that  $\mp i\Sigma^{c,\lessgtr}$  is PSD and vice versa. The PSD property of the exact  $i\chi^{\lessgtr}(\omega)$  is manifested from the Lehmann representation of this quantity. It is instead less obvious to prove the PSD property from the diagrammatic expansion. Here we provide such a proof and bring to light a diagrammatic structure which forms the basis of a general scheme to construct PSD approximations.

Consider for definiteness a  $\mathcal{F}^<$  correlator (4.4), the same reasoning applies to  $\mathcal{F}^>$ . We can use the standard assumption of the zero-temperature Green's function formalism that  $\Psi_0$  can be obtained by evolving backward the noninteracting ground state  $\Phi_0$  from a distant future time  $\tau$  (with  $\tau \rightarrow \infty$ ) to the arbitrary initial time  $t_0$  using an interaction which is switched-on adiabatically. Eq. (4.4) becomes (the limit  $\tau \rightarrow \infty$  is implied)

$$\mathcal{F}^<(1, 2) = i \left[ \sum_i \langle \Phi_0 | \hat{U}(\tau, t_2) \hat{f}^\dagger(\mathbf{x}_2) \hat{U}(t_2, \tau) | \chi_i \rangle \langle \chi_i | \hat{U}(\tau, t_1) \hat{f}(\mathbf{x}_1) \hat{U}(t_1, \tau) | \Phi_0 \rangle \right]_{\text{irr}}. \quad (4.31)$$

Here we inserted a completeness relation  $\sum_i |\chi_i\rangle\langle\chi_i| = 1$  (the sum runs over all states  $\chi_i$  in Fock space) and used the group property  $\hat{U}(t_1, t_0)\hat{U}(t_0, \tau) = \hat{U}(t_1, \tau)$  and  $\hat{U}^\dagger(t_0, \tau)\hat{U}(t_0, t_2) = \hat{U}^\dagger(\tau, t_2)$ . Let  $\hat{\mathcal{C}}_i$  denote an operator acting on the noninteracting ground state and producing the intermediate states, i. e.,  $|\chi_i\rangle = \hat{\mathcal{C}}_i|\Phi_0\rangle$ . It can be expanded in terms of the annihilation and creation operators. The intermediate states differ by the number of holes ( $M$ ) and

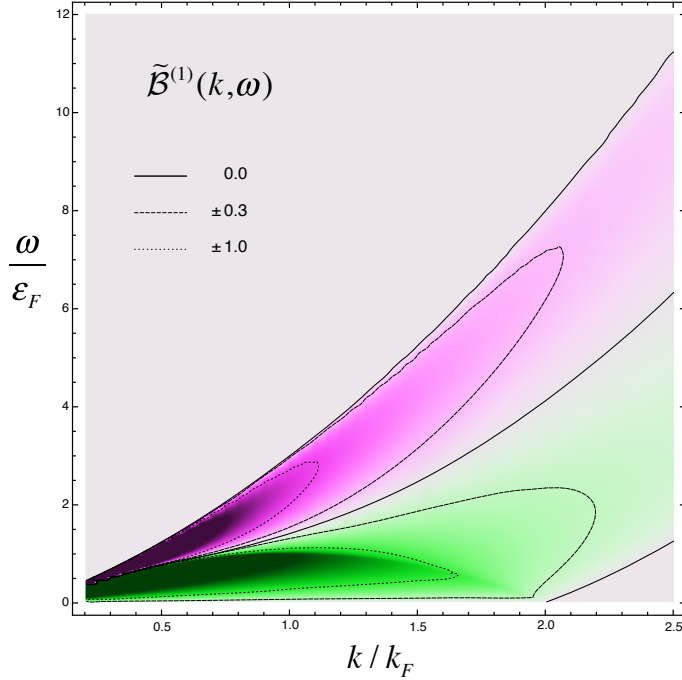


Figure 4.4: (Color online) Distribution of positive (green) and negative (pink) values of the first order spectral function in  $k - \omega$  plane.



particles ( $N$ ) they contain with respect to the ground state  $\Phi_0$

$$\hat{\mathcal{C}}_i |\Phi_0\rangle = \hat{c}_{q_N}^\dagger \dots \hat{c}_{q_1}^\dagger \hat{c}_{p_M} \dots \hat{c}_{p_1} |\Phi_0\rangle \equiv |\chi_{pq}^{(N,M)}\rangle. \quad (4.32)$$

Relation between  $N$  and  $M$  is fixed by the nature of operators  $\hat{f}$  in the correlator. For example, for self-energy we have  $M = N + 1$  (cf. Eq. 3.10), and for the density response  $M = N$  (cf. Eq. 3.11). With these definitions the completeness relation reads

$$\sum_i |\chi_i\rangle \langle \chi_i| \rightarrow \sum_{N=0}^{\infty} \frac{1}{M!N!} \sum_{pq} |\chi_{pq}^{(N,M)}\rangle \langle \chi_{pq}^{(N,M)}| = \hat{I}. \quad (4.33)$$

Defining the amplitudes

$$\begin{aligned} S_{pq}^{(N,M)*}(1) &\equiv \langle \chi_{pq}^{(N,M)} | \hat{U}(\tau, t_1) \hat{f}(\mathbf{x}_1) \hat{U}(t_1, \tau) | \Phi_0 \rangle, \\ S_{pq}^{(N,M)}(2) &\equiv \langle \Phi_0 | \hat{U}(\tau, t_2) \hat{f}^\dagger(\mathbf{x}_2) \hat{U}(t_2, \tau) | \chi_{pq}^{(N,M)} \rangle, \end{aligned}$$

the lesser correlator takes the following compact form

$$\mathcal{F}^<(1, 2) = i \left[ \sum_{N=0}^{\infty} \frac{1}{M!N!} \sum_{pq} S_{pq}^{(N,M)}(2) S_{pq}^{(N,M)*}(1) \right]_{\text{irr}}. \quad (4.34)$$

The adiabatic assumption implies that turning the interaction slowly on and off the state  $\Phi_0$  changes at most by a phase factor:  $\hat{U}(\tau, -\tau) |\Phi_0\rangle = e^{i\alpha} |\Phi_0\rangle$ . Hence we can rewrite the amplitudes as

$$\begin{aligned} S_{pq}^{(N,M)*}(\mathbf{x}_1 t_1) &= \frac{\langle \Phi_0 | \mathcal{T} \{ e^{-i \int_{-\tau}^{\tau} d\bar{\tau} \hat{H}(\bar{\tau})} \hat{c}_{p_1}^\dagger(\tau^+) \dots \hat{c}_{p_M}^\dagger(\tau^+) \hat{c}_{q_1}(\tau) \dots \hat{c}_{q_N}(\tau) \hat{f}(\mathbf{x}_1 t_1) \} | \Phi_0 \rangle}{\langle \Phi_0 | \mathcal{T} \{ e^{-i \int_{-T}^T d\bar{\tau} \hat{H}(\bar{\tau})} \} | \Phi_0 \rangle}, \\ S_{pq}^{(N,M)}(\mathbf{x}_2 t_2) &= \frac{\langle \Phi_0 | \bar{\mathcal{T}} \{ e^{i \int_{-\tau}^{\tau} d\bar{\tau} \hat{H}(\bar{\tau})} \hat{f}^\dagger(\mathbf{x}_2 t_2) \hat{c}_{q_N}^\dagger(\tau) \dots \hat{c}_{q_1}^\dagger(\tau) \hat{c}_{p_M}(\tau^+) \dots \hat{c}_{p_1}(\tau^+) \} | \Phi_0 \rangle}{\langle \Phi_0 | \bar{\mathcal{T}} \{ e^{i \int_{-\tau}^{\tau} d\bar{\tau} \hat{H}(\bar{\tau})} \} | \Phi_0 \rangle}, \end{aligned}$$

with  $\mathcal{T}$  and  $\bar{\mathcal{T}}$  the time-ordering and anti-time-ordering operators respectively. The time argument in the fermion creation and annihilation operators specifies the position of the operators on the time axis, and  $\tau^+$  denotes a time infinitesimally larger than  $\tau$ . Thus,  $S^{(N,M)*}$  and  $S^{(N,M)}$  have a typical form of interacting time-ordered, anti-time-ordered Green's functions, respectively. Hence they can be expanded diagrammatically using Wick's theorem [114]. An example of  $S$ ,  $S^*$  diagrams for the self-energy is illustrated in Fig. 4.5 and resembles half a  $\Sigma$  diagram. The left-half corresponds to  $S^{(N,M)*}$  with lines given by noninteracting time-ordered Green's functions  $g^{--}$  whereas the right-half corresponds to  $S^{(N,M)}$  with lines given by noninteracting anti-time-ordered Green's functions  $g^{++}$ .

It is now easy to show that  $i\mathcal{F}^<(\omega)$  is PSD. By Fourier transforming  $S$  with respect to  $t_2$  and  $S^*$  with respect to  $t_1$  we find (omitting the dependence on the spatial and spin variables)

$$i\mathcal{F}^<(t_1, t_2) = \sum_{N=1}^{\infty} \frac{1}{M!N!} \int \frac{d\omega}{2\pi} \frac{d\omega'}{2\pi} e^{-i\omega t_2 + i\omega' t_1} \sum_{pq} S_{pq}^{(N,M)}(\omega) S_{pq}^{(N,M)*}(\omega'). \quad (4.36)$$

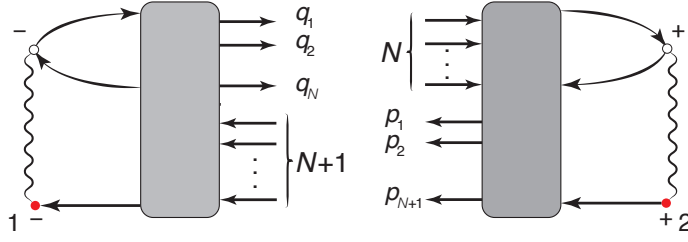


Figure 4.5: Diagrammatic structure of the functions  $S(1)$  and  $S^*(2)$  for the lesser self-energy. The external vertex points 1 and 2 have times on the  $-$  and  $+$  branch respectively. Green's functions are denoted by the lines with arrows, while wavy lines correspond to the bare interparticle interaction.

In equilibrium  $i\mathcal{F}^<$  is invariant under time translations, i. e., it depends on  $t_1 - t_2$  only. Imposing time translational invariance on the r.h.s. leads to

$$\sum_{N=1}^{\infty} \frac{1}{M!N!} \sum_{\underline{pq}} S_{\underline{pq}}^{(N,M)}(\omega) S_{\underline{pq}}^{(N,M)*}(\omega') = \mathcal{F}(\omega)\delta(\omega - \omega') \quad (4.37)$$

with  $\mathcal{F}$  some matrix function of the frequency  $\omega$ . Since for  $\omega = \omega'$  the l.h.s. is a sum of PSD matrices we conclude that  $\mathcal{F}$  is PSD. Inserting Eq. (4.37) back into Eq. (4.36) we see that  $\mathcal{F}(\omega)$  is the Fourier transform of  $i\mathcal{F}^<$  which, therefore, is PSD too.

In more general terms Eq. (4.37) tells us that  $i\mathcal{F}^<$  correlator (4.4) can be written in the Fermi Golden rule form (3.5). In Ref. [8] rules are formulated to turn an arbitrary diagrammatic approximation into PSD form. It rests on the following observations (We consider again only the case of lesser correlators. Greater correlators can be treated similarly.):

- For each diagram forming an approximation for  $\mathcal{F}^<$  specify position on the Keldysh contour for each vertex. This amounts to distributing pluses (time arguments on the backward branch) and minuses (forward branch) among the vertices. It can be shown that isolated islands of pluses or minuses are not permitted.
- In this way a lesser diagram corresponds to the sum of all possible *partitions* such as shown at Fig. 4.6.
- Each partition consists of two halves with internal time-vertices on opposite branches of the Keldysh contour.
- Analyze the full set of half-diagrams and amend it in such a way that the correlator can be represented as a sum of squares, i. e. in the form (4.37).

A requirement that the resulting approximation contains a *minimal set* of diagrams makes the treatment rather involved. Therefore, in the next section we only present results of such an analysis for the second-order self-energy.

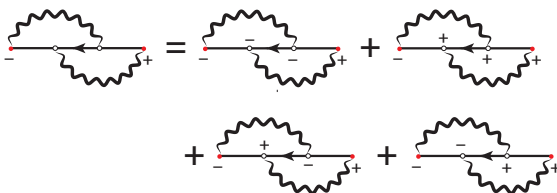


Figure 4.6: Next to leading order self-energy in the screened interaction  $W$ . Since  $W$  is non-local in time, the thick wavy lines denoting the screened interaction can connect points on different branches of the Keldysh contour.

## Vertex corrections in the homogeneous electron gas

Application of the rules to the full first and second order self-energy leads to PSD self-energy containing terms of the third and fourth orders. The numerical implementation of them is rather demanding. We observe, however, that the exclusion of the last two partitions of Fig. 4.6 leads to a much simpler PSD self-energy shown in Fig. 4.7 (*Left*). This self-energy too goes beyond the *GW* approximation, but the vertex correction is only partial.

We evaluate these diagrams for the 3d HEG using the analytical frequency and numerical Monte-Carlo momentum integrations, Fig. 4.7 (*Right*). The method was developed in Ref. [2], however, the analytical frequency integration part had to be substantially extended. As expected, the rate operator is everywhere positive despite a large negative contribution of the second order term. We notice an almost complete cancellations of different order terms beyond the singularities, i. e.  $\omega > \epsilon_k + \Omega(0)$  for particle ( $k > k_F$ ) and  $\omega < \epsilon_k - \Omega(0)$  for hole ( $k < k_F$ ) states, where  $\Omega(0)$  is the plasmon energy in the long wave-length limit. High accuracy of the Monte-Carlo integration was required to get the cancellations properly. This is especially important at metallic densities where different orders have comparable contributions. Due to the density scaling the first order self-energy ( $\sim \alpha r_s$ ) becomes dominant at large densities ( $r_s \rightarrow 0$ ), while the third order ( $\sim (\alpha r_s)^3$ ) is largest in the correlated low density regime ( $r_s \rightarrow \infty$ ).

In summary, in standard MBPT approximations the straightforward inclusion of vertex corrections inevitably ruin the PSD property and, hence, our additional diagrams must be included. Remarkably, these diagrams are of higher order. For instance, the inclusion of the *full first-order vertex* leads to diagrams of the fourth order in the screened interaction. Required computational power to numerically evaluate them is immense. Fortunately, excluding some partitions allows us to construct an approximation containing diagrams of maximally third order. They are feasible for numerics as our calculations for the 3d HEG demonstrate. Even though we only presented in detail the formalism for the spectral function, the same ideas apply to the spectrum of the density response function [115].

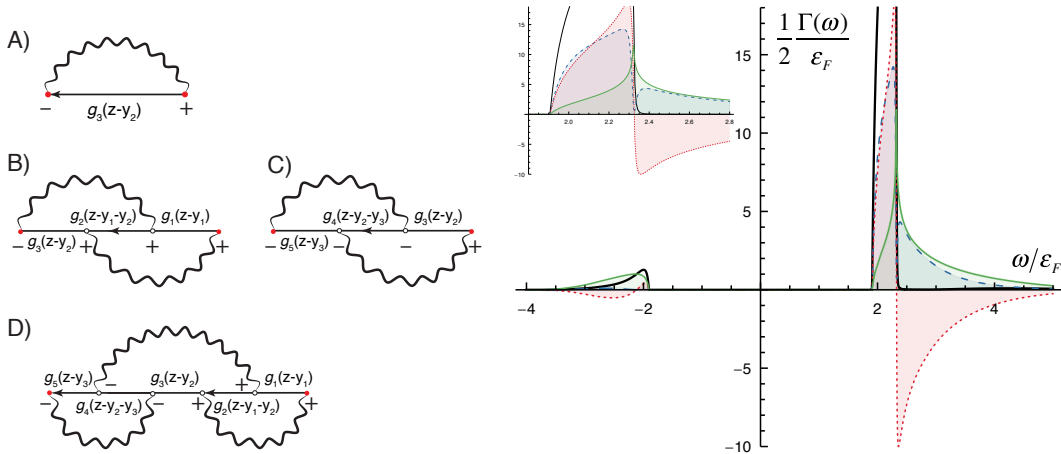


Figure 4.7: *Left*: Leading order beyond-*GW* self-energy with the PSD property. Thick wavy lines denote the screened Coulomb interaction in the random phase approximation. *Right*: The rate operator  $\frac{1}{2}\Gamma(k, \omega) = -\text{Im} \Sigma^R(k, \omega)$  of the homogeneous electron gas at the density of  $r_s = 4$  and  $k = 1.2k_F$  (the energy  $\omega$  is measured with respect to  $\mu$ ). Different line-styles denote contributions of different orders: full, dotted and dashed lines stand for first, second and third order, respectively. Thick solid line denotes the sum of all contributions. The inset magnifies the region of the logarithmic singularity. Notice the almost complete cancellation of  $\Sigma^{c,>}(k, \omega)$  for  $\omega > \epsilon_k + \Omega(0)$ .

#### 4.4 Processes involving emission of particles

Scattering experiments deliver the most detailed information on the structure of matter. For instance, the fully resolved spectra of an electron emitted from an electronic system upon photon or particle impact encode the spin and momentum-resolved spectral properties of the sample [116–120]. For direct information on the two-particle properties the detection of a correlated electron pair is necessary which is usually performed in a one-photon double-electron emission [119] or in a swift particle-impact double-electron emission experiment [121].

*Initial state preparation:* Let the wave-function  $|\Psi_0\rangle$  and corresponding energy  $E_0$  be the quantum state of a target with the Hamiltonian  $\hat{H}$  in remote past ( $t = -\infty$ ). We will use the letters ( $abcd$ ) for general orbitals, ( $ijnm$ ) for bound orbitals and bold-face letters for continuum states. When the system is perturbed by the interaction with external fields it evolves to a new state. As a typical mechanism we consider here the light-matter interaction

$$\hat{\phi}(t) = (\hat{\Delta}e^{-i\omega t} + \hat{\Delta}^\dagger e^{i\omega t})e^{\eta t}, \quad \hat{\Delta} = \sum_{ab} \Delta_{ab} \hat{c}_a^\dagger \hat{c}_b. \quad (4.38)$$

In this expression  $\hat{\phi}(t)$  is adiabatically turned on allowing to introduce a typical interaction time  $\sim (2\eta)^{-1}$ . The form (4.38) permits generalizations such as the process of impact ionization caused a projectile particle (e. g. an electron distinguishable from electrons of the system) impinging on the target system.

From the first-order time-dependent perturbation theory we obtain the *approximate* eigenstate  $|\tilde{\Psi}^{(+)}\rangle$  of the full Hamiltonian  $\hat{H} + \hat{\phi}(t)$  at time  $t = 0$ :

$$|\tilde{\Psi}^{(+)}\rangle = |\Psi_0\rangle + \lim_{\eta \rightarrow 0} \frac{1}{E_0 + \omega - \hat{H} + i\eta} \hat{\Delta} |\Psi_0\rangle. \quad (4.39)$$

*Observables:* Assuming we know the quantum state of the target at  $t = 0$  some observables can be computed. Since we are interested in photoemission these are the expectation values of the current operators. The one-electron current  $J_{\mathbf{k}}$  (as in the single photoemission (SPE) experiment) is defined as the number of electrons  $N_{\mathbf{k}}$  with a given momentum  $\mathbf{k}$  outside the target divided by the effective interaction time  $(2\eta)^{-1}$ . There is a detailed discussion [93] on why electrons in the sample give a negligible contribution to the current. Same arguments are valid for the two-electron case. Thus, we analogically define the two-electron current (double photoemission (DPE) experiment) as

$$J_{\mathbf{k}_1, \mathbf{k}_2} = \lim_{\eta \rightarrow 0} 2\eta \langle \hat{N}_{\mathbf{k}_1} \hat{N}_{\mathbf{k}_2} - \delta_{\mathbf{k}_1, \mathbf{k}_2} \hat{N}_{\mathbf{k}_1} \rangle. \quad (4.40)$$

In the expression above (and all subsequent derivations) we do not explicitly spell out the spin quantum numbers. The dependence on the spin can be recovered by substituting the continuum quantum numbers like  $\mathbf{k}$  by  $\mathbf{k}\sigma$  (likewise for bound indices). The second term excludes the one-electron current in the case when two momenta are equal. Eq. (4.40) gives access to the differential cross-section through the following relation:

$$\frac{d^2\sigma}{d\mathbf{k}_1 d\mathbf{k}_2} = \frac{\omega}{I} J_{\mathbf{k}_1, \mathbf{k}_2}, \quad (4.41)$$

where  $I/\omega$  is the photon flux density [122]. For the velocity gauge  $\hat{\Delta} = \frac{1}{c}\mathbf{A}_0 \cdot \hat{\mathbf{p}}$ ,  $I = \frac{\omega^2 A_0^2}{2\pi c}$ , where  $\mathbf{A}_0$  is the amplitude of the vector potential.

The average in Eq. (4.40) is performed over the perturbed state (4.39):

$$J_{\mathbf{k}_1, \mathbf{k}_2} = \lim_{\eta \rightarrow 0} 2\eta \left\langle \Psi_0 \left| \hat{\Delta}^\dagger \frac{1}{E_0 + \omega - \hat{H} - i\eta} \hat{c}_{\mathbf{k}_1}^\dagger \hat{c}_{\mathbf{k}_2}^\dagger \hat{c}_{\mathbf{k}_2} \hat{c}_{\mathbf{k}_1} \frac{1}{E_0 + \omega - \hat{H} + i\eta} \hat{\Delta} \right| \Psi_0 \right\rangle, \quad (4.42)$$

where we used the usual anti-commutation relations for the fermionic operators. The current is quadratic in  $\hat{\Delta}$  or linear in the number of absorbed photons. The first order in  $\hat{\Delta}$  gives the linear conductivity current and is of no interest here [96].

*Final state specification:* Equation (4.42) describes all possible processes leading to the emission of two-electrons including those in which the target is left in an unbound state, i. e. emission of more than two particles. They have to be excluded by the assumption  $\hat{c}_{\mathbf{k}} |\Psi_\beta^{2+}\rangle = 0$ , where  $\Psi_\beta^{2+}$  is the state of the system after the ionization event. One can show that it imposes following restrictions on the Green's functions:

$$G_{\mathbf{k}a}^<(\omega) = 0, \quad G_{\mathbf{k}a}^>(\omega) = 0, \quad (4.43)$$

$$\lim_{r_1 \rightarrow \infty} G^<(x_1 t_1, x_2 t_2) = \lim_{r_1 \rightarrow \infty} G^<(x_2 t_2, x_1 t_1) = 0. \quad (4.44)$$

These conditions are important when treating photoemission diagrammatically.

## Diagrammatic approach

Eq. (4.42) when transformed to the time domain gives rise to the ground state correlator:

$$Z(t, t') = \langle \Psi_0 | \hat{c}_b^\dagger(t) \hat{c}_a(t) \hat{c}_{\mathbf{k}_1}^\dagger(0) \hat{c}_{\mathbf{k}_2}^\dagger(0) \hat{c}_{\mathbf{k}_2}(0) \hat{c}_{\mathbf{k}_1}(0) \hat{c}_c^\dagger(t') \hat{c}_d(t') | \Psi_0 \rangle, \quad (4.45)$$

where the field operators are in the Heisenberg representation and  $t, t' \in (-\infty, 0]$  are *physical* times. For clarity, we omitted the indices in the notation of the correlator. It can be evaluated diagrammatically by adiabatically switching on the interaction in the remote past, i. e.  $\hat{H}_\delta = \hat{H}_0 + e^{-\delta|t|} \hat{H}_1$ . Now the average is performed over the non-interacting ground state  $|\Phi_0\rangle$  and the times  $t_2^- < t_1^+$  lie on forward, backward branches of Keldysh contour  $\gamma$  (Fig. 4.1), respectively:

$$Z(t, t') = \langle \Phi_0 | \mathcal{T} \left\{ e^{-i \int_\gamma \hat{H}_\delta(t) dt} \hat{c}_b^\dagger(t_+) \hat{c}_a(t_+) \times \hat{c}_{\mathbf{k}_1}^\dagger(0) \hat{c}_{\mathbf{k}_2}^\dagger(0) \hat{c}_{\mathbf{k}_2}(0) \hat{c}_{\mathbf{k}_1}(0) \hat{c}_c^\dagger(t'_-) \hat{c}_d(t'_-) \right\} | \Phi_0 \rangle. \quad (4.46)$$

$\mathcal{T}$  here is the usual contour ordering operator [89] with the order relation  $\prec$ .  $\hat{H}_\delta$  is such that it is equal to the Hamiltonian of noninteracting system  $\hat{H}_0$  in the remote past and is identical to  $\hat{H}$  at  $t = 0$ . Notice that it is different from adiabatic switching on of the electromagnetic field in Eq. (4.39).  $|\Phi_0\rangle$  is the ground state of  $\hat{H}_0$ . Using Wick's theorem we can contract the product of field operators in order to express the correlator in terms of products of single-particle Green's functions. Zeroth order obviously yields four fermionic lines. However, if we use restrictions (4.43) any zeroth order diagram vanishes. This is easy to understand

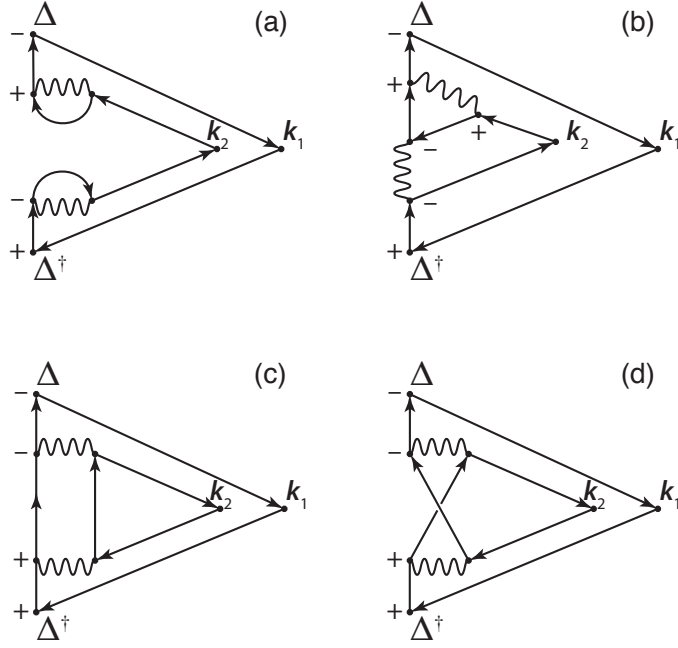


Figure 4.8: Second order diagrams (in bare Coulomb interaction) representing the DPE process. Notice that not all combinations of pluses and minuses are possible because Coulomb interaction can only connect vertices on the same branch of the Keldysh contour. (a) Diagram vanishes according to the assumption (4.43) for dressed GFs. (b) Diagram vanishes because it contains an isolated island of minuses. (c) and (d) are the lowest order non-zero diagrams. The remaining two are obtained by permuting  $\mathbf{k}_1$  and  $\mathbf{k}_2$ .

by comparing with SPE case. There, no-zero contributions are coming from the following contraction:

$$\langle \hat{c}_b^\dagger(t_+) \hat{c}_a(t_+) \overbrace{\hat{c}_p^\dagger(0) \hat{c}_p(0)} \overbrace{\hat{c}_c^\dagger(t'_-) \hat{c}_d(t'_-)} \rangle.$$

This is the only combination that results in greater GFs when one of the arguments is a scattering state (and is compatible with (4.43)). In particular, the above contraction equals to

$$g_{ap}^>(t) g_{db}^<(t' - t) g_{pc}^>(-t').$$

In DPE two creation operators with continuum state indices need to be contracted with two annihilation operators on the positive track. However, there is only one such operator. Hence, 0th order in interaction is zero. The argument that excludes the first order diagram is slightly different and is based on the fact that bare interaction is instantaneous, i. e. corresponding time-arguments necessarily lie on the same, positive or negative, track.

Second order non-vanishing contributions contain products of two Coulomb interaction operators (e. g. at contour times  $\bar{t}_+$  and  $\bar{t}_-$ ) and already a familiar product of six operators as in Eq. (4.46). From all possible contractions (they yield eight fermionic lines) we have to exclude many terms. Some of them immediately vanish because of the assumption (4.43) for non-interacting GF. Others, represent the Hartree-Fock renormalization of two fermionic lines and likewise vanish because of the same assumption for the full fermionic propagators (Fig. 4.8 (a)). Then, there are diagrams (Fig. 4.8 (b)) containing isolated islands of pluses and minuses which also vanish because otherwise the two-particle current cannot be written in the Fermi Golden rule form, see Sec. 4.3 and Ref. [8]. Finally, there are only four direct and eight exchange non-zero diagrams. Two of them are depicted at Fig. 4.8 (c,d).

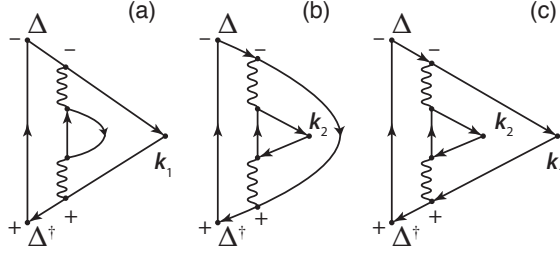


Figure 4.9: Diagrams for the plasmon assisted photoemission. SPE setup: only the primary (a), secondary electron (b) is observed, the fate of another electron is not specified. (c) DPE setup: both, primary and secondary electrons are observed in coincidence.

### Example of plasmon assisted DPE

As an example we consider the processes depicted in Fig. 4.9. The diagrams show a very common situation where a primary electron excited by the laser pulse is losing its energy on the way to the detector by exciting a secondary electron (the so-called extrinsic energy loss [97, 123, 124]). There could be either bare or screened Coulomb interaction between the two electrons. In the latter case some resonant phenomena related to the excitation of e. g. plasmon are expected. The SPE case (Figs. 4.9 (a, b)) is identical to the process of secondary electron excitation considered by Caroli *et al.* [96]. All DPE processes covered by the diagram at Fig. 4.9 (c) form a subset of the SPE process. The only difference between the two scenarios is whether primary, secondary or both electrons are observed in the detector. Using energy flows as shown in Fig. 4.10 (*Left*) the following expression for the two-particle current is obtained

$$\begin{aligned}
 J_{\mathbf{k}_1\mathbf{k}_2} &= 2\pi \int_{-\infty}^{\mu} \frac{d\zeta}{2\pi} \int_{-\infty}^{\mu} \frac{d\bar{\zeta}}{2\pi} \int_0^{\infty} \frac{d\xi}{2\pi} \delta(\xi + \varepsilon_{\mathbf{k}_1} - \omega - \zeta) \delta(\varepsilon_{\mathbf{k}_2} - \xi - \bar{\zeta}) \\
 &\times \int d(xx'zz') \langle \chi_{\mathbf{k}_1}^{(-)} | x' \rangle W_{z'x'}^{--}(\xi) W_{xz}^{++}(\xi) \langle x | \chi_{\mathbf{k}_1}^{(-)} \rangle \\
 &\times \langle \chi_{\mathbf{k}_2}^{(-)} | z' \rangle A_{z'z}(\bar{\zeta}) \langle z | \chi_{\mathbf{k}_2}^{(-)} \rangle \left[ G^{--}(\omega + \zeta) \hat{\Delta} A(\zeta) \hat{\Delta}^\dagger G^{++}(\omega + \zeta) \right]_{x'x}, \quad (4.47)
 \end{aligned}$$

where  $A(\zeta)$  is the spectral function and  $\chi_{\mathbf{k}}^{(-)}$  is the one-electron scattering function with asymptotic momentum  $\mathbf{k}$  that fulfills incoming boundary conditions. We evaluate this equation for a spherically symmetric jellium model of the  $C_{60}$  molecule [86, 125]. The optical response of this system is dominated by the plasmon resonance at  $\omega_p \sim 22$  eV. Therefore, a strong modification of the double photoemission due to the excitation of this mode can be expected. This is indeed the case as comparison of bare Coulomb, plasmonic and total contributions shows, Fig. 4.10 (*Right*). Our results also show excellent agreement with a coincidence DPE experiment performed on the surface-deposited  $C_{60}$  molecule [126].

In summary, we derive the diagrammatic expansions for one- and two-particle currents starting from the time-dependent perturbation theory and using the adiabatic switching of the electron-electron interaction. Hence, we have electromagnetic field switched on at the remote past (as  $e^{t'}$ ) and independently adiabatically switched on the interaction such that the total Hamiltonian takes a form  $\hat{H}_\delta = \hat{H}_0 + e^{-\delta|t|} \hat{H}_1$ . The diagrammatic structure of one- and two-particle currents is surprisingly simple: one starts with the density-density response function  $\chi^<$  which necessarily contains two blocks associated with the forward (“-”) and backward (“+”) parts of the Keldysh contour. Requesting that one or two lines flowing from “-” to “+” blocks are associated with scattering states (with momenta  $\mathbf{k}_i$ ) one obtains exactly the diagrams for SPE and DPE currents showing the close connection between these types of light-matter interaction. It is not difficult to generalize this approach to an arbitrary number of particles. Finally, we presented a detailed analysis of the plasmon-assisted DPE and showed that if one of the emitted particles is unobserved, its diagrammatic representation reduces to the one describing external losses in the SPE process considered

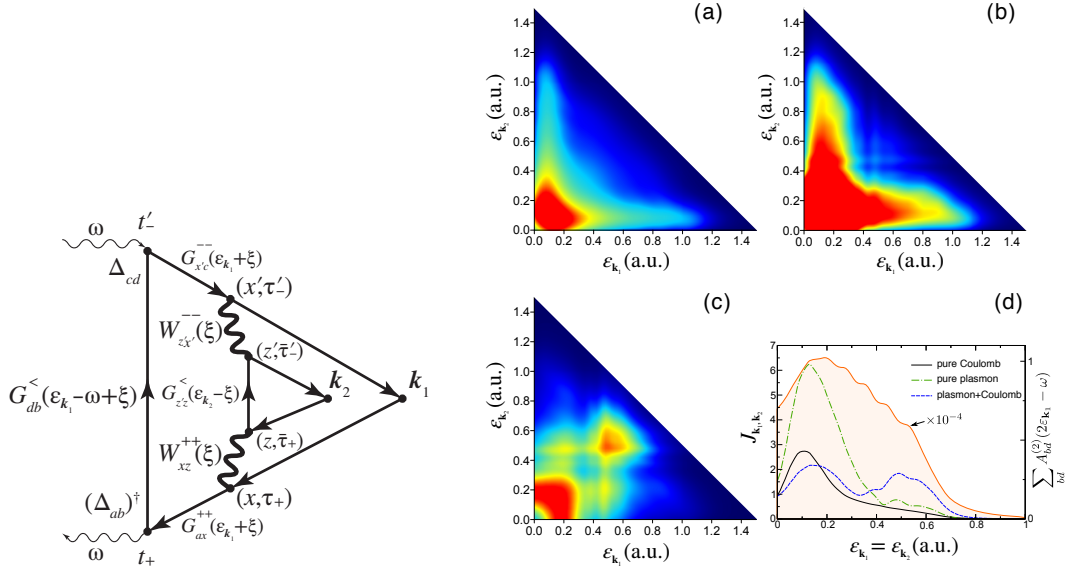


Figure 4.10: *Left*: Energy flows DPE diagram describing a related plasmon assisted process. *Right*: The symmetrized two-electron current as a function of the photoelectron energies (energy-sharing diagram) for typical parameters:  $\omega = 2.0$  and  $\omega_p = 0.8$ . (a) The process is mediated by the pure Coulomb interaction. (b) Pure plasmonic contribution. (c) Total (bare Coulomb and plasmonic contributions) signal including the interference terms. (d) Equal energy sharing ( $\epsilon_{k_1} = \epsilon_{k_2}$ ) for the current and trace of the two-particle spectral density (shaded curve).

by Caroli *et al.* [96]. Plasmon pole approximation was employed to derive computationally manageable expressions which were applied to the simple and yet realistic jellium model of the  $C_{60}$  molecule.



## 5 Classical and semi-classical approaches

---

The dielectric response of electronic matter encoded in the *density-density response function*  $\chi(\mathbf{r}, \mathbf{r}'; \omega)$  is a key quantity for a wide range of phenomena including the energy  $\omega$  and momentum  $\mathbf{k}$  exchange with a traversing particle and the refraction and absorption of light. Recent reviews on the interaction of nanoparticles with light [127] or electrons [128] provide an overview on these topics including the relevance for the nanotechnology and plasmonics. In the previous chapters I have presented the diagrammatic and configuration interaction approaches to the computation of dielectric response. They can efficiently be applied to either homogeneous systems or finite systems containing just a small number of electrons. However, in many relevant experimental situations such as nanoplasmonics a typical system does not fall in either category. Even though the size of a system does not permit a quantum-mechanical treatment gross features of its density-density response can be captured by the *semi-classical approximation*. The time-dependent density functional theory provides an exact relation between the density-density response function and the Kohn-Sham response function  $[\chi(\mathbf{r}, \mathbf{r}', \omega)]^{-1} = [\chi^{(0)}(\mathbf{r}, \mathbf{r}', \omega)]^{-1} - v(\mathbf{r} - \mathbf{r}') - f_{xc}(\mathbf{r}, \mathbf{r}', \omega)$ , where the non-local *exchange-correlation kernel*  $f_{xc}(\mathbf{r}, \mathbf{r}', \omega)$  plays a crucial role [59]. For vanishing exchange correlation kernel the theory reduces to random phase approximation for the Kohn-Sham ground state. In the long range limit it is nothing else as the classical theory of the collective oscillations.

There is a lot subtleties in going from the density-density response to realistic observables such as linear and non-linear optical cross-sections. I illustrate these technicalities by computing the angular resolved second harmonic generation from spherical particles (Sec. 5.1). The effect—nonlinear Mie scattering from spherical particles [10]—is very interesting from theoretical point of view and has a lot of practical applications [129]. Since SHG response from centrosymmetric systems is forbidden within the electric dipole approximation, its description must involve a *nonlocal* electron response to an external electrical field [130]. Our theory rests on the surface sheet model which assumes inversion symmetry breaking on the surface of a sphere. Thus, the system is characterized by just few material constants. In the following sections another step towards *ab initio* description of nanosystems is made: I will show how the theory can be further generalized to include all kinds of many-body effects beyond the random phase approximation (Sec. 5.2) and how the linear and non-linear optical responses can be computed starting from the *ground state electron density* and its gradient [11, 12] (Sec. 5.3).

### 5.1 Nonlinear Mie scattering from spherical particles

We describe second harmonic generation (SHG) from spherical particles using a classical electrodynamics approach. Although it is well known that SHG response from centrosymmetric systems is forbidden within the electric dipole approximation I show how the inver-

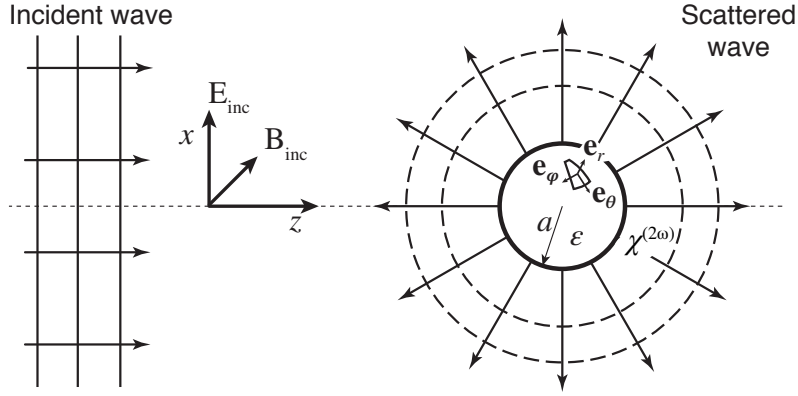


Figure 5.1: Scattering of light by a sphere. The sphere of radius  $a$  is characterized by the dielectric constants at fundamental and double frequency  $\epsilon(\omega)$ ,  $\epsilon(2\omega)$  respectively, and by the tensor of surface second-order nonlinear susceptibility  $\chi^{(2\omega)}$ .

sion symmetry breaking on the surface of a sphere leads to this nonlinear optical process. Presented theoretical analysis unifies existing theories which are valid in the special cases of small particle size (Rayleigh limit), small refractive index [131, 132], radiation by non-local dipole and quadrupole moments [130] and constitutes a non-linear generalization of the linear Mie theory. Since the original publication the method was extended by several authors: de Beer and Roke included the sum-frequency generation mechanism into the considerations [133], the cylindrical geometry was treated by Dadap [134] and finally the theory for arbitrarily shaped particles was developed by de Beer, Roke, and Dadap [135]. In turn, I will present a generalization to include quantum mechanical and many-body effects in Sec. 5.2 and illustrate the method with a realistic example in Sec. 5.3.

Already on classical level important observations can be made: absence of signal in the strict forward  $\theta = 0^\circ$  and backward  $\theta = 180^\circ$  directions, shape resonance phenomena leading to the SH intensity oscillations as a function of size parameter  $ka$ , existence of the transition regime between Rayleigh and Mie theories, interference between different multipole contributions leading to peaks in angular distributions. These findings were confirmed in numerous experimental works [136–139].

## Theory

Let us consider the scattering geometry of the problem as shown on Fig. 5.1. The theory consists of three steps as follows.

*Firstly*, we solve a problem of the electromagnetic field scattering by a sphere (Mie theory) in order to find electric fields close to its surface. We represent the electric and the magnetic fields as expansions in terms of *vector spherical harmonics*<sup>1</sup>:

$$\mathbf{E}_i = \frac{1}{2} \sum_{l,m} C(l) \left[ a_{(l,m)}^i f_l^{(i)}(kr) \mathbf{X}_{l,m}(\theta, \phi) + \alpha^i b_{(l,m)}^i \nabla \times f_l^{(i)}(kr) \mathbf{X}_{l,m}(\theta, \phi) \right], \quad (5.1)$$

$$c\mathbf{B}_i = \frac{1}{2} \sum_{l,m} C(l) \left[ b_{(l,m)}^i f_l^{(i)}(kr) \mathbf{X}_{l,m}(\theta, \phi) + \beta^i a_{(l,m)}^i \nabla \times f_l^{(i)}(kr) \mathbf{X}_{l,m}(\theta, \phi) \right], \quad (5.2)$$

<sup>1</sup>They are defined in Ref. [140] (Eq. 9.119) as  $\mathbf{X}_{l,m}(\theta, \phi) = \frac{1}{l(l+1)} \mathbf{L} Y_{l,m}(\theta, \phi)$ ,  $\mathbf{L} = \frac{1}{i}(\mathbf{r} \times \nabla)$ ,  $l \geq 1$ . The absence of the  $l = 0$  term results in the absence of an isotropic contribution to SHG.

where  $C(l) = \sqrt{4\pi(2l+1)l!}$ ,  $\alpha^i = \alpha^i(k)$ ,  $\beta^i = \beta^i(k)$ , and  $k^i$  are constants that depend on the medium being considered. Outside the sphere we have  $k^{out} = \frac{\omega}{c} = k$ , while inside  $k^{in} = \sqrt{\epsilon(\omega)}\frac{\omega}{c} = nk = k_1$ , where we also introduce the complex refraction index  $n$ . The index  $i$  refers to the incident ( $i \equiv inc$ ), the scattered ( $i \equiv sc$ ), or the internal ( $i \equiv in$ ) fields. The functions  $f^{(i)}$  are different depending on the region we consider:  $f_l^{(inc,in)} = j_l$  (spherical Bessel function of the first kind) and  $f_l^{(sc)} = h_l^{(1)}$  (spherical Hankel function of the first kind). The expansion coefficients are determined by four boundary conditions:

$$\mathbf{n} \times (\mathbf{E}_{sc} + \mathbf{E}_{inc}) = \mathbf{n} \times \mathbf{E}_{in}, \quad (5.3a)$$

$$\mathbf{n} \cdot (\mathbf{D}_{sc} + \mathbf{D}_{inc}) = \mathbf{n} \cdot \mathbf{D}_{in}, \quad (5.3b)$$

$$\mathbf{n} \times (\mathbf{B}_{sc} + \mathbf{B}_{inc}) = \mathbf{n} \times \mathbf{B}_{in}, \quad (5.3c)$$

$$\mathbf{n} \cdot (\mathbf{B}_{sc} + \mathbf{B}_{inc}) = \mathbf{n} \cdot \mathbf{B}_{in}. \quad (5.3d)$$

$\mathbf{n} = \mathbf{e}_r$  is a vector normal to the surface. Solution of the boundary value problem allows to express coefficients of the scattered and inner fields via the incident field.

In the second step of the calculation we determine the sources of the second harmonic fields, namely the surface charge  $\sigma$  and the surface current  $\mathbf{j}_s$ , which are expanded in terms of spherical harmonics  $Y_{l,m}(\theta, \phi)$  and vector spherical harmonics:

$$\sigma(\theta, \phi) = \frac{1}{2} \sum_{l,m} \sigma_{l,m} Y_{l,m}(\theta, \phi), \quad (5.4a)$$

$$\mathbf{j}_s(\theta, \phi) = \frac{1}{2} \sum_{l,m} \left[ j_{l,m}^{\parallel} \mathbf{X}_{l,m}(\theta, \phi) + j_{l,m}^{\perp} \mathbf{X}_{l,m}(\theta, \phi) \times \mathbf{n} \right] \quad (5.4b)$$

In each point of the surface of the sphere the  $\mathbf{e}_x$ ,  $\mathbf{e}_y$ ,  $\mathbf{e}_z$  unit vectors of the local coordinate system point along  $\mathbf{e}_\theta$ ,  $\mathbf{e}_\phi$ ,  $\mathbf{e}_r$  respectively. For the  $C_{4v}$  symmetry of the surface layer<sup>2</sup> the only non-zero nonlinear tensor elements are  $\chi_{zxx} = \chi_{zyy}$ ,  $\chi_{zzz}$ , and  $\chi_{xzx} = \chi_{yzy}$ . According to the surface sheet model SHG takes place in a thin layer at the surface. The second order polarization  $\mathbf{P}_{2\omega}$  is expressed via the electric field on the outer surface of the sphere  $\mathbf{E}_s$ :

$$\begin{aligned} P_{2\omega}^r &= \chi_{zxx} E_s^\theta E_s^\theta + \chi_{zyy} E_s^\phi E_s^\phi + \chi_{zzz} E_s^r E_s^r, \\ P_{2\omega}^\theta &= \chi_{xzx} E_s^r E_s^\theta, \\ P_{2\omega}^\phi &= \chi_{yzy} E_s^r E_s^\phi. \end{aligned}$$

The surface density is then  $\sigma = \mathbf{n} \cdot \mathbf{P}_{2\omega}$  and the surface current  $\mathbf{j}_s = -2i\delta\omega\mathbf{n} \times (\mathbf{P}_{2\omega} \times \mathbf{n})$ , where  $\delta$  is the thickness of the surface layer where SHG takes place. In order to find the coefficients of the expansion  $\sigma_{l,m}$  and  $j_{l,m}^{\parallel}$  we re-expand the electric field on the surface  $\mathbf{E}_s = \epsilon E_{in}^r \mathbf{e}_r + E_{in}^\theta \mathbf{e}_\theta + E_{in}^\phi \mathbf{e}_\phi \Big|_{r=a}$  in terms of vector spherical harmonics [141] as:

$$\mathbf{E}_s = \sum_{l,m} A_{l,m}^{(1)} \mathbf{Y}_{l,m}^{(1)} + A_{l,m}^{(0)} \mathbf{Y}_{l,m}^{(0)} + A_{l,m}^{(-1)} \mathbf{Y}_{l,m}^{(-1)}. \quad (5.5)$$

The third step of the calculation is very similar to the first one. We find the second harmonic fields from the known surface charge and the current by solving a boundary condition problem:

$$\mathbf{n} \times (\mathbf{E}_{out} - \mathbf{E}_{in}) = 0, \quad (5.6a)$$

<sup>2</sup>Since SHG cannot distinguish isotropic and  $C_{4v}$  symmetry within the electric-dipole approximation, we work with  $C_{4v}$  symmetry without loss of generality.

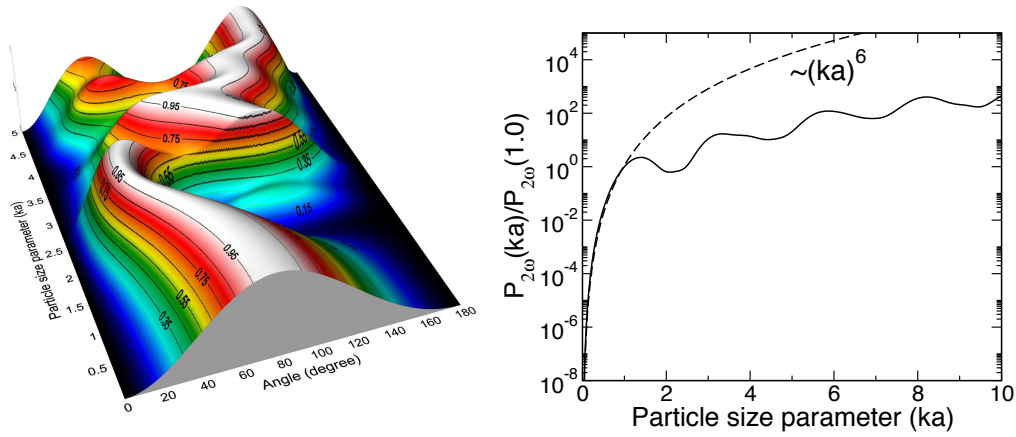


Figure 5.2: *Left*: angular distribution of the SHG intensity for water droplets as a function of particle size parameter laying within the range  $0.001 < ka < 5.0$ . At each value of  $ka$  the angular distribution is normalized, so that the maximum value is unity. At  $ka \sim 1.0$  the distribution starts to vary with the particle size indicating that the Rayleigh theory ceases to be valid. *Right*: integrated SH intensity  $P_{2\omega}(ka)$ . At small particle size parameter the Rayleigh theory is valid, yielding  $(ka)^6$  scaling. Intensity is normalized so that  $P_{2\omega}(1.0) = 1.0$ .

$$\mathbf{n} \cdot (\mathbf{D}_{out} - \mathbf{D}_{in}) = \sigma, \quad (5.6b)$$

$$\mathbf{n} \times (\mathbf{H}_{out} - \mathbf{H}_{in}) = \mathbf{j}_s, \quad (5.6c)$$

$$\mathbf{n} \cdot (\mathbf{B}_{out} - \mathbf{B}_{in}) = 0. \quad (5.6d)$$

Calculations show that only the  $j^{\parallel}$  component of the surface current contributes to the results. Lastly, we determine the angular distribution of the intensities in the far field approximation using the asymptotic expansions of the Hankel functions and their derivatives. The numerical algorithm based on the theory can be outlined as follows:

- Find coefficients of the surface electric field  $\mathbf{E}_s$  expansion (Eq. 5.5).
- Compute the surface charge  $\sigma$  and the current  $\mathbf{j}_s$  using Clebsch-Gordan algebra (Eqs. 5.4).
- Find coefficients of the SH electric field  $\mathbf{E}_{out}$  expansion and compute the angular dependence of SHG in far field approximation.

## Numerical results

We study the angular distribution and the intensity of SHG radiated in a unit solid angle for different sizes of particles. Water droplets of the size parameter ranging from  $ka = 10^{-3}$  to  $ka = 200.0$  with  $n(\omega) = 1.326 - 1.250 \cdot 10^{-7}i$  and  $n(2\omega) = 1.350 - 1.580 \cdot 10^{-9}i$  (complex refractive index approximately corresponds to the wave-length of incident light  $\lambda = 800$  nm) are considered. The number of significant terms in the multipole expansion (Eqs. 5.4) varies depending on the value of  $ka$ . For  $l > ka$  the terms decrease rapidly, whereas for  $l \ll ka$  they have comparable amplitudes. Only the  $\chi_{zzz}^{(2\omega)}$  tensor element is assumed to be non-zero. The theory is valid in the regime of small particle sizes ( $ka < 1$ , Rayleigh limit) as well as for large particles. In the former case the angular distribution of SH intensity remains independent on the size parameter, the integrated intensity grows as  $P_{2\omega}(ka) \sim (ka)^6$  (Fig. 5.2), in agreement with Ref. [130]. The small- $ka$  expansion of the first few coefficients of the SH electric field  $\mathbf{E}_{out}$ :

$$b_{1,0}^{out} = \sqrt{\frac{24}{\pi}} \frac{n^2(\omega)\chi_{zzz}}{(n^2(\omega) + 2)(2n^2(\omega) + 3)(n^2(2\omega) + 2)} (ka)^4, \quad (5.7a)$$

$$b_{2,0}^{out} = \sqrt{\frac{3}{10\pi}} \frac{n^2(\omega)\chi_{zzz}}{(n^2(\omega) + 2)^2(2n^2(2\omega) + 3)} i(ka)^4, \quad (5.7b)$$

$$b_{2,2}^{out} = -\sqrt{\frac{9}{20\pi}} \frac{n^2(\omega)\chi_{zzz}}{(n^2(\omega) + 2)^2(2n^2(2\omega) + 3)} i(ka)^4 \quad (5.7c)$$

shows that in the lowest order of  $ka$  the SH radiation results from the excitation of dipole and quadrupole moments, which have a comparable strength, as has been shown in Ref. [130]. The scaling of the SH power should be contrasted with the linear Rayleigh scattering, which is known to scale as  $P_\omega(ka) \sim (ka)^4$ .

## 5.2 Semi-classical sources

The theories based on classical electrodynamics rely on the knowledge of the frequency-dependent dielectric function and the non-linear optical susceptibility tensor. With the fabrication processes being perfected and the system tending smaller and smaller sizes one may wonder to which extent quantum effects are important and whether it is justified to use the same susceptibility tensor to describe semi-infinite and finite size systems on the nanometer range. To shed light on these issues, it is desirable to have a quantum theory for the non-linear response on the nanoscale. The fully atomistic approach seems to be out of reach for present computers, as currently maximally hundreds of atoms are possible to treat using quantum chemistry codes. Yet, the outstanding question is, how important are the electronic correlation effects and is there possibly a way to stay on the solid quantum theory basis while treating larger systems?

There is an affirmative answer to these questions as was demonstrated recently in the linear optics case by Prodan and Nordlander [142]. They succeeded to push the limits of the time-dependent density functional theory (TDDFT) to metallic systems containing millions of atoms. But at the same time they demonstrated that for these system sizes the semi-classical approach becomes very accurate. This is a marked finding as it allows to replace the complicated sum-over-states quantum mechanical expression [143] for the polarizability tensor with a single integral equation. Consequently, there is only one parameter in the theory: the ionic density distribution. With some reasonable assumptions about the ionic density such as in the jellium model<sup>3</sup> we can obtain the ground state electronic density from the solution of the Kohn-Sham equations and express the response function in its terms.

In the following I formulate integral equations describing linear and non-linear responses of electrons to the optical field generalizing the work of Liebsch and Schaich [146] to include many-body correlation effects. Finally I introduce the semi-classical approximation. It implies the high frequency limit and enables to express the source terms entering these equations solely in terms of electron density, its gradients and parameters of external perturbation. Explicit calculations, rather laborious for the second order response, were performed in a sequence of works [11, 12].

<sup>3</sup>This assumption is reasonable even for molecular structures, as we have shown recently [79, 86] for fullerenes. The usefulness of the jellium model was demonstrated by the pioneering works of Ekardt on sodium clusters [66, 144] or of Puska and Nieminen on  $C_{60}$  [145].

## Integral equations

Before considering any approximations let us write integral response equations in full generality. At the introduction to this chapter I have presented an algebraic equation that relates the full density-density and the Kohn-Sham response functions. In fact, it is only a formal writing as it presumes that these functions are invertible. It is well known, however, that at least  $\chi(\mathbf{r}, \mathbf{r}'; \omega)$  is singular; perfectly valid mathematically is the integral form:

$$\chi(\mathbf{r}, \mathbf{r}'; \omega) = \chi^{(0)}(\mathbf{r}, \mathbf{r}'; \omega) + \int d\mathbf{r}_1 \int d\mathbf{r}_2 \chi^{(0)}(\mathbf{r}, \mathbf{r}_1; \omega) (v(\mathbf{r}_1 - \mathbf{r}_2) + f_{xc}(\mathbf{r}_1, \mathbf{r}_2; \omega)) \chi(\mathbf{r}_2, \mathbf{r}'; \omega), \quad (5.8)$$

here  $v(\mathbf{r} - \mathbf{r}_1)$  is the Coulomb potential and  $\chi^{(0)}(\mathbf{r}, \mathbf{r}'; \omega)$  is the *non-interacting density-density response* function and  $f_{xc}(\mathbf{r}, \mathbf{r}'; \omega)$  is the Fourier transform from the time to frequency domain of the exchange-correlation kernel.

A rigorous definition of the kernel is not merely  $f_{xc}(\mathbf{r}t, \mathbf{r}'t') = \delta^2 A_{xc} / \delta n(\mathbf{r}t) \delta n(\mathbf{r}'t')$  but, as R. van Leeuwen showed [147, 148] requires use of the Keldysh formalism. Setting the kernel to zero corresponds to the random phase approximation.

Let us consider the response of the system subject to the harmonic electric field oscillating at the frequency  $\omega$ , i. e.  $\varphi^{(0)}(\mathbf{r}; t) = \varphi^{(0)}(\mathbf{r}) e^{-i\omega t}$ . Then, the induced density which oscillates at the frequency of the applied field is given by:

$$\delta n^{(1)}(\mathbf{r}) = \int d\mathbf{r}' \chi(\mathbf{r}, \mathbf{r}'; \omega) \varphi^0(\mathbf{r}') = \int d\mathbf{r}' \chi^{(0)}(\mathbf{r}, \mathbf{r}'; \omega) \varphi^{(1)}(\mathbf{r}'), \quad (5.9)$$

where  $\varphi^{(1)}(\mathbf{r})$  is the induced local field oscillating at the fundamental frequency and consisting of the external potential plus the Hartree potential corresponding to the induced density:

$$\varphi^{(1)}(\mathbf{r}) = \varphi^{(0)}(\mathbf{r}) + \int d\mathbf{r}' (v(\mathbf{r} - \mathbf{r}') + f_{xc}(\mathbf{r}, \mathbf{r}'; \omega)) \delta n^{(1)}(\mathbf{r}'). \quad (5.10)$$

The induced density oscillating at the double frequency results from the non-linear process described by the  $\chi_2^{(0)}$  response function and from the linear response to the local field  $\varphi^{(2)}(\mathbf{r})$  oscillating at  $2\omega$ :

$$\delta n^{(2)}(\mathbf{r}) = \int d\mathbf{r}' \int d\mathbf{r}'' \chi_2^{(0)}(\mathbf{r}; \mathbf{r}', \mathbf{r}''; \omega) \varphi^{(1)}(\mathbf{r}') \varphi^{(1)}(\mathbf{r}'') + \int d\mathbf{r}' \chi^{(0)}(\mathbf{r}, \mathbf{r}'; \omega) \varphi^{(2)}(\mathbf{r}'). \quad (5.11)$$

Because there is no external field at  $2\omega$  the local field at this frequency is given by the Hartree potential:

$$\varphi^{(2)}(\mathbf{r}) = \int d\mathbf{r}' (v(\mathbf{r} - \mathbf{r}') + f_{xc}(\mathbf{r}, \mathbf{r}'; \omega)) \delta n^{(2)}(\mathbf{r}'). \quad (5.12)$$

Equations (5.9) and (5.10) yield the integral equation for the linear density:

$$\delta n^{(1)}(\mathbf{r}) = \xi^{(1)}(\mathbf{r}) + \int d\mathbf{r}' \int d\mathbf{r}'' \chi^{(0)}(\mathbf{r}, \mathbf{r}'; \omega) (v(\mathbf{r}' - \mathbf{r}'') + f_{xc}(\mathbf{r}', \mathbf{r}''; \omega)) \delta n^{(1)}(\mathbf{r}''), \quad (5.13)$$

while eqs. (5.11) and (5.12) result in the integral equation for the second harmonic density:

$$\delta n^{(2)}(\mathbf{r}) = \xi^{(2)}(\mathbf{r}) + \int d\mathbf{r}' \int d\mathbf{r}'' \chi^{(0)}(\mathbf{r}, \mathbf{r}'; \omega) (v(\mathbf{r}' - \mathbf{r}'') + f_{xc}(\mathbf{r}, \mathbf{r}''; \omega)) \delta n^{(2)}(\mathbf{r}''). \quad (5.14)$$

We defined the source terms following [146] as:

$$\xi^{(1)}(\mathbf{r}) = \int d\mathbf{r}' \chi^{(0)}(\mathbf{r}, \mathbf{r}'; \omega) \varphi^{(0)}(\mathbf{r}'), \quad (5.15)$$

$$\xi^{(2)}(\mathbf{r}) = \int d\mathbf{r}' \int d\mathbf{r}'' \chi_2^{(0)}(\mathbf{r}; \mathbf{r}', \mathbf{r}''; \omega) \varphi^{(1)}(\mathbf{r}') \varphi^{(1)}(\mathbf{r}''). \quad (5.16)$$

Eqs. (5.13, 5.15) and eqs. (5.14, 5.16) are essentially exact. When coupled with an appropriate approximation for the non-interacting response functions and the exchange-correlation functional  $A_{xc}$  they allow to completely describe the linear and the second-harmonic optical responses.

We start from the microscopic expressions for the noninteracting first order linear (known as Lindhard function for the homogeneous electron gas in three dimensions):

$$\chi^{(0)}(\mathbf{r}, \mathbf{r}'; \omega) = 2 \sum_{i,j} \frac{f_i - f_j}{\omega + E_i - E_j + i\eta} \psi_i(\mathbf{r}) \psi_j^*(\mathbf{r}) \psi_j(\mathbf{r}') \psi_i^*(\mathbf{r}'), \quad (5.17)$$

and the second order non-linear:

$$\begin{aligned} \chi_2^{(0)}(\mathbf{r}; \mathbf{r}', \mathbf{r}''; \omega) = \sum_{i,j,k} \frac{\psi_k^*(\mathbf{r}) \psi_i(\mathbf{r}) \psi_i^*(\mathbf{r}') \psi_j(\mathbf{r}') \psi_j^*(\mathbf{r}'') \psi_k(\mathbf{r}'')}{2\omega + E_i - E_k + i\eta} \\ \times \left( \frac{f_k - f_j}{\omega + E_j - E_k + i\eta} - \frac{f_j - f_i}{\omega + E_i - E_j + i\eta} \right) \end{aligned} \quad (5.18)$$

response functions. In this expressions  $f$  is the Fermi function and  $i, j, k$  refer to the collections of quantum numbers that uniquely characterize the electronic states of the system. The infinitesimally small positive number  $\eta$  shifts the poles from the real axis and ensures, thus, the causality of the response function.

To stay completely at the microscopic level one needs some method to perform the summation over the infinite number of unoccupied states for the calculation of the response functions. Fortunately a trick suggested by Zangwill and Soven [149] allows to completely avoid explicit sums. This allowed for example Prodan and Nordlander to treat very large spherical systems at the TDDFT level [142].

We go one step further and introduce the semi-classical approximation  $|E_i - E_j| \ll \omega$ . This high frequency condition allows us to approximate the denominator in (5.17) as

$$\frac{f_i - f_j}{\omega + E_i - E_j} \approx \frac{f_i - f_j}{\omega} \left( 1 - \frac{E_i - E_j}{\omega} \right). \quad (5.19)$$

In the series of works we derived the semi-classical approximation for the  $\xi^{(1)}(\mathbf{r})$  [11]:

$$\xi^{(1)}(\mathbf{r}) = \frac{1}{\omega^2} \left( \nabla n(\mathbf{r}) \cdot \nabla \varphi^{(0)}(\mathbf{r}) - n(\mathbf{r}) \Delta \varphi^{(0)}(\mathbf{r}) \right) \quad (5.20)$$

and for the second-harmonic generation source term  $\xi^{(2)}(\mathbf{r})$  [12]:

$$\xi^{(2)}(\mathbf{r}) = \frac{1}{2\omega^4} \nabla \cdot \left( \nabla \varphi^{(1)}(\mathbf{r}) \left[ n(\mathbf{r}) \Delta \varphi^{(1)}(\mathbf{r}) + (\nabla \varphi^{(1)}(\mathbf{r}) \cdot \nabla n(\mathbf{r})) \right] + \frac{1}{4} n(\mathbf{r}) \nabla (\nabla \varphi^{(1)}(\mathbf{r}))^2 \right). \quad (5.21)$$

These results raise the question of whether it is sufficient to know the unperturbed ground state density to obtain the lowest order approximation for an arbitrary response function. We recall that from the point of view of the diagrammatic perturbation theory [150] SHG comprises three processes in which the  $2\omega$  photon is emitted before, between or after the absorption of two  $\omega$ -photons. Consequently, one might wonder if each diagram of this expansion can also be expressed in terms of  $n(\mathbf{r})$ . As was demonstrated in Ref. [12], the answer is negative, one additionally needs the one-particle density matrix  $\gamma(\mathbf{r}, \mathbf{r}')$  whose diagonal elements are given by  $n(\mathbf{r})$ . This comes not as a surprise if we consider the analogy with the orbital-free kinetic density functional theory [151] where this matrix enters the kinetic energy term.

Although quite technical, the derivation of Eq. (5.21) in Ref. [12] has its own merits as it establishes the equivalence between classical approaches of Wang, Chen and Bower [152] and Apell [153] and the high-frequency semi-classical expansion if the local fields effects are neglected. Finally, we notice that expressions (5.20) and (5.21) can be further simplified in the case of spherical symmetry. This will be demonstrated in the next section where numerical results for a realistic system are presented.

### 5.3 Linear scaling approach

Quantum theory accounts inherently for the non-locality of the dielectric function that can in principle be calculated fully *ab initio*. However, due to enormous computational cost a fully atomistic approach is feasible only for small molecular systems. Over the years several authors perfected the method (now the treatment of systems containing millions of electrons is possible [142]), and applied it to a range of geometries: starting from the simple spherical symmetry (spherical clusters, nanoshells) to systems without any symmetry [154] and used theories from the random phase approximations (RPA) to time-dependent density functional theory (TDDFT).

In this section we deal with a situation where a system has dimensions prohibitively large for atomistic approach, but still is treatable on quantum level within the jellium model. For frequencies of external fields  $\omega$  exceeding the single-particle gap  $E_g$  ( $\omega \gg E_g$ ) the semi-classical approximation becomes well justified and allows to formulate an integral equation for the optical response as was demonstrated for a number of relevant geometries by Mukhopadhyay and Lundqvist [155]. In comparison with RPA or TDDFT this semi-classical approximation (SCA) is substantially simpler as it is free from summations over the electronic states. Recent comparison of the two approaches reveals a remarkable agreement between them [142]. This is mostly expressed in the energy positions of collective resonances. Quantum effects such as discreteness of the electronic structure are manifested



as small deviations at the resonances' wings. In the case of abruptly varying density (expressible as a combination of the step-functions) the SCA integral equation can be reduced to an algebraic one. Analytical solutions in this case are in agreement with the classical Mie theory using the Drude dielectric function.

In view of its simplicity and accuracy SCA is potentially a practical tool for nanoplasmonics. However, its use was hindered by the difficulties of solving the integral equation and was considered to be a *formidable task* [156]. In fact, conventional methods require discretization of the integral equation and solution of the resulting system of linear equations. The method unfavorably scales as  $\mathcal{O}(N^3)$  with the number of mesh points and is, thus, not practical for large systems, where one necessarily uses very fine meshes to describe non-smooth electron densities at the interfaces. Here we go one step further towards analytic solution of the problem for systems with symmetries. I show that the SCA integral equation can be reduced to a system of two coupled differential equations. Although in general their solution cannot be obtained analytically it still presents a huge computation saving as the problem can be solved with  $\mathcal{O}(N)$  complexity. Below we discuss a *linear scaling* approach for the calculation of the multipole linear and second harmonic optical response in the semi-classical approximation and apply it to the icosahedrally ordered  $\text{Na}_{2869}^-$  cluster.

### Solution of generic integral equation

Equations obtained in the previous section simplify considerably if some symmetry assumptions are used. We consider below the case of spherical symmetry although axial symmetry can be treated similarly. After expansion of all quantities in terms of spherical harmonics and performing the integrations over the angular degrees of freedom one obtains the following generic integral equation for the induced densities [11, 12]:

$$\alpha(r; \omega) = \alpha^{(0)}(r; \omega) \left[ 1 - \int_0^\infty dr' G(r, r') \alpha(r'; \omega) \right], \quad (5.22)$$

where  $\alpha^{(0)}(r; \omega)$  is a known function of the ground state density distribution  $n(r)$  and the unknown function  $\alpha(r; \omega)$  typically has a meaning of the  $\ell$ -component of the induced density ( $\delta n_{\ell 0}^{(1)}$  or  $\delta n_{\ell 0}^{(2)}$ ). The  $\omega$  parameter is in general a complex number as it includes also the small broadening  $i\eta$ . Therefore, the response functions are also complex. The Green's function has the following structure:

$$G(r, r') = f(r) g(r') \theta(r - r') - h \theta(r' - r), \quad (5.23)$$

$f(r)$  and  $g(r)$  are typically given by the power functions. Eq. (5.22) belongs to the class of the *Fredholm integral equations of the second kind* [157]. The analytical solution of our particular form is not known and one has to resort to numerical methods. A standard approach, also broadly used for the computations of the polarizabilities [142, 156], is the *quadrature method*. Here one proceeds by using some quadrature rules for the integral, discretizing the kernel, and by posing the problem as a system of linear algebraic equations. The advantage of this approach is its universality, however, it is obliterated by the high computational cost. A mesh containing  $N$  point leads to a system of  $N$  linear equations which can only be solved at  $\mathcal{O}(N^3)$  cost. A further disadvantage of the method is in the difficulty to apply an iterative

refinement procedure: It is often necessary to obtain the solutions for a large number of  $\omega$ -values. For finite  $\eta$  response functions are continuous functions of the frequencies. Thus, one might want to use a known solution at  $\omega = \omega_i$  to find a solution for a neighboring point  $\omega = \omega_{i+1}$ . The implementation of this approach within the quadrature approach requires the use of sophisticated methods, and also may suffer from instabilities and cannot be implemented within standard numerical libraries. Therefore we propose a method that is free from these deficiencies: i) it scales linearly with the number of mesh points; ii) the iterative refinement can be implemented straightforwardly; and iii) the method is numerically stable.

Let us write (5.22) in the form:

$$\alpha(r; \omega) = \alpha^{(0)}(r; \omega) [1 + h a(\omega)] - \alpha^{(0)}(r; \omega) \int_0^r dr' [f(r) g(r') + h] \alpha(r'; \omega). \quad (5.24)$$

If  $a(\omega) = \int_0^\infty \alpha(r; \omega) dr$  were a known function Eq. (5.24) would belong to the type of the *Volterra integral equations of the second kind* with a degenerate kernel [157] which admits an analytic solution. Let us assume that on the  $n$ th iteration step an approximate value  $a^{(n)}$  has already been known. We solve the integral equation (5.24) in a standard way by introducing the two auxiliary functions:

$$w_1(r, \omega) = \int_0^r dr' g(r') \alpha(r'; \omega), \quad (5.25a)$$

$$w_2(r, \omega) = \int_0^r dr' \alpha(r'; \omega). \quad (5.25b)$$

Then the unknown function is given by

$$\alpha(r; \omega) = \alpha^{(0)}(r; \omega) [1 + h a^{(n)}(\omega) - f(r) w_1(r, \omega) - h w_2(r, \omega)] \quad (5.26)$$

and the improved approximation to  $a(\omega)$  by

$$a^{(n+1)}(\omega) = \lim_{r \rightarrow \infty} w_2(r, \omega). \quad (5.27)$$

Two auxiliary functions can be found as solutions to the system of the ordinary differential equations:

$$w_1'(r, \omega) = \alpha^{(0)}(r; \omega) g(r) [1 + h a^{(n)}(\omega) - f(r) w_1(r, \omega) - h w_2(r, \omega)], \quad (5.28a)$$

$$w_2'(r, \omega) = \alpha^{(0)}(r; \omega) [1 + h a^{(n)}(\omega) - f(r) w_1(r, \omega) - h w_2(r, \omega)]. \quad (5.28b)$$

These relations are derived by differentiating (5.25) and using (5.26). To solve (5.28) with the initial conditions  $w_i(r, \omega) = 0$  the standard *forth-order Runge-Kutta* method can be used. This turned out to be a good compromise between the speed and the accuracy. Let us focus now on the second component of our approach: the iterative update of  $a(\omega)$ . To explicitly show the functional dependence of  $w_2(r, \omega)$  on  $a(\omega)$  it can be written as:

$$a = \lim_{r \rightarrow \infty} w_2[a](r, \omega). \quad (5.29)$$

This relation can be viewed as a nonlinear algebraic equation for the complex  $a(\omega)$ . In general, the brute-force update (5.27) does not achieve convergence; with only one starting point it is successful under special conditions only. Therefore, we use here a simple and an efficient method for finding the complex roots based on a quadratic interpolation with three

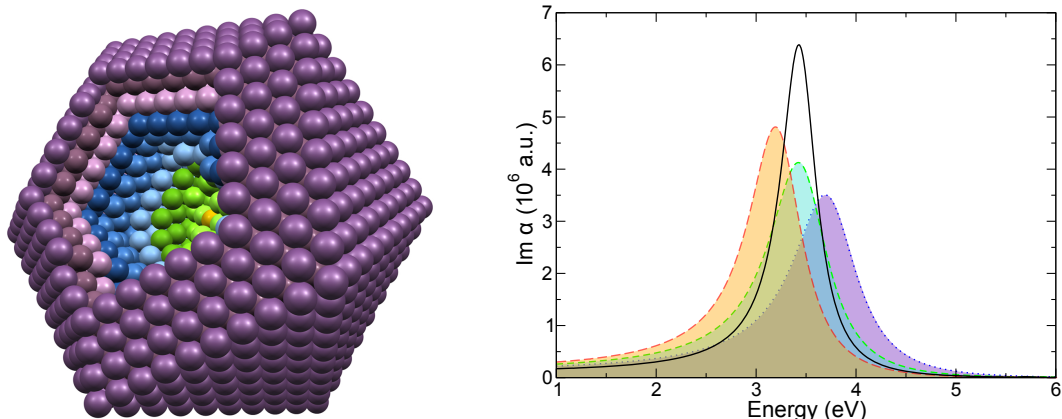


Figure 5.3: *Left*: Geometrical structure of 10-shell icosahedral  $\text{Na}_{2869}^{-}$  cluster. *Right*: The optical response obtained by solving Eq. 5.22. The solid line: the standard jellium model, the dotted line:  $a_s = 0.95a_{nm}$ , the short dashed line:  $a_s = a_{nm}$ , the long dashed line:  $a_s = 1.05a_{nm}$ .

distinct points needed to start the iteration. This approach is known as the *Müller's method*. The convergence can be greatly accelerated if already known  $a(\omega_i)$  is used to initialize the computation of  $a(\omega_{i+1})$ :

$$a^{(1)}(\omega_{i+1}) = a(\omega_i), \quad a^{(2,3)}(\omega_{i+1}) = (1 \pm \lambda)a(\omega_i),$$

where  $\lambda$  is a small parameter (typically  $\lambda = 0.1$ ). Our numerical tests indicate an excellent stability of the method. Typically one  $\omega$ -point is converged with an accuracy of  $10^{-12}$  within 10 iteration and the whole calculation linearly scales with the number of mesh points. This makes it a perfect candidate for the investigation of the optical properties of complex 3d-objects not necessarily possessing a high symmetry. Here, we demonstrate the usability of our approach by applying it to a spherically symmetric metal cluster.

## Numerical results

We apply our theory to  $\text{Na}_{2869}^{-}$  cluster. It is remarkable as it simultaneously possesses a magic structural number of the atoms and has completely filled electronic shells [158]. The atoms are organized according to an icosahedral symmetry: a central atom is surrounded by 12 neighboring atoms at the corners of the icosahedron, this 13-atom core is covered by a second layer of 42 atoms, forming again a perfect icosahedron, and so on (Fig. 5.3 (*Left*)). The standard jellium model assumes that ionic density is homogeneously distributed within the volume of a sphere and abruptly drops to zero at its boundaries [159]. The electronic properties are then determined by a single parameter: the ionic density  $n^{(i)}(r)$  which is selected to match the bulk value (for Na  $r_s = 3.96$ ) and, hence, is related to the bulk lattice constant (for Na  $a_b = 4.230 \text{ \AA}$ ) and to the number of valence electrons per unit cell. For our comparative study we fix the averaged ionic density and adjust all the other parameters. As anticipated, the ionic density exhibits an oscillatory behavior (Fig. 5.4).

*Ground state electronic properties* Let us assess the influence of the ionic density oscillations on the electronic properties by comparing electronic distributions (Fig. 5.4) resulting from the self-consistent LDA calculations based on the jellium model for the ionic density and on the realistic ionic density derived by smearing out the positive charges at idealized icosahedral positions. Our LDA calculations use the same exchange-correlation potential and the methodology as in Ref. [159]. The radial Kohn-Sham (or Schrödinger) equations

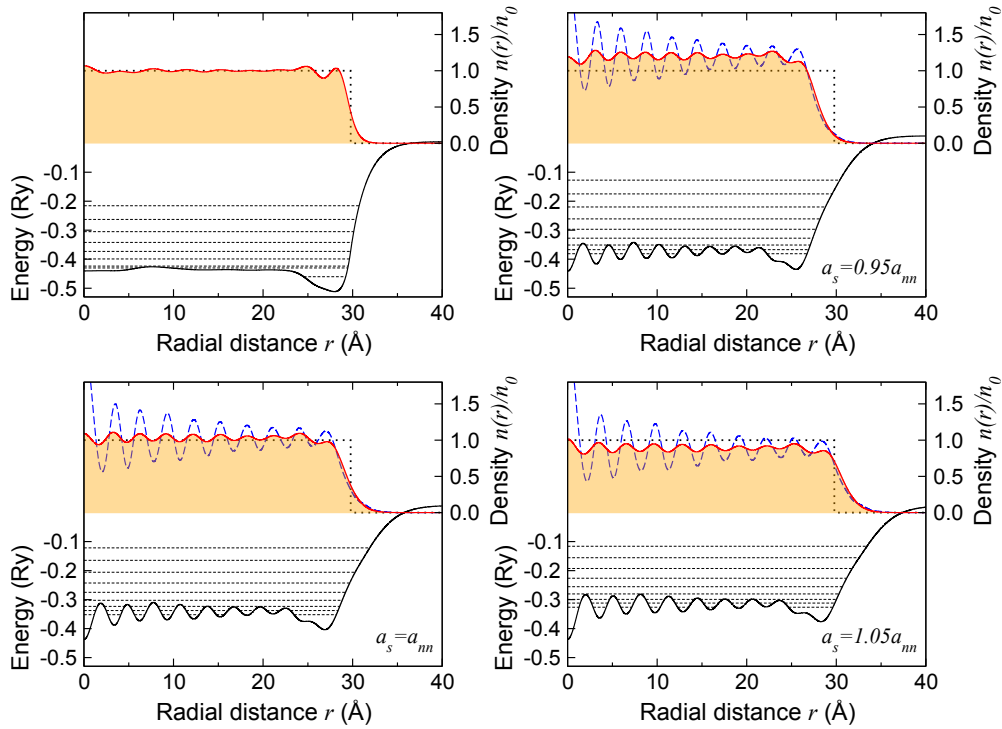


Figure 5.4: Electronic structure of the  $\text{Na}_{2869}^-$  cluster corresponding to different approximations to the ionic density: solid line denotes the self-consistent Kohn-Sham potential, the electronic states for  $\ell = 0$  shown as thin dashed lines; the filled area denotes the converged electronic density; the long-dashed line shows the ionic density; the dotted line marks the ideal jellium background.

are solved by the renormalized *Numerov method* [160] using the *Pulay method* [161] to accelerate the convergence.

Our calculations reveal interesting features of the jellium model approach. We find that the electronic density reproduces closely the oscillations of the positive background. The oscillations are in-phase, their magnitude is damped compared to the ionic distribution, and they are also reflected in the Kohn-Sham potential. In the next paragraph we will argue that they are also manifested in the optical response. In the asymptotic region the electron and the ionic densities are almost indistinguishable. We also notice that the spill-off region is significantly extended compared to the standard jellium model. This is in the first place a geometric not an electronic effect which originates from the deviation of the cluster's shape from the spherical or, in other words, from the reduced coordination number of the surface atoms. The Kohn-Sham potential for the system with a realistic ionic density is shallower compared to the standard jellium model. Consequently, the work-function in the latter case is increased by roughly 1 eV.

*Linear optical properties* Variation of the electronic density has a profound impact on the optical response, Fig. 5.3 (Right). The optical spectrum in all four scenarios is characterized by a major surface plasmon resonance at around classical value  $\omega_s = \omega_p / \sqrt{3}$  and some features at the bulk plasmon frequency  $\omega_p$ . Such “artificial features” were also observed in metallic shell systems. For our system they are only visible when plotted on the log-scale. We performed a sequence of calculations by varying the broadening parameter and found only a tiny influence of the spectrum. This signifies the intrinsic broadening of the

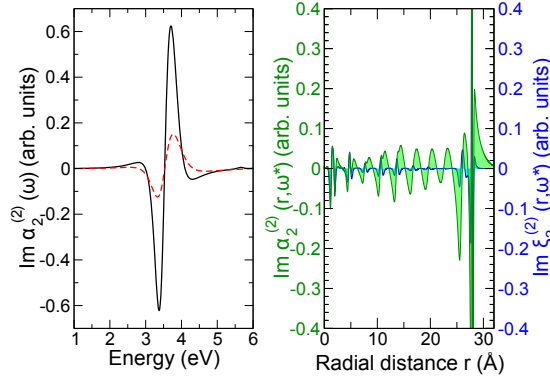


Figure 5.5: *Left*: The second-order non-linear  $\ell = 1$  (left) and  $\ell = 2$  (right) optical response of the icosahedral  $\text{Na}_{2869}^-$  cluster based on the standard jellium model (black solid line) and on the realistic ionic density (red dashed line). *Right*: Corresponding source terms  $\xi_\ell^{(2)}(r, \omega^*)$  and the resulting induced densities  $\delta n_\ell^{(2)}(r, \omega^*)$  for a particular frequency value  $\omega^* = 5.75$  eV.

optical absorption peaks in SCA. Contrary to fully quantum approach where finite systems necessarily possess electronic excitations of the discrete spectrum the response function in SCA has branch-cuts rather than poles. This can be traced back to a specific form of the free term  $\alpha^{(0)}(r; \omega)$  in the SCA integral equation having a branch-cut in the complex  $\omega$ -plane. The broadening of the excited states in the optical experiments is associated with different factors: the temperature, disorder, the electronic correlations. Our results emphasize the role of geometric ordering.

*Second harmonics generation* Computation of the second order optical processes is more involved. It includes several steps:

- i) The integral equation (5.13) is solved with a source term (5.20). It yields the first order density  $\delta n^{(1)}(\mathbf{r})$  and, therefore, the local potential  $\varphi^{(1)}(\mathbf{r})$ ;
- ii) Eq. (5.21) is applied to generate the source term for the equation (5.14);
- iii) This integral equation is solved similarly to (5.13) in order to obtain  $\delta n^{(2)}(\mathbf{r})$ .

Results of this program are shown at Fig. 5.5. For linear optical absorption the spill-off of the electron density in realistic systems mostly leads to the broadening of the surface plasmon resonances. To illustrate this fact for the second-harmonic generation we choose the off-resonance value of the frequency ( $\omega^* = 5.75$  eV) and plot the source  $\xi_\ell^{(2)}(r, \omega^*)$  and the induced density  $\delta n_\ell^{(2)}(r, \omega^*)$ . Numerous features associated with slow electronic density variations within the cluster are visible. They contribute to the optical absorption in the off-resonance regime. However, the relative weight of these oscillations decreases when the frequency approaches the resonance. The spectrum at the resonance is dominated by fast density variations at the surface. It is interesting to observe that two different excitation mechanisms (the quadrupole transition at  $\omega$  or  $2\omega$  frequency) lead to almost identical frequency dependence. Unlike in the linear case, the efficiency of the frequency conversion vanishes at the plasmon resonance and has two pronounced peaks at the energy slightly below and above. We also do not observe a strong correlation between the source and the induced density as in the off-resonant linear case (cf. blue and green curves). The complicated radial dependence is the result of the derivatives of the induced density and the potential in the non-linear source terms.



## 6 Conclusions

---

The new developments presented here are methodological to a large extent, and partly numerical. Both are interwound such that a progress in theory was supported by numerical calculations, and, vice versa, larger capabilities of modern computers stipulated new theoretical questions. We have seen following examples: using a computer algebra system enabled us to generate Feynman diagrams starting from the Hedin equations (Section 2.1) and to explicitly evaluate frequency integrals in higher order Feynman diagrams. Inspecting the results we were able to prove a more general statement about the self-energy of the  $S$ -model (Section 2.3). Same approach enabled us to resolve a controversy related to the Paley-Wiener theorem and decay of quasiparticle states in 3d homogeneous electron gas (Section 2.4). Finally, by improving the Monte-Carlo integrator we were able to evaluate a subset the self-energy diagrams up to the third order (Section 4.3). Inclusion of the third order diagrams was required to resolve a problem of negative spectral densities from diagrammatic expansions (Section 4.3). Understanding the fundamental role of the Fermi Golden rule (Section 3.1) in its resolution gave a hint on the diagrammatic structure of the two-particle current (Section 4.4). From another side, numerical obstacles in application of methods of MBPT to larger systems called for the development of semi-classical methods (Section 5.2). Even very large systems were possible to treat thanks to the linear scaling approach (Section 5.3).





# Bibliography

---

- [1] G. Giuliani and G. Vignale, *Quantum theory of the electron liquid* (Cambridge University Press, Cambridge, UK, 2005).
- [2] P. Nozières and D. Pines, *The theory of quantum liquids*, Advanced book classics (Westview Press, Perseus Books Group, Boulder, CO, 1999).
- [3] E. K. U. Gross, E. Runge, and O. Heinonen, *Many-particle theory* (A. Hilger, 1991).
- [4] L. Hedin, Phys. Rev. **139**, A796 (1965).
- [5] W. Pauli, Science **103**, 213 (1946).
- [6] W. Heitler and F. London, Zeitschrift für Physik **44**, 455 (1927).
- [7] K. Gavroglou and A. Simões, *Neither physics nor chemistry: a history of quantum chemistry* (MIT Press, Cambridge, Mass, 2012).
- [8] P. A. M. Dirac, Proc. R. Soc. Lond. A **123**, 714 (1929).
- [9] D. R. Hartree, Math. Proc. Cambridge **24**, 426 (1928).
- [10] D. R. Hartree, Math. Proc. Cambridge **24**, 89 (1928).
- [11] R. T. Sharp and G. K. Horton, Phys. Rev. **90**, 317 (1953).
- [12] P. Hohenberg and W. Kohn, Phys. Rev. **136**, B864 (1964).
- [13] W. Kohn and L. J. Sham, Phys. Rev. **140**, A1133 (1965).
- [14] J. Schwinger, J. Math. Phys. **2**, 407 (1961).
- [15] L. V. Keldysh, Sov. Phys. JETP **20**, 1018 (1965).
- [16] P. W. Anderson, Science **177**, 393 (1972).
- [17] L. D. Landau, Sov. Phys. JETP **3**, 920 (1956).
- [18] P. W. Anderson, *A Career in Theoretical Physics*, 2nd ed. (World Scientific, New Jersey, 2004).
- [19] P. W. Anderson, Phys. Rev. Lett. **18**, 1049 (1967).
- [20] P. Nozières and C. T. De Dominicis, Phys. Rev. **178**, 1097 (1969).
- [21] A. O. Gogolin, A. A. Nersesyan, and A. M. Tsvelik, *Bosonization and strongly correlated systems* (Cambridge University Press, Cambridge, U.K.; New York, NY, 1998).
- [22] G. Onida, L. Reining, and A. Rubio, Rev. Mod. Phys. **74**, 601 (2002).
- [23] M. Gell-Mann and K. A. Brueckner, Phys. Rev. **106**, 364 (1957).
- [24] K. Fuchs, P. R. Soc. A-Math. Phy. **151**, 585 (1935).
- [25] G. Strinati, Riv. Nuovo Cimento **11**, 1 (1988).

- [26] E. T. Whittaker and G. N. Watson, *A course of modern analysis: an introduction to the general theory of infinite processes and of analytic functions, with an account of the principal transcendental functions*, 4th ed. (Cambridge University Press ; Lightning Source Inc., Cambridge; Tennessee, 2005).
- [27] G. Lani, P. Romaniello, and L. Reining, *New J. Phys.* **14**, 013056 (2012).
- [28] J. A. Berger, P. Romaniello, F. Tandetzky, B. S. Mendoza, C. Brouder, and L. Reining, *New J. Phys.* **16**, 113025 (2014).
- [29] V. Pilaud and J. Rué, *Adv. Appl. Math.* **57**, 60 (2014).
- [30] D. Bar-Natan, *Topology* **34**, 423 (1995).
- [31] V. Hinich and A. Vaintrob, *Selecta Math. (N.S.)* **8**, 237 (2002).
- [32] A. Stoimenow, *Discrete Mathematics* **218**, 209 (2000).
- [33] B. I. Lundqvist, *Phys. Kondens. Mater.* **9**, 236 (1969).
- [34] G. D. Mahan, *Phys. Rev.* **153**, 882 (1967).
- [35] B. Roulet, J. Gavoret, and P. Nozières, *Phys. Rev.* **178**, 1072 (1969).
- [36] P. Nozières, J. Gavoret, and B. Roulet, *Phys. Rev.* **178**, 1084 (1969).
- [37] R. Markiewicz, J. Rehr, and A. Bansil, *Phys. Rev. Lett.* **112**, 237401 (2014).
- [38] D. C. Langreth, *Phys. Rev. B* **1**, 471 (1970).
- [39] M. Cini and A. D'Andrea, *J. Phys. C* **21**, 193 (1988).
- [40] N. S. Wingreen, K. W. Jacobsen, and J. W. Wilkins, *Phys. Rev. Lett.* **61**, 1396 (1988).
- [41] N. S. Wingreen, K. W. Jacobsen, and J. W. Wilkins, *Phys. Rev. B* **40**, 11834 (1989).
- [42] L. K. Dash, H. Ness, and R. W. Godby, *J. Chem. Phys.* **132**, 104113 (2010).
- [43] H. Ness, L. K. Dash, M. Stankovski, and R. W. Godby, *Phys. Rev. B* **84**, 195114 (2011).
- [44] S. M. Story, J. J. Kas, F. D. Vila, M. J. Verstraete, and J. J. Rehr, *Phys. Rev. B* **90**, 195135 (2014).
- [45] F. Aryasetiawan, L. Hedin, and K. Karlsson, *Phys. Rev. Lett.* **77**, 2268 (1996).
- [46] B. Holm and F. Aryasetiawan, *Phys. Rev. B* **56**, 12825 (1997).
- [47] M. Guzzo, G. Lani, F. Sottile, P. Romaniello, M. Gatti, J. J. Kas, J. J. Rehr, M. G. Silly, F. Sirotti, and L. Reining, *Phys. Rev. Lett.* **107**, 166401 (2011).
- [48] M. Guzzo, J. J. Kas, L. Sponza, C. Giorgetti, F. Sottile, D. Pierucci, M. G. Silly, F. Sirotti, J. J. Rehr, and L. Reining, *Phys. Rev. B* **89**, 085425 (2014).
- [49] J. J. Kas, J. J. Rehr, and L. Reining, *Phys. Rev. B* **90**, 085112 (2014).
- [50] J. Winter, *Nucl. Phys. A* **194**, 535 (1972).
- [51] L. Hedin, J. Michiels, and J. Inglesfield, *Phys. Rev. B* **58**, 15565 (1998).
- [52] B. Bergersen, F. W. Kus, and C. Blomberg, *Can. J. Phys.* **51**, 102 (1973).
- [53] L. Hedin, *Phys. Scr.* **21**, 477 (1980).
- [54] M. Vogt, R. Zimmermann, and R. J. Needs, *Phys. Rev. B* **69**, 045113 (2004).
- [55] S. M. Bose and J. Fitchek, *Phys. Rev. B* **12**, 3486 (1975).
- [56] R. E. Paley and N. Wiener, *Fourier transforms in the complex domain* (American

- Math. Soc., New York, 1934).
- [57] B. Gumhalter, Prog. Surf. Sci. **87**, 163 (2012).
- [58] F. Bruneval, F. Sottile, V. Olevano, R. Del Sole, and L. Reining, Phys. Rev. Lett. **94**, 186402 (2005).
- [59] S. Botti, A. Schindlmayr, R. D. Sole, and L. Reining, Rep. Prog. Phys. **70**, 357 (2007).
- [60] Y. Pavlyukh, J. Berakdar, and A. Rubio, Phys. Rev. B **87**, 125101 (2013).
- [61] S. Ethofer and P. Schuck, Zeitschrift für Physik **228**, 264 (1969).
- [62] P. Knowles and N. Handy, Chem. Phys. Lett. **111**, 315 (1984).
- [63] J. Olsen, B. O. Roos, P. Jørgensen, and H. J. A. Jensen, J. Chem. Phys. **89**, 2185 (1988).
- [64] J. Olsen, P. Jørgensen, and J. Simons, Chem. Phys. Lett. **169**, 463 (1990).
- [65] Y. Pavlyukh and W. Hübner, Phys. Lett. A **327**, 241 (2004).
- [66] W. Ekardt, Phys. Rev. Lett. **52**, 1925 (1984).
- [67] R. Pauncz, *Spin eigenfunctions: construction and use* (Plenum Press, New York, 1979).
- [68] A. Stan, N. E. Dahlen, and R. v. Leeuwen, EPL (Europhysics Letters) **76**, 298 (2006).
- [69] M. Weinelt, J. Phys. Condens. Matter **14**, R1099 (2002).
- [70] M. L. Tiago and J. R. Chelikowsky, Phys. Rev. B **73**, 205334 (2006).
- [71] H. Nakatsuji and K. Hirao, J. Chem. Phys. **68**, 2053 (1978).
- [72] Y. Pavlyukh and W. Hübner, Appl. Phys. A **82**, 67 (2006).
- [73] C. Baldacchini, L. Chiodo, F. Allegretti, C. Mariani, M. G. Betti, P. Monachesi, and R. Del Sole, Phys. Rev. B **68**, 195109 (2003).
- [74] K. S. Thygesen, L. B. Hansen, and K. W. Jacobsen, Phys. Rev. Lett. **94**, 026405 (2005).
- [75] M. Bauer, S. Pawlik, and M. Aeschlimann, Surf. Sci. European Conference on Surface Science, **377-379**, 350 (1997).
- [76] M. Bauer, S. Pawlik, and M. Aeschlimann, Phys. Rev. B **60**, 5016 (1999).
- [77] M. Feng, J. Zhao, and H. Petek, Science **320**, 359 (2008).
- [78] J. Zhao, M. Feng, J. Yang, and H. Petek, ACS Nano **3**, 853 (2009).
- [79] Y. Pavlyukh and J. Berakdar, Chem. Phys. Lett. **468**, 313 (2009).
- [80] T. Huang, J. Zhao, M. Feng, H. Petek, S. Yang, and L. Dunsch, Phys. Rev. B **81**, 085434 (2010).
- [81] J. Schirmer, L. S. Cederbaum, and O. Walter, Phys. Rev. A **28**, 1237 (1983).
- [82] M. Altarelli, D. L. Dexter, H. M. Nussenzveig, and D. Y. Smith, Phys. Rev. B **6**, 4502 (1972).
- [83] U. von Barth and B. Holm, Phys. Rev. B **54**, 8411 (1996).
- [84] Y. Pavlyukh and J. Berakdar, Comp. Phys. Commun. **184**, 387 (2012).
- [85] B. L. Altshuler, Y. Gefen, A. Kamenev, and L. S. Levitov, Phys. Rev. Lett. **78**, 2803 (1997).

- [86] Y. Pavlyukh and J. Berakdar, *Phys. Rev. A* **81**, 042515 (2010).
- [87] P. B. Corkum and F. Krausz, *Nature Phys.* **3**, 381 (2007).
- [88] H. Petek and S. Ogawa, *Prog. Surf. Sci.* **56**, 239 (1997).
- [89] G. Stefanucci and R. van Leeuwen, *Nonequilibrium Many-Body Theory of Quantum Systems: A Modern Introduction* (Cambridge University Press, Cambridge, 2013).
- [90] P. Lipavský, V. Špička, and B. Velický, *Phys. Rev. B* **34**, 6933 (1986).
- [91] G. Baym and L. P. Kadanoff, *Phys. Rev.* **124**, 287 (1961).
- [92] F. Green, D. Neilson, and J. Szymański, *Phys. Rev. B* **31**, 2779 (1985).
- [93] C.-O. Almbladh, *Phys. Scr.* **32**, 341 (1985).
- [94] A.-M. Uimonen, G. Stefanucci, and R. v. Leeuwen, *J. Chem. Phys.* **140**, 18A526 (2014).
- [95] J. Berakdar, *Phys. Rev. B* **58**, 9808 (1998).
- [96] C. Caroli, D. Lederer-Rozenblatt, B. Roulet, and D. Saint-James, *Phys. Rev. B* **8**, 4552 (1973).
- [97] L. Hedin and J. D. Lee, *Phys. Rev. B* **64**, 115109 (2001).
- [98] S. Grabowski, M. E. Garcia, and K. H. Bennemann, *Phys. Rev. Lett.* **72**, 3969 (1994).
- [99] M. Quijada, R. Díez Muiño, and P. M. Echenique, *Nanotechnology* **16**, S176 (2005).
- [100] B. Holm and U. von Barth, *Phys. Rev. B* **57**, 2108 (1998).
- [101] G. Strinati, H. J. Mattausch, and W. Hanke, *Phys. Rev. B* **25**, 2867 (1982).
- [102] N.-H. Kwong and M. Bonitz, *Phys. Rev. Lett.* **84**, 1768 (2000).
- [103] G. Baym, *Phys. Rev.* **127**, 1391 (1962).
- [104] Y. Takada, *Phys. Rev. Lett.* **87**, 226402 (2001).
- [105] N. E. Dahlen and R. van Leeuwen, *Phys. Rev. Lett.* **98**, 153004 (2007).
- [106] F. Jahnke, M. Kira, and S. W. Koch, *Zeitschrift Fur Physik B-Condensed Matter* **104**, 559 (1997).
- [107] S. Ismail-Beigi and S. G. Louie, *Phys. Rev. Lett.* **90**, 076401 (2003).
- [108] T. Reiners, W. Orlik, C. Ellert, M. Schmidt, and H. Haberland, *Chem. Phys. Lett.* **215**, 357 (1993).
- [109] P. Minnhagen, *J. Phys. C* **7**, 3013 (1974).
- [110] A. Schindlmayr and R. W. Godby, *Phys. Rev. Lett.* **80**, 1702 (1998).
- [111] A. Schindlmayr, T. J. Pollehn, and R. W. Godby, *Phys. Rev. B* **58**, 12684 (1998).
- [112] J. Hubbard, *P. R. Soc. A-Math. Phys.* **243**, 336 (1958).
- [113] A. Holas, P. K. Aravind, and K. S. Singwi, *Phys. Rev. B* **20**, 4912 (1979).
- [114] R. van Leeuwen and G. Stefanucci, *Phys. Rev. B* **85**, 115119 (2012).
- [115] A.-M. Uimonen, G. Stefanucci, Y. Pavlyukh, and R. van Leeuwen, *Phys. Rev. B* **91**, 115104 (2015).
- [116] M. Cardona and L. Ley, eds., *Photoemission in Solids I General Principles* (Springer, Berlin, 1978).
- [117] S. Hüfner, *Photoelectron spectroscopy: principles and applications*, 3rd ed., Ad-

- vanced texts in physics (Springer, Berlin; New York, 2003).
- [118] W. Schattke and M. A. Van Hove, eds., *Solid-state photoemission and related methods: theory and experiment* (Wiley-VCH, Weinheim, 2002).
- [119] V. Schmidt, *Electron spectrometry of atoms using synchrotron radiation*, Cambridge monographs on atomic, molecular, and chemical physics No. 6 (Cambridge University Press, Cambridge; New York, 1997).
- [120] E. Weigold, *Electron momentum spectroscopy*, Physics of atoms and molecules (Kluwer Academic/Plenum Publishers, New York, 1999).
- [121] J. Berakdar, A. Lahmam-Bennani, and C. Dal Cappello, Phys. Rep. **374**, 91 (2003).
- [122] J. Berakdar, *Concepts of highly excited electronic systems*, 1st ed. (Wiley-VCH, Weinheim, 2003).
- [123] L. Campbell, L. Hedin, J. J. Rehr, and W. Bardyszewski, Phys. Rev. B **65**, 064107 (2002).
- [124] E. Klevak, J. J. Kas, and J. J. Rehr, Phys. Rev. B **89**, 085123 (2014).
- [125] M. E. Madjet, H. S. Chakraborty, J. M. Rost, and S. T. Manson, J. Phys. B **41**, 105101 (2008).
- [126] F. U. Hillebrecht, A. Morozov, and J. Kirschner, Phys. Rev. B **71**, 125406 (2005).
- [127] N. J. Halas, S. Lal, W.-S. Chang, S. Link, and P. Nordlander, Chem. Rev. **111**, 3913 (2011).
- [128] F. J. García de Abajo, Rev. Mod. Phys. **82**, 209 (2010).
- [129] S. Roke and G. Gonella, Annu. Rev. Phys. Chem. **63**, 353 (2012).
- [130] J. I. Dadap, J. Shan, K. B. Eisenthal, and T. F. Heinz, Phys. Rev. Lett. **83**, 4045 (1999).
- [131] N. Yang, W. E. Angerer, and A. G. Yodh, Phys. Rev. Lett. **87**, 103902 (2001).
- [132] S. Roke, W. G. Roeterdink, J. E. G. J. Wijnhoven, A. V. Petukhov, A. W. Kleyn, and M. Bonn, Phys. Rev. Lett. **91**, 258302 (2003).
- [133] A. G. F. de Beer and S. Roke, Phys. Rev. B **79**, 155420 (2009).
- [134] J. I. Dadap, Phys. Rev. B **78**, 205322 (2008).
- [135] A. G. F. de Beer, S. Roke, and J. I. Dadap, J. Opt. Soc. Am. B **28**, 1374 (2011).
- [136] J. Butet, G. Bachelier, I. Russier-Antoine, C. Jonin, E. Benichou, and P.-F. Brevet, Phys. Rev. Lett. **105**, 077401 (2010).
- [137] G. Gonella and H.-L. Dai, Phys. Rev. B **84**, 121402 (2011).
- [138] J. Butet, I. Russier-Antoine, C. Jonin, N. Lascoux, E. Benichou, and P.-F. Brevet, Nano Lett. **12**, 1697 (2012).
- [139] G. Gonella, W. Gan, B. Xu, and H.-L. Dai, J. Phys. Chem. Lett. **3**, 2877 (2012).
- [140] J. Jackson, *Classical electrodynamics*, 3rd ed. (Wiley, New York, 1999).
- [141] D. A. Varshalovich and A. N. Moskalev, *Quantum Theory of Angular Momentum* (World Scientific Pub Co Inc, 1988).
- [142] E. Prodan and P. Nordlander, Nano Lett. **3**, 543 (2003).
- [143] B. Orr and J. Ward, Mol. Phys. **20**, 513 (1971).
- [144] W. Ekardt, Phys. Rev. B **31**, 6360 (1985).

- [145] M. J. Puska and R. M. Nieminen, *Phys. Rev. A* **47**, 1181 (1993).
- [146] A. Liebsch and W. L. Schaich, *Phys. Rev. B* **40**, 5401 (1989).
- [147] R. van Leeuwen, *Phys. Rev. Lett.* **80**, 1280 (1998).
- [148] R. Van Leeuwen, *Int. J. Mod. Phys. B* **15**, 1969 (2001).
- [149] A. Zangwill and P. Soven, *Phys. Rev. A* **21**, 1561 (1980).
- [150] J. F. Ward, *Rev. Mod. Phys.* **37**, 1 (1965).
- [151] Y. Wang and E. Carter, in *Theoretical Methods in Condensed Phase Chemistry*, Progress in Theoretical Chemistry and Physics (Kluwer Academic Publishers, Dordrecht, 2002) pp. 117–184.
- [152] C. Wang, J. Chen, and J. Bower, *Optics Commun.* **8**, 275 (1973).
- [153] P. Apell, *Phys. Scr.* **27**, 211 (1983).
- [154] I. Grigorenko, S. Haas, and A. F. J. Levi, *Phys. Rev. Lett.* **97**, 036806 (2006).
- [155] G. Mukhopadhyay and S. Lundqvist, *Nuovo Cim. B* **27**, 1 (1975).
- [156] B. Vasvári, *Phys. Rev. B* **55**, 7993 (1997).
- [157] A. D. Polyanin and A. V. Manzhirov, *Handbook of integral equations* (CRC Press, Boca Raton, Flo., 1998).
- [158] T. Martin, *Phys. Rep.* **273**, 199 (1996).
- [159] W. Ekardt, *Phys. Rev. B* **29**, 1558 (1984).
- [160] B. R. Johnson, *J. Chem. Phys.* **67**, 4086 (1999).
- [161] D. Bowler and M. Gillan, *Chem. Phys. Lett.* **325**, 473 (2000)

# Index

---

- GW* approximation, 25
- S*-model, 9, 11, 14
- $\alpha$  constant, 5
- f*-sum rule, 36
  
- asymptotic expansions, 30
- asymptotic series, 9
- atomic orbital basis, 31
- attosecond streaking, 33
  
- band gap, 9
- Bethe-Salpeter equation, 6, 37, 40
- Bose distribution, 38
  
- chord diagrams, 7, 12, 14
- configuration interaction, 21, 25, 51
- conserving approximations, 36
- contour evolution operator, 35
- contour-ordering operator, 34
- core electron, 9
- correlational shift, 9
- Coulomb matrix elements, 24, 31
- cumulant function, 10
  
- density functional theory, 4, 21
- density-density response, 51
- double photoemission, 46
- Drude dielectric function, 59
- Dyson equation, 13, 14, 25, 29
  
- electron-plasmon interaction, 14
- electron-plasmon scattering, 13
- exchange-correlation kernel, 51, 56
  
- Fermi distribution, 38
- Fermi edge singularity, 14
- Fermi Golden rule, 48
- Fermi liquid, 4, 14
- Fluctuation potential, 14
- fluctuation-dissipation theorem, 22, 33
  
- Fock space, 31, 42
  
- Galitskii-Migdal equation, 25
- generalized Kadanoff-Baym Ansatz, 34
- Green's function, 10
  
- Hartree approximation, 7
- Hartree-Fock Hamiltonian, 3
- Hedin's equations, 7
- highest occupied molecular orbital, 25
- Hopf algebra, 8
  
- incoming boundary conditions, 49
  
- jellium model, 25, 27, 50, 55, 58, 61
  
- Keldysh contour, 42, 47, 49
- Kohn-Sham potential, 31, 62
  
- ladder approximation, 25
- Langreth rules, 35
- local field factor, 41
- lowest unoccupied molecular orbital, 25
  
- Mie theory, 52
- molecular orbital basis, 31
- Monte-Carlo integration, 18, 45
  
- non-degenerate chord diagram, 8
  
- one-electron current, 46
- optimized effective potential, 3
- orbital-free kinetic density functional theory, 58
- orthogonality catastrophe, 4
  
- Padé approximation, 13, 14, 41
- Paley-Wiener theorem, 18, 19, 65
- photoemission, 4
- plasmon, 49
- plasmon pole approximation, 50

plasmonic satellites, 10  
polarization, 6, 7  
positive definite approximations, 41  
  
quasiparticle, 4, 10, 14, 17  
  
random phase approximation, 6, 45, 51,  
56  
Rayleigh scattering, 55  
reductionism, 3  
  
scattering state, 48  
screened interaction, 6  
second harmonic generation, 51  
Seitz radius, 5  
self-energy, 6, 7  
spectral function, 10  
spectral moments, 30  
spherical Bessel function, 53  
spherical Hankel function, 53  
structure factor, 15  
superatomic molecular orbitals, 21  
superconvergence theorem, 31  
surface sheet model, 51  
  
time-dependent density functional theory,  
27, 51, 55  
time-ordering operator, 34  
time-resolved two-photon photoemission,  
33  
time-resolved two-photon photoemission,  
25, 26  
  
vector spherical harmonics, 53  
vertex, 6, 7  
vertex correction, 9  
  
Whittaker functions, 7  
Wick's theorem, 43, 47  
  
x-ray absorption, 9



# Eidesstattliche Erklärung

---

Hiermit erkläre ich, dass ich die Habilitationsschrift selbstständig und ohne fremde Hilfe verfasst und andere als die angegebenen Quellen und Hilfsmittel nicht benutzt und die den benutzten Werken wörtlich oder inhaltlich entnommenen Stellen als solche kenntlich gemacht habe.

Halle (Saale), den Juni 25, 2015

Yaroslav Pavlyukh



---



# Lebenslauf

---

Martin-Luther-Universität Halle-Wittenberg  
Karl-Freiherr-von-Fritsch Str. 3  
D-06120 Halle (Saale)  
Telefon: +49 345 5528 527  
Fax: +49 345 5527 393  
Email: yaroslav.pavlyukh@physik.uni-halle.de



## Persönliche Details

Geburtsdatum: 26.02.1976, Staatsangehörigkeit: ukrainisch, Ehestand: verheiratet mit Khompat Satitkovitchai, Kinder: Nadija, Taras

## Wissenschaftliche Ausbildung

**2003** Promotion in Physik, Max-Planck-Institut für Mikrostrukturphysik und Martin-Luther-Universität Halle-Wittenberg, Prädikat: Magna Cum Laude, Dissertation: “*Ab initio* theory for ultrafast electron dynamics in metallic nanoparticles”, Betreuer: Prof. W. Hübner

**1998** Diplom in Physik, Nationale Iwan-Franko-Universität Lwiw, Lemberg, Ukraine, Diplomarbeit: “Simulation of the topological structure of highly dispersed disordered systems”, Betreuer der Abschlussarbeit: Prof. Z. M. Yaremko

## Wissenschaftlicher Werdegang

**ab 4/2007** Wissenschaftlicher Mitarbeiter an der Martin-Luther-Universität Halle-Wittenberg in der Arbeitsgruppe von Prof. Jamal Berakdar

**01/2003-03/2007** Postdoc mit Prof. Wolfgang Hübner an der Technischen Universität Kaiserslautern

**01/2000-12/2002** Doktorand am Max-Planck-Institut für Mikrostrukturphysik

Halle (Saale), den Juni 25, 2015

Yaroslav Pavlyukh

A handwritten signature in blue ink, appearing to read 'Yaroslav Pavlyukh', written over a horizontal line.



## List of the appended publications

---

- [1] Y. Pavlyukh and W. Hübner, *J. Math. Phys.* **48**, 052109 (2007).
- [2] Y. Pavlyukh, A. Rubio, and J. Berakdar, *Phys. Rev. B* **87**, 205124 (2013).
- [3] Y. Pavlyukh and W. Hübner, *Phys. Rev. B* **75**, 205129 (2007).
- [4] Y. Pavlyukh, J. Berakdar, and W. Hübner, *Phys. Rev. Lett.* **100**, 116103 (2008).
- [5] Y. Pavlyukh and J. Berakdar, *J. Chem. Phys.* **135**, 201103 (2011).
- [6] G. Pal, Y. Pavlyukh, H. C. Schneider, and W. Hübner, *Eur. Phys. J. B* **70**, 483 (2009).
- [7] G. Pal, Y. Pavlyukh, W. Hübner, and H. C. Schneider, *Eur. Phys. J. B* **79**, 327 (2011).
- [8] G. Stefanucci, Y. Pavlyukh, A.-M. Uimonen, and R. van Leeuwen, *Phys. Rev. B* **90**, 115134 (2014).
- [9] Y. Pavlyukh, M. Schüler, and J. Berakdar, *Phys. Rev. B* **91**, 155116 (2015).
- [10] Y. Pavlyukh and W. Hübner, *Phys. Rev. B* **70**, 245434 (2004).
- [11] Y. Pavlyukh, J. Berakdar, and K. Köksal, *Phys. Rev. B* **85**, 195418 (2012).
- [12] Y. Pavlyukh, J. Berakdar, and W. Hübner, *New J. Phys.* **14**, 093044 (2012)